Title

Sensory Tuning of Thalamic and Intracortical Excitation in Primary Visual Cortex and Novel Methods for Circuit Analysis

Author

Lien, Anthony D.

Publication Date

2013

Peer reviewed|Thesis/dissertation

UNIVERSITY OF CALIFORNIA, SAN DIEGO

Sensory Tuning of Thalamic and Intracortical Excitation in Primary Visual Cortex and Novel Methods for Circuit Analysis

A dissertation submitted in partial satisfaction

of the requirements for the degree Doctor of Philosophy

in

Neurosciences

by

Anthony D. Lien

Committee in charge:

Professor Massimo Scanziani, Chair
Professor Edward M. Callaway
Professor E.J. Chichilnisky
Professor Timothy Q. Gentner
Professor Jeffry S. Isaacson
Professor Takaki Komiyama

2013

The Dissertation of Anthony D. Lien is approved and it is acceptable in quality and form for publication on microfilm and electronically:

_____

_____

_____

_____

_____

_____

Chair

University of California, San Diego

2013

Table of Contents

Signature Page iii

Table of Contents iv

List of Figures vi

Acknowledgements vii

Vita ix

Abstract x

Chapter 1. Thalamic and intracortical excitation and sensory tuning in the visual cortex 1

Introduction 1
Tuning properties of V1 neurons 2
Anatomical and synaptic properties of thalamic excitation 4
Tuning properties of thalamic neurons 6
Circuit mechanisms for orientation tuned thalamic excitation 7
Experimental evidence for orientation tuning of thalamic excitation 8
Silencing the cortex to isolate thalamic excitation 11
Results on thalamic excitation 13
What are the tuning properties of cortical inputs? 15
Results on cortical excitation 18
Conclusion 20
The origin of direction selectivity 20
Contribution of thalamic and intracortical excitation to tuning properties in other cortical layers 23
References 33

Chapter 2. Tuned thalamic excitation is amplified by visual cortical circuits 38

Abstract 38
Introduction 38
Results 41
Discussion 49
Methods 56
Acknowledgements 84
References 84

Chapter 3. *In vivo* labeling of constellations of functionally identified neurons for targeted *in vitro* recordings 88

Preface 88
Abstract 89
Introduction 90
Results 91
Discussion 96
Methods 98
Acknowledgments 107
References 107

List of Figures

Chapter 1

Figure 1.1 Tuning properties of cortical neurons 26

Figure 1.2 Tuning properties of thalamic neurons 27

Figure 1.3 Possible circuits for orientation selective thalamic excitation 28

Figure 1.4 Experimental evidence for oriented spatial arrangement of thalamic inputs onto a cortical neuron 29

Figure 1.5 Experimental evidence for tuning of thalamic excitation 30

Figure 1.6 Predicted orientation tuning of thalamic excitation in response to drifting gratings 31

Figure 1.7 Proposed intracortical and thalamic excitatory connectivity scheme .. 32

Chapter 2

Figure 2.1 Isolating thalamic excitation 67

Figure 2.2 Receptive field structure of thalamic excitation 69

Figure 2.3 Orientation tuning of thalamic excitation 71

Figure 2.4 Separation of ON and OFF thalamic subfields predicts preferred orientation of thalamic excitation 72

Figure 2.5 Tuning of non-thalamic excitatory charge 74

Figure 2.6 Tuning of non-thalamic excitatory F1 modulation 75

Figure 2.7 Co-tuning and phase relationship between thalamic and non-thalamic excitation 76

Supplementary Figure 2.1 Suppression of the local field potential is correlated with the degree of cortical silencing 77

Supplementary Figure 2.2 Cortical depth of recorded neurons 78

Supplementary Figure 2.3 Tuning of isolated dLGN units 79

Supplementary Figure 2.4 Blocking $GABA_B$ receptors does not affect grating-evoked local field potential during cortical silencing 81

Supplementary Figure 2.5 Additional measures of orientation tuning 82

Chapter 3

Figure 3.1 *In vivo* photo-labeling of functionally identified cortical neurons followed by *in vitro* targeted recording. 105

Figure 3.2 Matching *in vivo* and *in vitro* identities of photo-labeled neurons to correlate visual response properties with intrinsic electrophysiological properties. 106

Acknowledgements

I thoroughly enjoyed my time in graduate school. This would not be possible without the kind support of my mentors, friends, and family. My most sincere gratitude goes to:

Massimo Scanziani for his elegant approach to science, for sharing his enthusiasm and joy of discovery, for his outstanding guidance and mentorship, for his willingness to step with me into the unknown, for his refined aesthetic sense, and for his humor and wit.

Shaul Hestrin for patiently teaching me when I knew nothing and inspiring me to pursue science.

Bassam Atallah for his infectious passion for science and life and for teaching me how to ride the waves at Scripps pier.

Mingshan Xue for his humor, compassion, good nature, camaraderie, and conversation.

Members of the Scanziani and Isaacson labs past and present for making the lab a wonderful place to be.

My fellow students in the Neurosciences Graduate Program for being so smart, talented, creative, and fun.

Marina Garrett for her friendship and for inspiring me through our freeform scientific discourse.

My family for raising me, encouraging me to think scientifically, and supporting my aspirations.

My wife Lisa for her unconditional love and support, her incredible perseverance, and the joy she brings to my life.

Chapter 2, in full, is a reprint of material as it appears in: Lien AD, Scanziani M (2013) Tuned thalamic excitation is amplified by visual cortical circuits. Nature Neuroscience 16:1315–1323. The dissertation author was the primary investigator and author of this paper.

Chapter 3, in full, is a reprint of material as it appears in: Lien AD, Scanziani M (2011) In vivo labeling of constellations of functionally identified neurons for targeted in vitro recordings. Frontiers in Neural Circuits 5:16. The dissertation author was the primary investigator and author of this paper.

Vita

2007	B.S., Biological Sciences, Stanford University, Stanford, CA
2007-08	Research Assistant, Stanford University, Stanford, CA
2013	Ph.D., Neurosciences, University of California, San Diego, San Diego, CA

Publications

Lien AD, Scanziani M. (2013) Tuned thalamic excitation is amplified by visual cortical circuits. *Nature Neuroscience.* 16, 1315-1323.

Lien AD, Scanziani M. (2011) In vivo labeling of constellations of functionally identified neurons for targeted in vitro recordings. *Frontiers in Neural Circuits.* 5, 16.

Robey IF, **Lien AD**, Welsh SJ, Baggett BK, Gillies RJ (2005). Hypoxia-Inducible Factor-1α and the glycolytic phenotype in tumors. *Neoplasia.* 7(4), 324–330.

ABSTRACT OF THE DISSERTATION

Sensory Tuning of Thalamic and Intracortical Excitation in Primary Visual Cortex and Novel Methods for Circuit Analysis

by

Anthony D. Lien

Doctor of Philosophy in Neurosciences

University of California, San Diego, 2013

Professor Massimo Scanziani, Chair

The mammalian brain contains many regions in which feedforward excitatory afferents impinge on neurons that are interconnected by recurrent excitatory circuits. The functional *in vivo* properties of feedforward versus recurrent excitation are poorly understood due to the technical difficulty of distinguishing between these two sources of excitation in individual neurons. To address these issues I developed novel techniques for measuring the *in vivo* functional properties of the specific neuronal circuits that impinge onto individual neurons.

Chapters 1 and 2 describe how feedforward and recurrent excitation onto individual neurons in the mouse primary visual cortex respond to visual stimuli. In the primary visual cortex, individual neurons are tuned to specific features of visual stimuli namely their orientation, direction of movement, and retinal location of bright and dark regions. I examined the extent to which these sensory tuning properties are present in the

thalamic versus intracortical excitation onto single cortical neurons using *in vivo* intracellular recording techniques during optogenetic silencing of cortical excitatory neurons to isolate thalamic excitation. These results reveal that the main tuning properties observed in the primary visual cortex, namely receptive field structure, orientation selectivity, and direction selectivity, are already present in the thalamic excitation onto individual neurons. Estimation of the intracortical excitation from the total excitation recorded in the absence of cortical silencing revealed that thalamic and intracortical excitation share similar tuning properties demonstrating that tuned feedforward thalamic excitation is amplified by recurrent intracortical excitation.

Chapter 3 describes a novel photolabeling method that allows neurons with known *in vivo* functional properties to be studied in *in vitro* brain slice preparations in order to reveal their cellular, synaptic, and circuit properties. This technique helps bridge the gap between systems and cellular neuroscience and opens up new possibilities for understanding how neuronal circuits underlie neuronal function in the intact brain.

Together, these novel experimental approaches allow us to understand a fundamental aspect of neuronal circuit operation: the transfer and integration of information via synaptic connections. Such knowledge will aid in our understanding of the neuronal mechanisms underlying sensation, learning, and behavior.

Chapter 1. Thalamic and intracortical excitation and sensory tuning in the visual cortex

This chapter is an extended introduction and discussion of the published data and experiments described in Chapter 2: Tuned thalamic excitation is amplified by visual cortical circuits.

Introduction

Neurons in the primary visual cortex (V1) are tuned to specific features of the visual world meaning that they fire more action potentials (spikes) in response to certain visual stimuli but than others. The depolarization of the neuronal membrane to reach spike threshold is mediated by synaptic excitation. In V1, cortical neurons receive excitation from two main sources: feedforward inputs from the thalamus that provide sensory information, and intracortical inputs from other cortical neurons. What is the relative amount of excitation that is contributed by thalamic versus intracortical inputs in cortical neurons during visual stimulation? How are thalamic and intracortical excitation tuned to specific features of visual stimuli?

While the experiments described herein focus specifically on V1, many brain areas share a similar circuit architecture in which the major feedforward excitatory afferents impinge on neurons embedded in recurrently connected excitatory networks. This circuit architecture applies not only for thalamic projections to neocortex in general but also for other systems. For example, in the olfactory system the olfactory bulb projects to recurrently connected pyramidal neurons in the piriform cortex and in the

hippocampus, the dentate gyrus sends excitatory projections via mossy fibers onto a recurrent network of CA3 pyramidal neurons. By dissecting the tuning properties of feedforward and recurrent excitation in V1, we may begin to understand the operating principles of this ubiquitous neuronal circuit architecture.

Tuning properties of V1 neurons

The pioneering studies of Hubel and Wiesel were the first to describe how V1 neurons fire in response to visual stimuli (i.e., their tuning properties) (Hubel and Wiesel, 1959). Neurons in V1 respond only to stimuli presented within a constrained region of visual space called the receptive field. In so-called "simple cells", the receptive field can be divided into multiple spatially offset subregions that respond to increases (ON receptive field) or decreases (OFF receptive field) in luminance (Fig. 1.1a, Hubel and Wiesel, 1962). These regions are often elongated in the dimension perpendicular to the axis of spatial offset.

A consequence of this receptive field structure is that V1 neurons are highly selective for the orientation of bars or edges, firing only in response to stimuli oriented so that the luminance pattern is matched to the ON and OFF subregions of the neuron's receptive field (Fig. 1.1b, Hubel and Wiesel, 1959; Lampl et al., 2001; Usrey et al., 2003; Liu et al., 2011; Zhuang et al., 2013). Orientation tuning is a ubiquitous feature of cortical neurons and is observed in the majority of V1 neurons in all mammalian species examined.

In addition to being orientation selective, some V1 neurons are selective for the direction of movement of a visual stimulus. In these cells, a stimulus of the preferred

orientation evokes more spiking when it moves across the visual field in one direction as compared to the opposite direction (Fig. 1.1c, Hubel and Wiesel, 1959).

In cortical neurons, changes in the membrane potential result from the combination of the two opposing forces of synaptic excitation and inhibition, which respectively drive the membrane potential above and below spike threshold. The tuning properties of cortical spiking could result from either tuned excitation or untuned excitation combined with tuned inhibition. While the tuning properties of inhibition are still controversial (Anderson et al., 2000; Liu et al., 2011, 2010; Monier et al., 2003), it is clear that in V1 cortical neurons, excitation is largest for those stimuli that drive the strongest spiking responses. Hence, synaptic excitation and spiking share the same stimulus preference and are tuned to the same stimuli. Nevertheless, spiking responses tend to be more selective than excitation. That is, the difference in spiking between the preferred and non-preferred stimulus is larger than the difference in excitation in response to the same stimuli. This is because spike rate increases with increasing excitation only if the amount of excitation is large enough to depolarize the membrane potential to spike threshold. Thus, stimuli that evoke subthreshold amounts of excitation produce no spiking, resulting in spiking responses being more selective than excitation.

As mentioned above, synaptic excitation in V1 neurons comes from two main sources: feedforward inputs from the thalamus that provide sensory information and intracortical inputs from other cortical neurons. Do these two excitatory pathways carry the same information about the stimulus? What is the relative amount of excitation that comes from thalamic versus intracortical excitation? Do they prefer the same stimuli? Are they equally selective or is one more selective than the other?

Anatomical and synaptic properties of thalamic excitation

Studies of the anatomical and synaptic properties of the thalamic inputs to V1 can provide some insight into how thalamic inputs influence cortical spiking. Visual information reaches V1 via thalamocortical projection neurons of the lateral geniculate nucleus (LGN) of the thalamus. The axons of this projection contact V1 neurons to form excitatory synapses that utilize the neurotransmitter glutamate. These projections primarily target layer 4 (L4) of V1 however smaller projections are observed in all other cortical layers (LeVay and Gilbert, 1976; Antonini et al., 1999)

Despite the fact that the thalamus is the source of all visual input to V1, electron microscopy shows that LGN axonal boutons comprise only 6% of the total number of excitatory boutons in L4 (da Costa and Martin, 2009). Estimates of the fraction of excitatory synapses onto individual L4 excitatory neurons are similarly low (6%)(Ahmed et al., 1994).

The total number of thalamic neurons that converge on a single L4 neuron has not been directly measured. In cat V1, the innervation of a single L4 neuron by LGN projections consists of ~100-200 synapses (da Costa and Martin, 2011; Peters and Payne, 1993) and single LGN axons formed 1-8 synapses per cortical neuron(Freund et al., 1985), leading to an estimate of ~10-200 LGN neurons converging on a single cortical neuron. Roughly similar numbers (~85) were estimated obtained from paired recordings between thalamic and cortical neurons in the rat barrel cortex (Bruno and Sakmann, 2006).

Even though thalamic inputs make up a tiny fraction of the excitatory inputs to a L4 neuron, individual presynaptic thalamic axons in cat V1 produce larger, more reliable excitatory postsynaptic potentials (EPSPs) onto L4 neurons than intracortical excitatory axons at least as established in brain slices (Stratford et al., 1996). In mouse barrel cortex brain slices, thalamic axons have many more release sites and higher probability of release than intracortical axons, resulting in greater synaptic efficacy (Gil et al., 1999). Nevertheless, the mean amplitude of putative single thalamic axon EPSPs is only 2 mV in cat visual cortical slices (Stratford et al., 1996) and only ~0.5 mV in the rat barrel cortex *in vivo* (Bruno and Sakmann, 2006). Furthermore, the amplitude of thalamocortical EPSPs depresses strongly with repeated stimulation (Stratford et al., 1996; Gil et al., 1999). Since the resting potential of cortical neurons is 30-40 mV below spike threshold, a single thalamic input is too weak to drive a cortical neuron to spike. Therefore, during visual stimulation cortical neurons must rely on the concurrent activity of multiple thalamic inputs to reach spike threshold. Overall, cortical neurons appear to integrate input from multiple thalamic neurons. This integration may have crucial functional consequences; as originally suggested by Hubel and Wiesel, it might allow cortical neurons to derive tuning properties not present in individual thalamic neurons. Thus, the capacity of thalamic excitation to contribute to the tuning properties of cortical neurons critically depends on the tuning properties of the thalamic inputs that converge onto individual cortical neurons.

Tuning properties of thalamic neurons

In contrast to V1 neurons, the majority of thalamic neurons are poorly selective for both orientation and direction, firing a similar number of action potentials regardless of stimulus orientation or direction (Fig. 1.2c-d, Piscopo et al., 2013). Instead, they respond to changes in luminance in a circular region of visual space relative to background light levels. These neurons come in two types: ON-center that respond to increases in luminance and OFF-center that respond to decreases in luminance (Fig. 1.2a-b). This thalamic receptive field structure is directly inherited from retinal ganglion cells (RGCs), which make strong monosynaptic connections onto thalamic neurons.

However, the retina contains diverse types of RGCs with heterogeneous functional properties. Both direction and orientation selective RGCs exist in rabbits and rodents (Barlow and Hill, 1963; Yoshida et al., 2001) and at least some of the direction selective RGCs are known to project to LGN (Huberman et al., 2009; Rivlin-Etzion et al., 2011; Kay et al., 2011) suggesting that some LGN neurons may inherit orientation or direction selectivity from the retina. Recently, direction and/or orientation selective neurons were found in mouse LGN (Fig. 1.2c-d, Marshel et al., 2012; Piscopo et al., 2013; Scholl et al., 2013; Zhao et al., 2013) and orientation selective neurons were found in marmoset monkey (Cheong et al., 2013) although these constitute a small (~10%) fraction of LGN neurons.

Cortical neurons have the potential to receive thalamic input from poorly selective ON-center and OFF-center neurons as well as neurons that are highly selective for orientation and direction. The tuning of thalamic excitation onto a cortical neuron will result from the combined tuning properties of the thalamic neurons that converge onto it.

Circuit mechanisms for orientation tuned thalamic excitation

How could thalamic inputs be combined to produce orientation selective thalamic excitation? Orientation selective thalamic excitation could be generated either by combining the receptive fields of untuned thalamic inputs to construct a spatially oriented receptive field or by inheriting orientation selectivity from the subset of thalamic neurons that are already orientation selective (Fig. 1.3).

The hypothesis that orientation selective thalamic excitation results from the spatial arrangement of the receptive fields of untuned thalamic inputs was first proposed by Hubel and Wiesel (1962). Orientation selectivity can be achieved with at least two non-mutually exclusive distinct receptive field arrangements. First, the thalamic receptive fields could cover an elongated region of visual space (Fig. 1.3a). In this case, a bar oriented parallel to the elongation would simultaneously activate all of the thalamic inputs whereas a perpendicular bar would only activate a small fraction.

Second, orientation selective thalamic excitation could be achieved if the receptive fields of ON-center and OFF-center inputs were spatially offset from each other (Fig 3a). In this case, a contrast edge consisting of adjacent dark and bright regions would simultaneously activate all ON and OFF inputs if it were positioned so the dark region covered the OFF-center receptive fields and the bright region covered the ON-center whereas the same edge rotated to a perpendicular orientation would activate only a small fraction of the inputs.

The alternative hypothesis is that cortical neurons directly inherit their orientation selectivity from the orientation selectivity of individual thalamic neurons. Under this

hypothesis, cortical neurons receive thalamic inputs from orientation selective thalamic neurons that are tuned to the same orientation (Fig 3b). Thus, there are multiple possible ways of combining thalamic inputs to generate orientation selective thalamic excitation.

Experimental evidence for orientation tuning of thalamic excitation

Orientation selective thalamic excitation in a cortical neuron could be generated by combining the receptive fields of untuned thalamic neurons to construct an elongated and/or ON/OFF separated receptive field or by pooling inputs from orientation selective thalamic neurons tuned to the same orientation. In order to distinguish these hypotheses, it is necessary to measure orientation tuning and receptive field properties of thalamic input onto a cortical neuron, which is technically challenging.

Several experimental efforts have been made to map the receptive fields of thalamic and cortical neurons with known connectivity. These studies provide some evidence that the spatial arrangement of the receptive fields of untuned thalamic inputs onto an individual cortical neuron could produce orientation selective thalamic excitation.

One set of studies mapped the receptive fields of thalamic neurons that innervate a group of cortical neurons tuned to the same orientation. This is experimentally possible in carnivores and primates because V1 in these species contains orientation domains in which groups of neurons clustered within several hundred μm with receptive fields in roughly the same region of visual space are tuned to the same orientation. Thus the thalamic inputs to cortical neurons tuned to the same orientation can be isolated by recording from thalamic axons in a single orientation domain (Chapman et al., 1991) or

by recording thalamic neurons that project to the same orientation domain (Jin et al., 2011).

In ferret V1, the receptive fields of thalamic inputs in the same orientation domain were scattered across an elongated region of space that matched the cortical preferred orientation (Fig 4a, Chapman et al., 1991) whereas in cat V1, the ON and OFF thalamic inputs tended to be spatially offset from each other in a manner that matched the preferred orientation (Fig 4b, Jin et al., 2011). These results are significant because they demonstrate that the receptive fields of thalamic inputs onto a cortical orientation domain are, as a whole, capable of producing orientation tuned thalamic excitation either through an elongation or ON/OFF separation mechanism. However, because an individual cortical neuron probably samples from only a subset of the thalamic inputs that innervate a orientation domain and the precise connectivity between individual thalamic and cortical neurons is not known in these experiments, the contribution of this "population thalamic receptive field" to the thalamic excitation of individual cortical neurons is unclear.

A second set of studies mapped the receptive fields of thalamic neurons that formed putative monosynaptic connections with a simultaneously recorded cortical neuron (Fig. 1.4c, Tanaka, 1985; Reid and Alonso, 1995). In this approach, a thalamic neuron was assumed to innervate a simultaneously recorded cortical neuron if a significant fraction of cortical spikes were time-locked to preceding thalamic spikes with a latency consistent with an excitatory monosynaptic connection (5-10 ms). In pairs of such putatively connected thalamic and cortical neurons, the receptive field of the thalamic neuron overlapped with elongated cortical receptive field subregions that

preferred the same luminance (ie, ON-center thalamic receptive fields overlapped with cortical ON subregions) while avoiding cortical subregions of opposite luminance (ie, ON-center thalamic receptive fields avoid cortical OFF subregions). These results show that individual thalamic inputs can contribute to both the elongation and segregation of ON and OFF receptive fields of a postsynaptic cortical neuron. A major caveat of this approach is that the presence of a monosynaptic connection is inferred indirectly through spike train correlations. This does not allow direct measurement of the relative synaptic strength of connections and is biased toward detecting inputs with highly precise temporal relationships with postsynaptic spiking, which may not reflect the vast majority of thalamic inputs. Additionally, the paired recording technique severely undersamples the total ensemble of thalamic inputs to a cortical neuron.

Little is known about how orientation selective LGN neurons connect to individual cortical neurons in L4. In the aforementioned studies, the orientation selectivity of thalamic neurons was not assessed although they exhibited other functional properties characteristic of untuned ON-center and OFF-center neurons. Preliminary work suggests that orientation selective thalamic neurons may preferentially project to superficial L2/3 rather than L4 of V1 (Cruz-Martin et al., 2013). Given that orientation selective neurons comprise less than 10% of all LGN neurons, it would be surprising if this population were responsible for cortical orientation selectivity although it remains an open possibility.

Ultimately, in order to understand how the thalamus contributes to cortical orientation selectivity, it is necessary to directly record thalamic excitation in individual cortical neurons and characterize its receptive field structure and orientation tuning

properties. A series of studies from David Ferster's lab were the first to isolate thalamic excitation and examine its orientation tuning properties. They made intracellular recordings from cortical neurons while silencing intracortical inputs via either cooling of the cortex (Ferster et al., 1996) or recruitment of inhibition by electrical stimulation (Chung and Ferster, 1998) to isolate thalamic excitation. These studies showed that thalamic excitation was indeed orientation selective (Fig. 1.5). However, because they did not map the receptive field of thalamic excitation, they could not specify whether this orientation selectivity resulted from an elongated or ON/OFF separated receptive field arrangement. Furthermore, because of how the orientation tuning of thalamic excitation was quantified, the contribution of orientation selective thalamic neurons could not be determined.

To address these unanswered questions, I isolated thalamic excitation onto cortical neurons using a novel optogenetic approach for cortical silencing in mouse V1. I mapped the ON and OFF receptive fields of thalamic excitation as well as its orientation tuning. Finally, I analyzed these data to determine the potential contribution of orientation selective thalamic neurons in the orientation tuning of thalamic excitation.

Silencing the cortex to isolate thalamic excitation

While total excitation can be measured using *in vivo* intracellular recording, it is difficult to separate thalamic from intracortical excitation because they occur concurrently during visual stimulation and are pharmacologically indistinguishable. Previous methods for isolating thalamic excitation utilized either cooling of the cortical surface (Ferster et al., 1996) or electrical stimulation-evoked inhibition (Chung and

Ferster, 1998) to strongly suppress cortical spiking. Cortical cooling drastically alters neurotransmitter release from thalamic terminals thus distorting thalamic excitation. Electrical stimulation only silences the cortex for a brief time window (~100 ms), restricting the use of dynamic stimuli such as drifting gratings.

I developed a novel method for isolating thalamic excitation by combining whole-cell voltage clamp recordings with optogenetic activation of parvalbumin (PV) expressing cortical GABAergic interneurons to silence the cortex. Because of their dense and divergent inhibitory connectivity, PV interneurons exert powerful inhibition onto local cortical excitatory neurons. PV neurons can be targeted for optogenetic manipulation in a transgenic mouse that expresses Cre recombinase specifically in PV neurons (Hippenmeyer et al., 2005) using viral delivery of Cre-dependent gene expression constructs for optogenetic tools. Photostimulation of PV interneurons expressing the light-gated cation channel channelrhodopsin 2 (ChR2) (Nagel et al., 2003; Boyden et al., 2005) results in complete suppression of spiking in cortical excitatory neurons. This method is rapid, reversible and can silence cortical spiking for several seconds, allowing for the use of longer duration stimuli.

An alternative optogenetic approach to silencing the cortex is to directly photosuppress cortical excitatory neurons expressing hyperpolarizing light-activated ion pumps such as Arch or Halorhodopsin (Zhang et al., 2007; Han and Boyden, 2007; Chow et al., 2010). However, in this approach complete cortical silencing necessitates complete transfection of the entire excitatory neuron population, which is difficult to achieve. In contrast, PV photostimulation can silence the cortex even in cases of incomplete

transfection of the PV neuron population because individual cortical excitatory neurons receive powerful inhibition from many PV neurons (Packer and Yuste, 2011).

Results on thalamic excitation

Using these new methods, I found that in mouse V1, thalamic excitation comprised approximately 30% of the total excitation onto cortical neurons in response to both flashed black and white squares as well as drifting gratings. This value is in close agreement to previous measurements from cat V1 (Ferster et al., 1996; Chung and Ferster, 1998).

The ON and OFF receptive fields of thalamic excitation were mapped using flashed black and white squares in various spatial locations. The receptive field of thalamic excitation was organized into overlapping, yet spatially offset ON and OFF subregions that exhibited little elongation.

As described above, such a receptive field structure can produce thalamic excitation that is selective for the orientation of a contrast edge even if they are contributed by ON-center and OFF-center thalamic neurons that are not orientation selective. Alternatively, orientation selectivity of thalamic excitation could be generated by inputs from the subset of thalamic neurons that are highly orientation selective. These two possibilities can be distinguished by examining thalamic excitation in response to drifting grating stimuli (Fig. 1.6), which consist of alternating black and white bars that move in a direction perpendicular to the bars of the grating.

If the spatially offset ON and OFF subregions are contributed by poorly tuned thalamic neurons, then drifting gratings oriented such that the bars are perpendicular to

the axis connecting the ON and OFF receptive fields will cause high amplitude fluctuations in thalamic excitation at the temporal frequency of the grating (F1 amplitude) because the ON and OFF subregions are activated simultaneously once per grating cycle. Orthogonal orientations produce sustained thalamic excitation with small F1 amplitude because the ON and OFF subregions are activated sequentially. Therefore, spatial offset between ON-center and OFF-center thalamic receptive fields can generate orientation selectivity in the F1 amplitude of thalamic excitation in response to drifting gratings. However, the average thalamic excitation across the grating cycle (F0) is not orientation selective because the inputs themselves are not orientation selective.

If instead, the ON and OFF subregions are contributed by orientation selective thalamic neurons tuned to the same orientation, then the F0 of thalamic excitation should be orientation selective because, at least in mice, these neurons exhibit F0 spiking responses that are tuned for orientation (Piscopo et al., 2013).

Thalamic excitation exhibited large F1 amplitude in response to specific orientations of drifting grating stimuli, but not to perpendicular orientations, demonstrating that the F1 amplitude of thalamic excitation is orientation selective. In contrast, the F0 response of thalamic excitation was poorly selective for orientation. Finally, the axis of spatial offset of the ON and OFF receptive fields of thalamic excitation was predictive of the preferred orientation of F1 modulation. Thus, orientation selectivity of thalamic excitation is unlikely to be generated by inputs from orientation selective thalamic neurons. Instead, it is likely that tuned thalamic excitation comes from poorly tuned ON-center and OFF-center thalamic neurons whose ON and OFF receptive fields are spatially offset from each other.

What are the tuning properties of cortical inputs?

The cortical silencing experiments show that intracortical inputs contribute the majority (~70%) of synaptic excitation to L4 neurons during visual stimulation. What are the tuning properties of intracortical excitation with regard to orientation and receptive field structure?

As mentioned previously, V1 of carnivores and primates contains orientation domains in which groups of neurons clustered within several hundred μm are tuned to the same orientation. These domains are organized across the cortical sheet in repeated pinwheel patterns in which the preferred orientation changes smoothly around the pinwheel center although there are occasional fractures where preferred orientation changes suddenly (Ohki et al., 2005). Thus, aside from the small population of neurons near pinwheel centers and fractures, the vast majority of cortical neurons are surrounded by neighbors that are tuned to the same orientation. Connectivity rates between cortical excitatory neurons are highest for nearby cells and decrease with distance (Holmgren et al., 2003), so a cortical neuron is more likely to receive intracortical excitatory inputs from other neurons that share its orientation preference. Remarkably this connectivity scheme does not require the spatial clustering of co-tuned neurons that occurs in orientation domains. In mouse V1, which lacks orientation domains such that neurons tuned to different orientations are intermingled, pairs of excitatory neurons in L2/3 that were tuned to the same orientation were twice as likely to be synaptically connected as compared to neurons with orthogonal preferred orientations (Ko et al., 2011). Orientation specific intracortical excitatory connectivity is expected to generate orientation selective

intracortical excitation. Furthermore, because cortical neurons are tuned in their F0 firing rates (Niell and Stryker, 2008; Ringach et al., 2002; Zhuang et al., 2013), orientation selectivity of intracortical excitation onto an individual cortical neuron should be seen in the F0 response.

How might the putative orientation selectivity of intracortical excitation be related to that of thalamic excitation? Given that the population receptive field of thalamic inputs to an orientation domain exhibits elongation (Chapman et al., 1991) or ON/OFF separation (Jin et al., 2011) that matches the preferred orientation of the cortical neurons in that domain (see above) it is likely that thalamic and intracortical excitation are tuned to the same orientation.

In addition to being orientation selective, cortical "simple cells" have spatially offset ON and OFF receptive fields. Is this organization contributed exclusively by the spatially offset ON and OFF subregions of thalamic excitation, or does intracortical excitation also contribute spatially offset ON and OFF subregions?

For the latter to occur, a cortical neuron would preferentially receive excitatory input not only from cortical neurons tuned to the same orientation but also from cortical neurons that had matching spatially offset ON and OFF receptive field subregions. This would result in an individual cortical neuron receiving intracortical excitation with spatially offset ON and OFF subregions. Alternatively, a cortical neuron might receive excitatory input from cortical neurons tuned to the same orientation but with non-matching ON and OFF subregions. In this case, the ON subregions would overlap with OFF subregions from different inputs, resulting in intracortical excitation with little spatial offset between ON and OFF subregions. Receptive field structure is not correlated

among neighboring cortical neurons (DeAngelis et al., 1999; Bonin et al., 2011) and so any preferential connectivity due to receptive field structure would require additional specificity beyond a connectivity rule based on interneuronal distance. The existence of such preferential intracortical connectivity has not been addressed experimentally.

In order to understand the tuning properties of intracortical excitation and its relationship to thalamic excitation, it is necessary to measure both thalamic excitation and intracortical excitation in isolation in the same neuron. Previous studies related the orientation selectivity of thalamic excitation during cortical silencing to that of the membrane potential in the absence of silencing (Ferster et al., 1996; Chung and Ferster, 1998). The thalamic excitation was tuned to a similar orientation as the membrane potential in the absence of silencing. However, the membrane potential in the absence of silencing results from a combination of synaptic excitation and inhibition, and so intracortical excitation could not be isolated.

I investigated the orientation tuning of intracortical excitation and its relationship to thalamic excitation by recording synaptic excitation from the same cortical neuron in the presence and absence of optogenetic cortical silencing. Importantly, the neurons were voltage clamped at the reversal potential for synaptic inhibition to isolate synaptic excitation. Intracortical excitation was estimated by subtracting thalamic excitation (recorded during cortical silencing) from total excitation (recorded in the absence of cortical silencing). This procedure assumes linearity of the interaction between excitatory currents of thalamic and cortical origin. While this assumption is reasonable as long as cortical neurons are properly voltage clamped, the consequences of improper voltage

clamp and ensuing nonlinearities are discussed in the discussion section of the attached paper.

Results on cortical excitation

The F0 component of intracortical excitation was orientation selective as opposed to that of thalamic excitation. This implies that a cortical neuron receives more excitation from cortical neurons tuned to specific orientations than to others, suggesting that cortical excitatory neurons tuned to the same orientation are more likely to be connected and/or form stronger connections with each other (Fig. 1.7a).

The intracortical excitation also exhibited large F1 modulation at specific orientations. The orientation tuning of the F1 amplitude shared similar orientation preference with the F0 response. Because F1 amplitude is related to the separation between ON and OFF subregions along the axis perpendicular to the bars of the grating, this result suggests that similar to thalamic excitation, intracortical excitation also exhibits spatially offset ON and OFF subregions. Thus, in addition to receiving more excitation from other cortical neurons tuned to the same orientation, these co-tuned inputs are likely to have matching ON and OFF receptive field subregions (Fig. 1.7b).

In an individual cortical neuron, the F0 and F1 of intracortical excitation were tuned to the same orientation as the F1 of thalamic excitation. Intracortical excitation thus preserves the orientation preference contributed by thalamic excitation. Because of this, a cortical neuron likely receives enhanced intracortical excitatory connectivity from other cortical neurons whose orientation preference matches that of its thalamic excitation. Furthermore, the F1 amplitude of thalamic excitation and intracortical excitation show

similar degrees of orientation selectivity, suggesting once again that intracortical excitation plays a role in preserving rather than enhancing or disrupting the orientation selectivity of thalamic excitation.

Thalamic and intracortical excitation also had similar temporal phase of F1 modulation in response to their mutual preferred grating orientation. Because the temporal phase of F1 modulation is related to the time point in the grating cycle at which the white and black bars are respectively matched to ON and OFF subregions, differences in temporal phase can be ascribed to spatial differences in ON and OFF subregions. The small temporal phase differences between thalamic and intracortical excitation suggest that thalamic and intracortical excitation have matching ON and OFF receptive field structure (Fig. 1.7c). This demonstrates that intracortical excitation also preserves the spatially offset ON and OFF receptive field structure of thalamic excitation. Hence, intracortical excitation amplifies both the orientation selectivity and the receptive field structure contributed by thalamic excitation.

We propose a circuit in which a cortical neuron receives excitatory inputs from untuned thalamic neurons with spatially offset ON and OFF receptive fields resulting in orientation selective thalamic excitation (Fig. 1.7). These thalamic inputs are accompanied by preferential excitatory connectivity from cortical neurons tuned to the same orientation as thalamic excitation. Finally, these intracortical excitatory inputs exhibit ON and OFF receptive fields that match those of thalamic excitation. Such functional organization of the excitatory inputs onto a cortical neuron allows the cortex to faithfully amplify novel sensory tuning properties arising from the combination of multiple thalamic inputs onto an individual cortical neuron.

Conclusion

In this section, points of interest that are not discussed in detail in the paper in the following chapter will be elaborated.

The origin of direction selectivity

A subset of orientation selective neurons in V1 are also direction selective. The mechanism of cortical direction selectivity is highly debated. Both thalamocortical and intracortical circuits have been implicated in the generation of direction selectivity. I found that in L4, direction selectivity is observed in the thalamic excitation onto individual neurons, suggesting a thalamic origin for direction selectivity. Notably, direction selectivity of thalamic excitation onto individual cortical neurons was observed in the F1 but not F0 response to drifting gratings. In other words, the temporal dynamics (F1 modulation) of thalamic excitation, but not the temporal integral (F0) differed in response to the same spatial pattern moving in opposite directions. While for gratings drifting in the preferred direction, thalamic excitation occurs at the same temporal phase of the grating cycle (ie simultaneous F1 modulation) for the null (opposite) direction, thalamic excitation is more temporally distributed across the grating cycle. The lack of direction tuning in the F0 component of thalamic excitation argues against direction selective thalamic neurons as the source of cortical direction selectivity because such thalamic neurons exhibit strong direction selectivity in their F0 responses (Piscopo et al., 2013).

How can the temporal dynamics of thalamic excitation be so different in response to the same spatial pattern moving in opposite directions? One possibility is that temporal dynamics of thalamic excitation in response to visual stimuli vary as a function of stimulus location within the receptive field. This could be achieved by a spatial gradient of visual response latencies across the receptive field such that the latency of thalamic excitation is high on one side of the receptive field and low on the opposite side. In response to a stimulus moving from the high latency to low latency region of the receptive field, the stimulus will initially activate the high latency region followed by the low latency region. If the latency of thalamic excitation in the high latency region is equal to the time it takes for the stimulus to reach the low latency region, then the high and low latency thalamic excitation occur coincidently and can summate, producing a large peak thalamic excitation. If a stimulus moves across the receptive field in the opposite direction, activating the low latency region followed by the high latency region, the thalamic excitation from the low latency region will decay before it can summate with that from the high latency region, producing a small peak thalamic excitation.

Recordings of thalamic excitation in response to both moving and stationary stimuli could test this hypothesis. If a gradient of latency of thalamic excitation across the receptive field generates direction selectivity, then it should be seen in the temporal dynamics of thalamic excitation in response to stationary stimuli in different parts of the receptive field. Furthermore, the direction and strength of this gradient should predict the preferred direction and degree of direction selectivity of thalamic excitation in response to moving stimuli. Specifically, thalamic excitation should exhibit the large peak response for stimuli that move from high to low latency regions and low peak response

for movement in the opposite direction. Additionally, direction selectivity should be observed only within the range of stimulus speeds in which the time it takes to move from high to low latency regions of the receptive field matches the difference in visual response latency.

What could cause differences in the latency of thalamic excitation? There is considerable variation in visual response latency across the population of thalamic neurons. In the cat LGN, thalamic neurons with different visual response latency were classified into two groups: high latency "lagged" cells and low latency "non-lagged" cells (Mastronarde, 1987). The latency differences between lagged and non-lagged thalamic neurons are on the order of tens of milliseconds, which is sufficient to produce direction selectivity at stimulus speeds at which cortical neurons are known to exhibit direction selectivity. If a cortical neuron received both lagged and non-lagged thalamic inputs but the receptive fields of the lagged inputs were spatially offset from those of the non-lagged thalamic inputs, its thalamic excitation would be direction selective.

The hypothesis that differences in visual response latency across the thalamic population are used to generate cortical direction selectivity could be tested by experimentally manipulating visual response latencies in the thalamus. A recent report showed that the onset of visually evoked synaptic excitation was similar across thalamic neurons, but in lagged cells the onset of spiking was delayed by synaptic inhibition (Vigeland et al., 2013). This inhibition is likely to come from inhibitory interneurons within the LGN. Specific inactivation of this inhibitory interneuron population using optogenetic or other methods could be used to test whether the elimination of visual

response latency differences among thalamic neurons affects direction selectivity in L4 of V1.

Contribution of thalamic and intracortical excitation to tuning properties in other cortical layers

How do thalamic and intracortical excitation contribute to the tuning properties of neurons outside of L4? Neurons in other cortical layers could inherit their tuning properties from L4 neurons. In the canonical cortical circuit model, L4 distributes sensory information from the thalamus to other cortical layers via feedforward excitatory projections to L2/3 and L5, which are reciprocally connected (Binzegger et al., 2004). At each cortical layer, neurons could inherit tuning properties from presynaptic neurons in the previous layer by integrating inputs with similar tuning properties. Neurons could also construct novel tuning properties by integrating functionally diverse inputs. For example, Hubel and Wiesel proposed that complex cells, neurons that are tuned for orientation but respond to both ON and OFF stimuli throughout their receptive field, are generated by the convergence of cortical simple cells tuned to the same orientation but whose ON and OFF receptive fields are not matched.

While there is compelling anatomical evidence for strong excitatory connectivity across layers (Binzegger et al., 2004; Lefort et al., 2009), whether these intracortical connections are the primary determinants of the tuning properties of cortical neurons outside of L4 remains an open question. Previous efforts to disrupt activity in specific cortical layers have yielded conflicting results. Reversible pharmacological silencing of a

specific layer of the cat LGN abolished activity in L4 while the responses and tuning properties in L2/3 and L5 were largely unaffected (Malpeli, 1983). However, a different study performing the same manipulation showed that responses in L2/3 were mostly suppressed in the absence of L4 activity (Martinez and Alonso, 2001). One possibility for this discrepancy is that some neurons rely on L4 for their tuning properties whereas others derive their tuning properties completely independently of L4 via direct thalamic input. Furthermore, inactivation of L2/3 and parts of L4 via cooling or cryogenic lesion also had little effect on the tuning properties of most L5 neurons suggesting that they may obtain their tuning properties independently of the superficial layers (Schwark et al., 1986).

A recent study in the rat barrel cortex provides compelling evidence that thalamic input alone can drive sensory responses outside of L4 (Constantinople and Bruno, 2013). The authors demonstrated that L5 neurons receive direct thalamic input and that the strength and connectivity of thalamic input was comparable to that of L4 neurons. Furthermore, the membrane potential and spiking responses to sensory stimulation in L5 neurons were unaffected by pharmacological silencing of L4 and L2/3. Thus, it is possible that neurons outside of L4 in V1 may also receive their tuning properties through thalamic excitation.

How could thalamic inputs to neurons outside of L4 contribute to their tuning properties? The mechanism could be similar to that seen in L4 neurons where selectivity to orientation (and possibly direction) is constructed from the receptive field arrangement of thalamic inputs that are poorly tuned for orientation and direction. Or, neurons could inherit the tuning properties of orientation and direction selective neurons. Different

populations of thalamic neurons are known to project to different cortical layers (Callaway, 1998) suggesting that neurons in different layers could inherit the functional properties specific to the thalamic inputs that target that layer. For example, preliminary anatomical tracing data suggests that direction selective thalamic neurons primarily target superficial L2/3, opening up the possibility that unlike in L4, direction selectivity in some L2/3 neurons is inherited from direction selective thalamic neurons (Cruz-Martin et al., 2013).

The cortical silencing approach applied in the current study could be used to investigate the tuning properties of thalamic and intracortical excitation to neurons in different cortical layers. The development of new strains of transgenic mice will allow for the targeted manipulation of thalamic and cortical neurons with increasing anatomical and functional specificity, enabling experiments to firmly establish how specific elements of thalamic and intracortical circuitry generate the rich sensory representation encoded by the cortex.

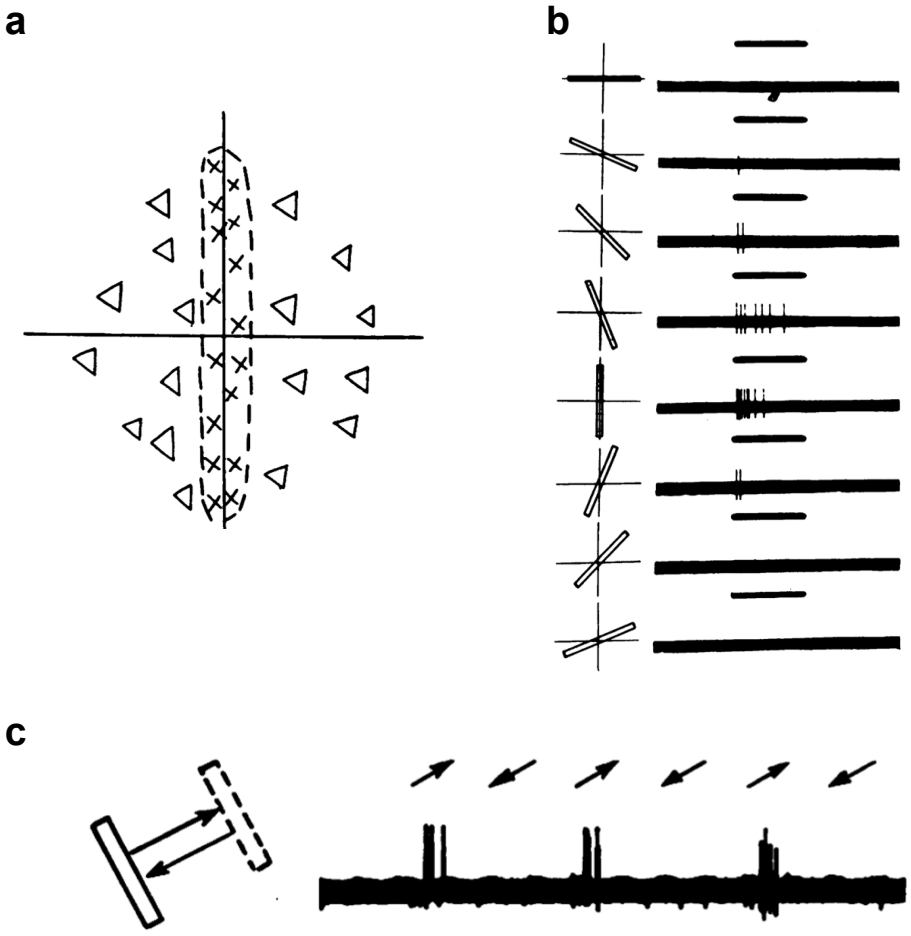

Figure 1.1 Tuning properties of cortical neurons

(**a**) Receptive field of a simple cell in cat V1 mapped by Hubel and Wiesel by flashing a small circular spot of light in different locations of the animal's visual field. Crosses and triangles indicate locations evoking spiking during light onset (ON subregion) and offset (OFF subregion), respectively. (**b**) Response of the same neuron in **a** to a bright bar at different orientations. The orientation and location of the bar are depicted to the left and spiking responses are shown in the traces on the right. The horizontal bar above the traces depicts the onset and duration of the stimulus, which lasted for 1 second. Maximal spiking occurs in response to the vertical bar, which is oriented and positioned to maximally cover the ON subregion. (**c**) Example of a direction selective cortical neuron. The trace shows spiking responses to a light bar moving in opposite directions across the neuron's receptive field as indicated by the arrows above the trace. The neuron responds only to rightward movement. Figures in **a**-**c** adapted from Hubel and Wiesel, 1959.

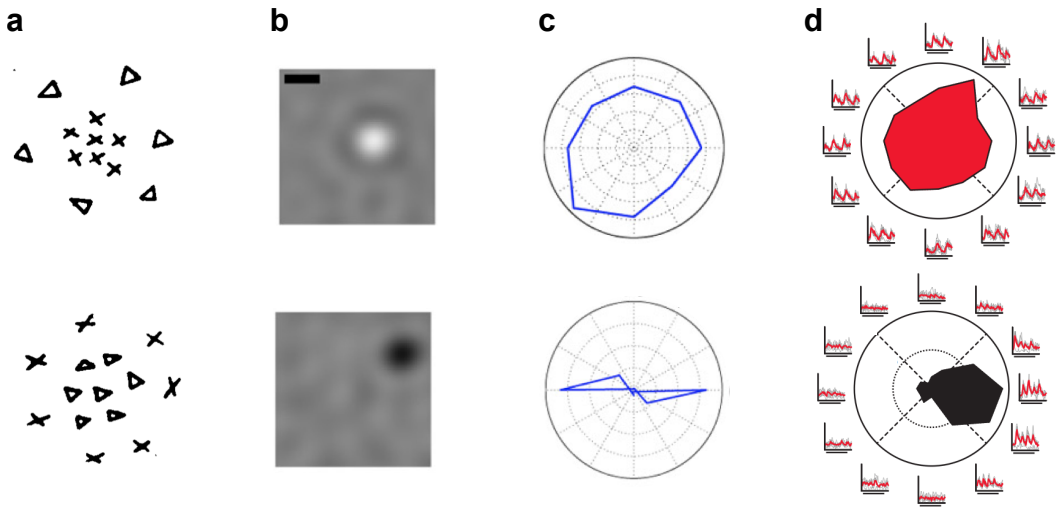

Figure 1.2 Tuning properties of thalamic neurons

(**a**) Circular receptive fields of ON-center (top) and OFF-center (bottom) neurons in LGN of the cat. Crosses and triangles indicate ON and OFF responses, respectively. (**b**) Receptive field of ON-center neuron (top) and OFF-center neurons recorded in the mouse LGN. The receptive fields were mapped using spike-triggered averaging of responses to white-noise. (**c**) Polar orientation tuning curves of poorly orientation selective (top) and strongly orientation selective (bottom) neurons in mouse LGN. The poorly selective neuron is the ON-center neuron in **b**. The tuning curve plots the firing rate (distance from the center) as a function of drifting grating orientation (angle). (**d**) Poorly selective (top) and direction selective (bottom) neurons recorded with calcium imaging in the mouse LGN. Polar tuning curves plot the amplitude of fluorescence signals as a function of drifting grating orientation. Small traces surrounding the polar plots show the fluorescence response at each orientation. Figures adapted from Hubel & Wiesel, 1962 (**a**), Piscopo et al., 2013 (**b-c**), and Marshel et al., 2012 (**d**).

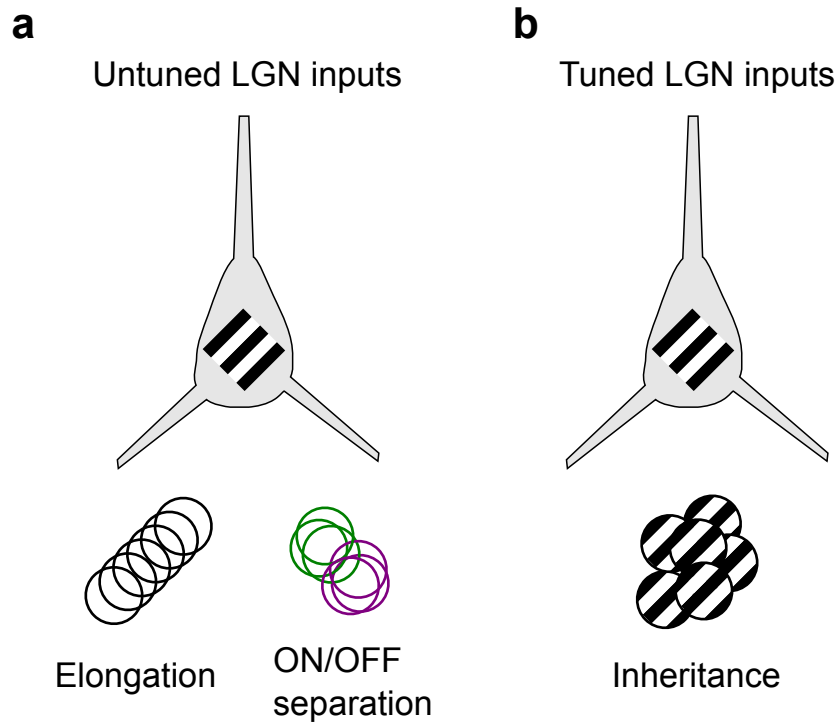

Figure 1.3 Possible circuits for orientation selective thalamic excitation

Schematic showing how thalamic inputs with different functional properties could be combined to generate orientation selective thalamic excitation. The cortical neuron is shown in the top portion with the preferred orientation of its thalamic excitation represented by a black and white grating. In (**a**), orientation selectivity is generated by thalamic neurons with circular receptive fields (empty circles) that are poorly tuned for orientation. In the elongation model (left), the cortical neuron receives inputs from thalamic neurons with receptive fields that cover an elongated region of space resulting in selectivity for the orientation of elongated stimuli. In the ON/OFF separation model, ON-center thalamic inputs (green) have receptive fields that are spatially offset from OFF-center thalamic neurons (magenta) resulting in selectivity for the orientation of contrast edges. In (**b**), orientation selectivity is generated by orientation selective thalamic neurons (circles containing gratings depicting the preferred orientation). The cortical neuron receives inputs from thalamic neurons tuned to the same orientation and directly inherits their orientation selectivity.

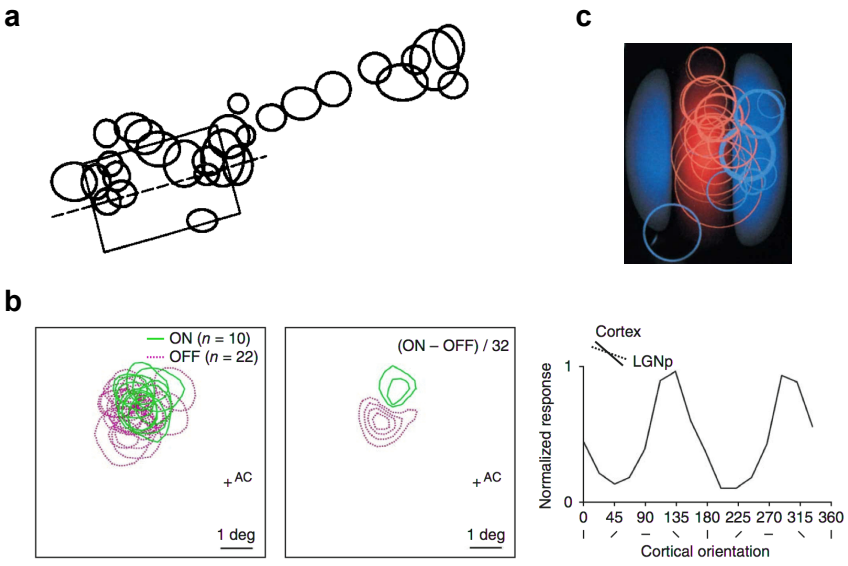

Figure 1.4 Experimental evidence for oriented spatial arrangement of thalamic inputs onto a cortical neuron

(**a**) Receptive fields of thalamic inputs to an orientation domain are scattered across an elongated region of space that matches the preferred cortical orientation. Ovals indicate the position and shape of receptive fields of thalamic axons recorded in the course of a single radial penetration through an orientation domain in ferret V1. The rectangle shows the receptive field of a L4 neuron recorded during the same penetration and the dashed line shows its preferred orientation. The axis of elongation matches the cortical preferred orientation. (**b**) ON and OFF receptive fields of thalamic inputs to an orientation domain are spatially offset in a direction that matches the preferred cortical orientation. Left, receptive fields of ON-center (green) and OFF-center (magenta) thalamic neurons that innervate the same orientation domain in cat V1. Middle, Contour plot of regions in which ON-center (green) or OFF-center (magenta) thalamic receptive fields outnumber their counterparts of opposite ON/OFF type, showing overall spatial segregation of ON and OFF receptive fields of the thalamic inputs. Right, Orientation tuning curve of cortical multiunit activity from the same orientation domain. Solid line in the upper left of the tuning curve shows the measured cortical preferred orientation. Dotted line shows the preferred orientation estimated from the overall spatial separation of ON-center and OFF-center thalamic inputs. The cortical orientation preference matches that predicted from the spatial offset of ON and OFF thalamic receptive fields. (**c**) Matching receptive field location and ON/OFF type in pairs of putatively connected thalamic and cortical neurons. The receptive fields of 23 pairs of thalamic and cortical neurons with significant spike correlation in a time window consistent with a monosynaptic delay are depicted. Cortical receptive fields were scaled, rotated, and aligned to the dominant cortical subregion (the stronger of the ON or OFF subregions) and merged to produce a population cortical receptive field with a central dominant subregion (solid red) and flanking subregions of the opposite ON/OFF type (solid blue). The empty circles indicate the location, size, and ON/OFF type of each thalamic neuron's receptive field relative to its cortical partner's. Thalamic receptive fields are distributed across the elongated structure of the cortical subregion of matching ON/OFF type. Figures adapted from Chapman et al., 1991 (**a**), Jin et al., 2011 (**b**), and Reid and Alonso, 1995 (**c**).

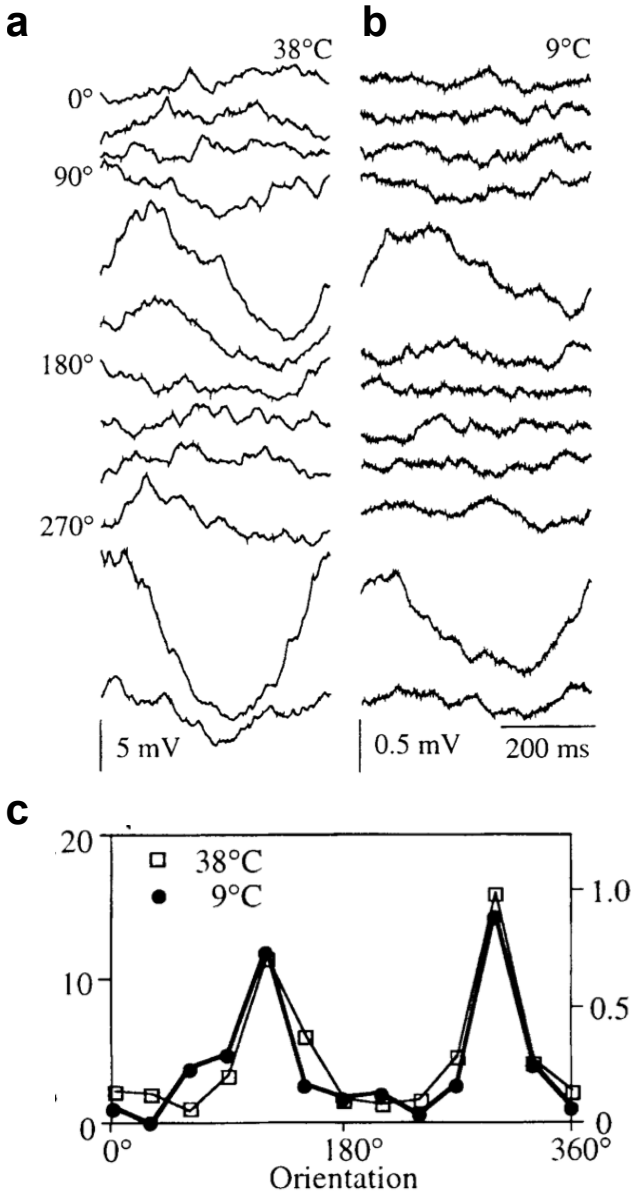

Figure 1.5 Experimental evidence for tuning of thalamic excitation

(**a**) Membrane potential response in response to drifting gratings of different orientations from an intracellular recording in cat V1 at physiological temperature. (**b**) Response of the same cell in **a** after silencing cortical spiking by cooling the cortex. The remaining membrane potential response is presumably thalamic in origin. (**c**) Orientation tuning curve of the normalized amplitude of membrane potential responses before and during cooling. The orientation tuning of the membrane potential is nearly identical in the presence and absence of cortical spiking demonstrating that thalamic excitation is selective for orientation. Figures adapted from Ferster, et al., 1996.

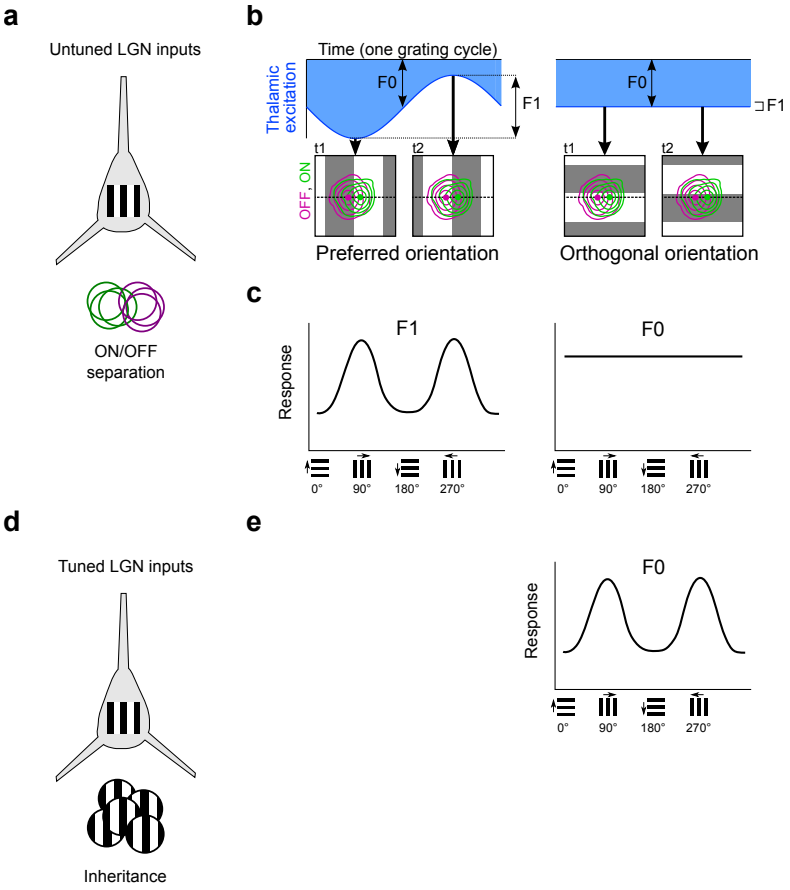

Figure 1.6 Predicted orientation tuning of thalamic excitation in response to drifting gratings

Diagrams showing the expected orientation tuning of thalamic excitation in response to drifting gratings for ON/OFF separation (**a**-**c**) and inheritance (**d**-**e**) models of thalamocortical connectivity. In (**b**), the thalamic excitation (blue) in response to one grating cycle (top) is shown for a cortical neuron receiving thalamic excitation with ON and OFF receptive fields offset along the horizontal dimension (bottom, contour plots depict the strength of thalamic excitation in response to ON and OFF stimuli with the filled dots denoting the location of peak response). In response to vertical gratings (left), thalamic excitation is maximally activated at time t1 in the grating cycle, when the black and white bars simultaneously activate the peaks of the ON and OFF receptive fields and minimally activated at t2 when the grating bars are out of phase with the peaks, resulting in a large amplitude periodic modulation occurring once per cycle (F1 modulation). In response to horizontal gratings (right), thalamic excitation is constant throughout the grating cycle because only one peak is activated at a time, resulting in small F1 modulation. However, the average thalamic excitation across the grating cycle (F0) is the same for both orientations because the thalamic inputs are untuned for orientation and fire the same number of spikes in response to every orientation. (**c**) Expected orientation tuning curves for F1 and F0 response of thalamic excitation under the ON/OFF separation model. F1 is well tuned for orientation whereas F0 is poorly tuned. (**e**) Expected orientation tuning curve for F0 response of thalamic excitation under the inheritance model. F0 is orientation selective because individual thalamic inputs exhibit orientation selectivity in their F0 responses.

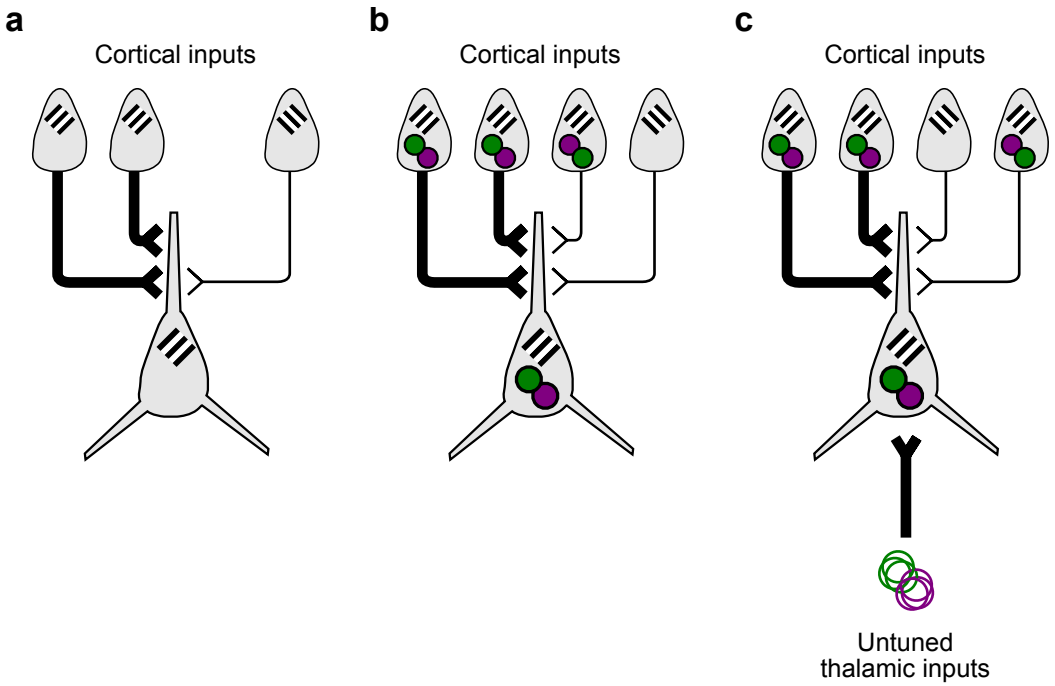

Figure 1.7 Proposed intracortical and thalamic excitatory connectivity scheme

Schematic of intracortical and thalamic excitatory circuits suggested by recordings of thalamic and intracortical excitation. (**a**) A cortical neuron receives more excitation from other cortical neurons tuned to the same orientation. (**b**) Cortical neuron receives more excitation from other cortical neurons tuned to the same orientation and sharing similar ON/OFF receptive field structure. (**c**) A cortical neuron receives more excitation from other cortical neurons tuned to the same orientation and sharing similar ON/OFF receptive field structure. Both the orientation selectivity and the ON/OFF receptive field structure are matched to that expected from the ON/OFF separation of thalamic inputs.

References

1. Ahmed, B., Anderson, J. C., Douglas, R. J., Martin, K. a, and Nelson, J. C. (1994). Polyneuronal innervation of spiny stellate neurons in cat visual cortex. *J. Comp. Neurol.* 341, 39–49.

2. Anderson, J. S., Carandini, M., and Ferster, D. (2000). Orientation tuning of input conductance, excitation, and inhibition in cat primary visual cortex. *J. Neurophysiol.* 84, 909–26.

3. Antonini, a, Fagiolini, M., and Stryker, M. P. (1999). Anatomical correlates of functional plasticity in mouse visual cortex. *J. Neurosci.* 19, 4388–406.

4. Barlow, H. B., and Hill, R. M. (1963). Selective sensitivity to direction of movement in ganglion cells of the rabbit retina. *Science (80-.).* 139, 412–4.

5. Binzegger, T., Douglas, R. J., and Martin, K. a C. (2004). A quantitative map of the circuit of cat primary visual cortex. *J. Neurosci.* 24, 8441–53.

6. Bonin, V., Histed, M. H., Yurgenson, S., and Reid, R. C. (2011). Local diversity and fine-scale organization of receptive fields in mouse visual cortex. *J. Neurosci.* 31, 18506–21.

7. Boyden, E. S., Zhang, F., Bamberg, E., Nagel, G., and Deisseroth, K. (2005). Millisecond-timescale, genetically targeted optical control of neural activity. *Nat. Neurosci.* 8, 1263–8.

8. Bruno, R. M., and Sakmann, B. (2006). Cortex is driven by weak but synchronously active thalamocortical synapses. *Science* 312, 1622–7.

9. Callaway, E. M. (1998). Local circuits in primary visual cortex of the macaque monkey. *Annu. Rev. Neurosci.* 21, 47–74.

10. Chapman, B., Zahs, K. R., and Stryker, M. P. (1991). Relation of cortical cell orientation selectivity to alignment of receptive fields of the geniculocortical afferents that arborize within a single orientation column in ferret visual cortex. *J. Neurosci.* 11, 1347–58.

11. Cheong, S. K., Tailby, C., Solomon, S. G., and Martin, P. R. (2013). Cortical-like receptive fields in the lateral geniculate nucleus of marmoset monkeys. *J. Neurosci.* 33, 6864–76.

12. Chow, B. Y., Han, X., Dobry, A. S., Qian, X., Chuong, A. S., Li, M., Henninger, M. a, Belfort, G. M., Lin, Y., Monahan, P. E., et al. (2010). High-performance genetically targetable optical neural silencing by light-driven proton pumps. *Nature* 463, 98–102.

13. Chung, S., and Ferster, D. (1998). Strength and orientation tuning of the thalamic input to simple cells revealed by electrically evoked cortical suppression. *Neuron* 20, 1177–89.

14. Constantinople, C. M., and Bruno, R. M. (2013). Deep cortical layers are activated directly by thalamus. *Science* 340, 1591–4.

15. Da Costa, N. M., and Martin, K. a C. (2011). How thalamus connects to spiny stellate cells in the cat's visual cortex. *J. Neurosci.* 31, 2925–37.

16. Da Costa, N. M., and Martin, K. a C. (2009). The proportion of synapses formed by the axons of the lateral geniculate nucleus in layer 4 of area 17 of the cat. *J. Comp. Neurol.* 516, 264–76.

17. Cruz-Martin, A., El-Danaf, R. N., Osakada, F., Nguyen, P. L., Callaway, E. M., Ghosh, A., and Huberman, A. D. (2013). A "labeled line" linking direction selective circuits in retina to superficial layers of primary visual cortex. in *Society for Neuroscience Abstract*.

18. DeAngelis, G. C., Ghose, G. M., Ohzawa, I., and Freeman, R. D. (1999). Functional micro-organization of primary visual cortex: receptive field analysis of nearby neurons. *J. Neurosci.* 19, 4046–64.

19. Ferster, D., Chung, S., and Wheat, H. (1996). Orientation selectivity of thalamic input to simple cells of cat visual cortex. *Nature* 380, 249–52.

20. Freund, T. F., Martin, K. a, Somogyi, P., and Whitteridge, D. (1985). Innervation of cat visual areas 17 and 18 by physiologically identified X- and Y- type thalamic afferents. II. Identification of postsynaptic targets by GABA immunocytochemistry and Golgi impregnation. *J. Comp. Neurol.* 242, 275–91.

21. Gil, Z., Connors, B. W., and Amitai, Y. (1999). Efficacy of thalamocortical and intracortical synaptic connections: quanta, innervation, and reliability. *Neuron* 23, 385–97.

22. Han, X., and Boyden, E. S. (2007). Multiple-color optical activation, silencing, and desynchronization of neural activity, with single-spike temporal resolution. *PLoS One* 2, e299.

23. Hippenmeyer, S., Vrieseling, E., Sigrist, M., Portmann, T., Laengle, C., Ladle, D. R., and Arber, S. (2005). A developmental switch in the response of DRG neurons to ETS transcription factor signaling. *PLoS Biol.* 3, e159.

24. Holmgren, C., Harkany, T., Svennenfors, B., and Zilberter, Y. (2003). Pyramidal cell communication within local networks in layer 2/3 of rat neocortex. *J. Physiol.* 551, 139–53.

25. Hubel, D. H., and Wiesel, T. N. (1959). Receptive fields of single neurones in the cat's striate cortex. *J. Physiol.* 148, 574–91.

26. Hubel, D. H., and Wiesel, T. N. (1962). Receptive fields, binocular interaction and functional architecture in the cat's visual cortex. *J. Physiol.* 160, 106–54.

27. Huberman, A. D., Wei, W., Elstrott, J., Stafford, B. K., Feller, M. B., and Barres, B. A. (2009). Genetic identification of an On-Off direction-selective retinal ganglion cell subtype reveals a layer-specific subcortical map of posterior motion. *Neuron* 62, 327–34.

28. Jin, J., Wang, Y., Swadlow, H. A., and Alonso, J. M. (2011). Population receptive fields of ON and OFF thalamic inputs to an orientation column in visual cortex. *Nat. Neurosci.* 14, 232–8.

29. Kay, J. N., De la Huerta, I., Kim, I., Zhang, Y., Yamagata, M., Chu, M. W., Meister, M., and Sanes, J. R. (2011). Retinal ganglion cells with distinct directional preferences differ in molecular identity, structure, and central projections. *J. Neurosci.* 31, 7753–62.

30. Ko, H., Hofer, S. B., Pichler, B., Buchanan, K. a, Sjöström, P. J., and Mrsic-Flogel, T. D. (2011). Functional specificity of local synaptic connections in neocortical networks. *Nature* 473, 87–91.

31. Lampl, I., Anderson, J. S., Gillespie, D. C., and Ferster, D. (2001). Prediction of orientation selectivity from receptive field architecture in simple cells of cat visual cortex. *Neuron* 30, 263–74.

32. Lefort, S., Tomm, C., Floyd Sarria, J.-C., and Petersen, C. C. H. (2009). The excitatory neuronal network of the C2 barrel column in mouse primary somatosensory cortex. *Neuron* 61, 301–16.

33. LeVay, S., and Gilbert, C. D. (1976). Laminar patterns of geniculocortical projection in the cat. *Brain Res.* 113, 1–19.

34. Liu, B. H., Li, P., Sun, Y. J., Li, Y., Zhang, L. I., and Tao, H. W. (2010). Intervening inhibition underlies simple-cell receptive field structure in visual cortex. *Nat. Neurosci.* 13, 89–96.

35. Liu, B. H., Li, Y., Ma, W., Pan, C., Zhang, L. I., and Tao, H. W. (2011). Broad inhibition sharpens orientation selectivity by expanding input dynamic range in mouse simple cells. *Neuron* 71, 542–54.

36. Malpeli, J. G. (1983). Activity of cells in area 17 of the cat in absence of input from layer a of lateral geniculate nucleus. *J. Neurophysiol.* 49, 595–610.

37. Marshel, J. H., Kaye, A. P., Nauhaus, I., and Callaway, E. M. (2012). Anterior-posterior direction opponency in the superficial mouse lateral geniculate nucleus. *Neuron* 76, 713–20.

38. Martinez, L. M., and Alonso, J. M. (2001). Construction of complex receptive fields in cat primary visual cortex. *Neuron* 32, 515–25.

39. Mastronarde, D. N. (1987). Two classes of single-input X-cells in cat lateral geniculate nucleus. I. Receptive-field properties and classification of cells. *J. Neurophysiol.* 57, 357–80.

40. Monier, C., Chavane, F., Baudot, P., Graham, L. J., and Frégnac, Y. (2003). Orientation and direction selectivity of synaptic inputs in visual cortical neurons: a diversity of combinations produces spike tuning. *Neuron* 37, 663–80.

41. Nagel, G., Szellas, T., Huhn, W., Kateriya, S., Adeishvili, N., Berthold, P., Ollig, D., Hegemann, P., and Bamberg, E. (2003). Channelrhodopsin-2, a directly light-gated cation-selective membrane channel. *Proc. Natl. Acad. Sci. U. S. A.* 100, 13940–5.

42. Niell, C. M., and Stryker, M. P. (2008). Highly selective receptive fields in mouse visual cortex. *J. Neurosci.* 28, 7520–36.

43. Ohki, K., Chung, S., Ch'ng, Y. H., Kara, P., and Reid, R. C. (2005). Functional imaging with cellular resolution reveals precise micro-architecture in visual cortex. *Nature* 433, 597–603.

44. Packer, A. M., and Yuste, R. (2011). Dense, unspecific connectivity of neocortical parvalbumin-positive interneurons: a canonical microcircuit for inhibition? *J. Neurosci.* 31, 13260–71.

45. Peters, A., and Payne, B. R. (1993). Numerical relationships between geniculocortical afferents and pyramidal cell modules in cat primary visual cortex. *Cereb. Cortex* 3, 69–78.

46. Piscopo, D. M., El-Danaf, R. N., Huberman, A. D., and Niell, C. M. (2013). Diverse visual features encoded in mouse lateral geniculate nucleus. *J. Neurosci.* 33, 4642–56.

47. Reid, R. C., and Alonso, J. M. (1995). Specificity of monosynaptic connections from thalamus to visual cortex. *Nature* 378, 281–4.

48. Ringach, D. L., Shapley, R. M., and Hawken, M. J. (2002). Orientation selectivity in macaque V1: diversity and laminar dependence. *J. Neurosci.* 22, 5639–51.

49. Rivlin-Etzion, M., Zhou, K., Wei, W., Elstrott, J., Nguyen, P. L., Barres, B. A., Huberman, A. D., and Feller, M. B. (2011). Transgenic mice reveal unexpected diversity of on-off direction-selective retinal ganglion cell subtypes and brain structures involved in motion processing. *J. Neurosci.* 31, 8760–9.

50. Scholl, B., Tan, A. Y. Y., Corey, J., and Priebe, N. J. (2013). Emergence of orientation selectivity in the Mammalian visual pathway. *J. Neurosci.* 33, 10616–24.

51. Schwark, H. D., Malpeli, J. G., Weyand, T. G., and Lee, C. (1986). Cat area 17. II. Response properties of infragranular layer neurons in the absence of supragranular layer activity. *J. Neurophysiol.* 56, 1074–87.

52. Stratford, K. J., Tarczy-Hornoch, K., Martin, K. A., Bannister, N. J., and Jack, J. J. (1996). Excitatory synaptic inputs to spiny stellate cells in cat visual cortex. *Nature* 382, 258–61.

53. Tanaka, K. (1985). Organization of geniculate inputs to visual cortical cells in the cat. *Vision Res.* 25, 357–64.

54. Usrey, W. M., Sceniak, M. P., and Chapman, B. (2003). Receptive fields and response properties of neurons in layer 4 of ferret visual cortex. *J. Neurophysiol.* 89, 1003–15.

55. Vigeland, L. E., Contreras, D., and Palmer, L. a (2013). Synaptic mechanisms of temporal diversity in the lateral geniculate nucleus of the thalamus. *J. Neurosci.* 33, 1887–96.

56. Yoshida, K., Watanabe, D., Ishikane, H., and Tachibana, M. (2001). A key role of starburst amacrine cells in originating retinal directional selectivity and optokinetic eye movement. *Neuron* 30, 771–780.

57. Zhang, F., Wang, L.-P., Brauner, M., Liewald, J. F., Kay, K., Watzke, N., Wood, P. G., Bamberg, E., Nagel, G., Gottschalk, A., et al. (2007). Multimodal fast optical interrogation of neural circuitry. *Nature* 446, 633–9.

58. Zhao, X., Chen, H., Liu, X., and Cang, J. (2013). Orientation-selective responses in the mouse lateral geniculate nucleus. *J. Neurosci.* 33, 12751–63.

59. Zhuang, J., Stoelzel, C. R., Bereshpolova, Y., Huff, J. M., Hei, X., Alonso, J.-M., and Swadlow, H. a (2013). Layer 4 in primary visual cortex of the awake rabbit: contrasting properties of simple cells and putative feedforward inhibitory interneurons. *J. Neurosci.* 33, 11372–89.

Chapter 2. Tuned thalamic excitation is amplified by visual cortical circuits

Abstract

Cortical neurons in thalamic recipient layers receive excitation from the thalamus and the cortex. The relative contribution of these two sources of excitation to sensory tuning is poorly understood. Here we optogenetically silence the visual cortex of mice to isolate thalamic excitation onto layer 4 neurons during visual stimulation. Thalamic excitation contributes to a third of total excitation and is organized in spatially offset, yet overlapping ON and OFF receptive fields. This receptive field structure predicts the orientation tuning of thalamic excitation. Finally, thalamic and total excitation are similarly tuned to orientation and direction, and have the same temporal phase relationship to the visual stimulus. Our results indicate that tuning of thalamic excitation is unlikely to be imparted by direction or orientation selective thalamic neurons and that a principal role of cortical circuits is to amplify tuned thalamic excitation.

Introduction

Synaptic excitation plays an important role in shaping the sensory tuning properties of cortical neurons (Anderson et al., 2000; Brecht & Sakmann, 2002; Liu et al., 2010, 2011; Liu, Wu, Arbuckle, Tao, & Zhang, 2007; Nelson, Toth, Sheth, & Sur, 1994). When located in thalamic recipient layers these neurons receive synaptic excitation from two major sources: thalamic and cortical neurons. The relative contribution of these two sources to the tuning of cortical neurons is debated.

In the visual system both thalamic and cortical neurons respond robustly to visual stimuli consisting of alternating bars of high and low luminance (gratings) that move across the visual field causing cyclical changes in luminance at each location in visual space. Due to the spatial arrangement of their receptive fields, many neurons spike preferentially at specific temporal phases of the grating cycle and are thus modulated at the temporal frequency of the grating. In addition to phase modulation, neurons may exhibit sensitivity to the orientation of the grating, responding with more spikes at certain orientations as compared to others.

In their classic feedforward model, Hubel and Wiesel (Hubel & Wiesel, 1962) proposed that thalamic excitation of a cortical neuron could be orientation selective via the convergence of multiple untuned thalamic inputs with properly aligned spatial receptive fields. There is evidence for such receptive field arrangements among the population of thalamic neurons projecting to the same orientation domain of visual cortex in ferrets (Chapman et al., 1991) and cats (Jin et al., 2011). Additionally, cortical neurons whose receptive field structure overlaps with the receptive field structure of individual thalamic neurons are indeed more likely to receive input from these neurons as compared to neurons with non matching receptive fields (Reid & Alonso, 1995; W M Usrey, Alonso, & Reid, 2000). Yet, the tuning properties of synaptic excitatory currents resulting from the convergence of a set of thalamic inputs onto individual cortical neurons are still unclear.

Furthermore, the impact of cortical excitation in shaping the total excitation received by visual cortical neurons is largely unknown. In mouse visual cortex, L2/3 neurons with similar orientation preference are more likely to be connected (Ko et al.,

2011) and long-range intracortical projections in the visual cortex of other species preferentially connect domains sharing similar orientation preference (Bosking, Zhang, Schofield, & Fitzpatrick, 1997; Gilbert & Wiesel, 1989; Malach, Amir, Harel, & Grinvald, 1993), suggesting that cortical excitation might contribute to the orientation tuning of total excitation.

A pivotal study combining intracellular recording in cat visual cortex with cooling-mediated cortical silencing isolated thalamic excitation onto cortical neurons and demonstrated its tuning to orientation (Ferster et al., 1996). However, because the receptive field structure of thalamic excitation, i.e. the spatial organization of ON and OFF receptive fields, was not assessed in these studies, the mechanisms underlying the observed orientation tuning could not be addressed. Furthermore, the relationship between thalamic and total excitation could not be established because synaptic activity recorded without cortical cooling reflected the combined effects of excitation and inhibition.

We have used an optogenetic strategy for cortical silencing in which we photostimulate parvalbumin-expressing (PV) cortical GABAergic interneurons (Olsen, Bortone, Adesnik, & Scanziani, 2012) expressing the light-gated cation channel channelrhodopsin 2 (ChR2) (Boyden et al., 2005; Nagel et al., 2003). By harnessing the dense and divergent inhibitory axons of PV cells we can completely silence the cortex for prolonged periods of time without affecting the dynamics of transmitter release from thalamic terminals.

Using this approach we reveal how the ON and OFF receptive field structure of thalamic excitation onto layer 4 cortical neurons can account for its orientation tuning

properties. Consistent with this hypothesis, we show that in response to drifting gratings, the phase modulation of thalamic excitation was tuned to orientation and direction, but the integral of thalamic excitatory current across the stimulus duration was untuned. Finally we demonstrate that the orientation and direction tuning as well as the phase of cortical excitation onto layer 4 neurons matches that of their thalamic excitation. These findings indicate that orientation tuning of thalamic excitation is generated by individually untuned thalamic inputs.

Results

Isolating thalamic excitation

To isolate the thalamic component of visually evoked synaptic excitation in layer 4 (L4) neurons *in vivo*, we optogenetically silenced the mouse visual cortex (Fig. 2.1a). The cortex was silenced by photostimulation of inhibitory parvalbumin-expressing (PV) GABAergic cortical interneurons that conditionally expressed the light-sensitive cation channel channelrhodopsin 2 (ChR2). We evaluated the robustness of cortical silencing by recording, in loose-patch configuration, the spiking responses of individual V1 neurons to visual stimuli consisting of drifting gratings with and without PV cell photostimulation on interleaved trials (Fig. 2.1b). Illumination of the cortical surface with a blue (470 nm) light-emitting diode (LED) for 2.6 s completely silenced both the spontaneous and visual stimulus-evoked spiking of all recorded neurons throughout the entire illumination period (Fig. 2.1b, n=14 cells, 2 mice). Experiments in which the local field potential (LFP) was simultaneously recorded with a second electrode while the LED intensity was varied to decrease cortical activity to different levels revealed a strong correlation between the

reduction in visually evoked firing rate and LFP amplitude (11 cells, 4 mice; Supplementary Fig. 2.1). Complete cortical silencing reduced the amplitude of the visually-evoked LFP by ~80 % (Supplementary Fig. 2.1). Thus, the LFP is a reliable indicator of cortical activity and was routinely monitored in subsequent experiments to verify cortical silencing (see Methods). These data indicate that complete cortical silencing can be achieved by photostimulating ChR2-expressing PV cells, consistent with previous reports from our lab (Atallah, Bruns, Carandini, & Scanziani, 2012; Olsen et al., 2012).

We recorded from L4 neurons (average depth: 386 ± 7 μm, restricted to 300-550 μm, n = 49 cells, 40 mice; Supplementary Fig. 2.2) in the whole-cell voltage clamp configuration and used visual stimulation to evoke excitatory postsynaptic currents (EPSCs) with and without cortical silencing on interleaved trials. Visual stimuli consisted of either an 8x8 grid of individually flashed black or white squares (Fig. 2.1c) or full-field gratings drifting in 12 different directions (Fig. 2.1d). Cortical silencing reduced the total excitatory postsynaptic charge (Q: the time integral of the EPSC) evoked by the flashed square of optimal location and luminance (i.e. the luminance and location that evoked the largest Q in control conditions) by 68 ± 3% (Fig. 2.1c; control: mean EPSC: -60 ± 9 pA, Q: 15 ± 2 pC; cortical silencing: mean EPSC: -17 ± 2 pA, Q: 4.4 ± 0.6 pC, n = 18 cells, 16 mice) and gratings drifting in the preferred direction (i.e. the direction that evoked the largest Q in control conditions) by 64 ± 2% (Fig. 2.1d; control: mean EPSC: -143 ± 10 pA, Q: 239 ± 17 pC; cortical silencing: mean EPSC: -46 ± 3 pA, Q: 78 ± 4 pC, n = 42 cells, 33 mice). Thus, because in the absence of cortical activity the principal remaining synaptic input to cortical neurons comes from the thalamus, these results

indicate that the thalamic component of excitation contributes to 32 ±3% and 36 ± 2% of the total excitation evoked by flashed squares and drifting grating stimuli, respectively (Fig. 2.1c-d). This estimate is likely to be an upper bound as cortical silencing under these conditions has been shown to increase the activity of thalamic relay neurons due to the elimination of the cortico-thalamic feedback loop (Olsen et al., 2012) (Supplementary Fig. 2.3g). In contrast, the release of GABA (by photostimulated PV cells) did not, per se, substantially affect the estimate of the thalamic component: The decrease in the membrane resistance of the recorded neuron via the activation of $GABA_A$ receptors was only 32 ± 3% (n = 15 cells, 11 mice) and a decrease in transmitter release via activation of presynaptic $GABA_B$ receptors on thalamic terminals could be ruled out (Supplementary Fig. 2.4). Below, we refer to the EPSC and Q recorded during control trials as $EPSC_{Tot}$ and Q_{Tot}, respectively, and to the EPSC and Q recorded during cortical silencing trials as $EPSC_{Thal}$ and Q_{Thal}, respectively.

Receptive field structure of thalamic excitation

To determine the receptive field structure of thalamic excitation onto individual layer 4 cortical neurons we silenced the cortex while presenting the 8x8 grid of flashed black or white squares (see above) and recorded $EPSC_{Thal}$ evoked at each grid location. (Fig. 2.2a).

We generated separate receptive field maps of thalamic excitation for black (OFF) and white (ON) stimuli based on the value of Q_{Thal} for a 100 ms window following stimulus onset for each grid location (Fig. 2.2a heat map). Individual OFF and ON

subfields were defined as spatially continuous regions of the receptive field map exceeding the background (Fig. 2.2b, see methods).

In 17 out of 18 cells, at least one subfield could be identified. Out of these cells, 13 had both a single ON and single OFF subfield while the remaining 4 had a single OFF subfield. We quantified the spatial properties of the receptive field in those 13 cells (12 mice) that exhibited both ON and OFF subfields.

The average area of a subfield for $EPSC_{Thal}$ was 242 ± 21 deg^2 (n = 26 subfields; Fig. 2.2f). However, the ON and OFF subfields for individual cells were highly overlapping in space with an average overlap area of 167 ± 26 deg^2 (n = 13 cells; Fig. 2.2f, overlap area). To quantify the overlap of the ON and OFF subfields we used the overlap index, defined as the fraction of the smaller subfield that was overlapped by the larger subfield. The average overlap index was 0.79 ± 0.07 (n = 13 cells; Fig. 2.2f, overlap index).

Despite the high degree of overlap, many neurons exhibited a spatial offset between the peaks of the ON and OFF subfields. The average distance between ON and OFF peaks was 5.1 ± 0.5 degrees (n = 13 cells; Fig. 2.2g).

To ensure that the separation between the peaks of ON and OFF subfields that we measured was not due to noise in the estimate of peak location, we simulated the probability that a pair of identical subfields would exhibit a similar degree of peak separation given the variability of responses measured in pixels outside of the receptive field (see Methods). The probability that the measured separation between the peaks of ON and OFF subfields was less than the separation between identical subfields was below 0.05 for 12/13 cells and below 0.005 for 9/13 cells.

We measured the elongation of the subfields by comparing the width of each subfield along the axis connecting the peaks of the ON and OFF subfields (ON-OFF axis) with the width along the orthogonal axis (Fig. 2.2h). The subfield widths along these two axes were similar (ON/OFF axis width = 10.6 ± 0.7 degrees, orthogonal axis width = 11.4 ± 0.7degrees, $p = 0.3$, not statistically significant; n = 26 subfields). The aspect ratio, the width along the orthogonal axis divided by the width along the ON-OFF axis, was close to 1 (aspect ratio = 1.15 ± 0.07; n = 26 subfields).

Thus the spatial receptive field of the thalamic excitatory input onto an individual cortical neuron consists of roughly symmetric spatially overlapping ON and OFF subfields whose peaks are offset by about 5 degrees in visual space.

Orientation tuning of thalamic excitation

The separation between the peaks of the ON and OFF $EPSC_{Thal}$ subfields suggests that in response to drifting gratings, $EPSC_{Thal}$ could, in principle, be orientation tuned without the average firing rate (averaged over the stimulus duration) of thalamic neurons contributing to $EPSC_{Thal}$ being itself orientation tuned. If the drifting grating is presented at an orientation where the bars of the grating are perpendicular to the axis connecting the peaks of ON and OFF thalamic subfields, it should produce simultaneous activation of ON and OFF thalamic subfields at the same temporal phase of the grating cycle (Fig. 2.4h, left). The resulting $EPSC_{Thal}$ will fluctuate in amplitude at the same temporal frequency of the grating (F1 modulation) and be maximal when the two thalamic subfields are activated together. The difference between the peak and the trough of this $EPSC_{Thal}$ fluctuation is the F1 amplitude ($F1_{Thal}$). In contrast, orthogonal gratings would

activate the subfields sequentially at different temporal phases producing a smaller $F1_{Thal}$ (Fig. 2.4h, right). In other words, $F1_{Thal}$ should be tuned to grating orientation.

Furthermore, if the average firing rate of thalamic neurons that contribute to $EPSC_{Thal}$ is not orientation selective, the number of action potentials generated in these neurons over the entire stimulus duration should be the same regardless of the orientation of the grating. Hence, the integral of $EPSC_{Thal}$ over the stimulus duration, Q_{Thal}, should be the same at each orientation and so Q_{Thal} should be untuned to grating orientation.

In contrast, if a cortical neuron receives input from a population of thalamic neurons whose average firing rate is orientation tuned and share similar orientation preference, then Q_{Thal} should be tuned to grating orientation. The tuning of $F1_{Thal}$ in this case would depend on the degree to which the thalamic inputs fire at the same phase of the grating cycle.

Thus, to examine the orientation tuning of thalamic excitation we extracted two values from $EPSC_{Thal}$ recorded during drifting gratings: $F1_{Thal}$ and Q_{Thal} (Fig. 2.3a, right). Note that Q is equivalent to the traditionally used F0, which is the average value of the response across the entire stimulus duration.

Q_{Thal} was remarkably similar across all grating orientations, resulting in a flat tuning curve and a low value of the orientation and direction selectivity index (OSI = 0.026 ± 0.003; DSI = 0.083 ± 0.009; n = 42 cells; Fig. 2.3b-e). In contrast to Q_{Thal}, $F1_{Thal}$ was clearly selective for orientation and direction (OSI $F1_{Thal}$ = 0.23 ± 0.017, significantly different than OSI Q_{Thal}, p = 5.8e-15; DSI $F1_{Thal}$ = 0.28 ± 0.03, significantly different than DSI Q_{Thal}, p = 4.4e-9; n = 42 cells; Fig. 2.3b-e). Thus orientation and direction tuning is present in $F1_{Thal}$, but not in Q_{Thal}.

Consistent with the absence of Q_{Thal} tuning, recordings from single units in the dorsal lateral geniculate nucleus (dLGN) during cortical silencing indicated that the average firing rate of individual thalamic neurons was poorly tuned to orientation (OSI = 0.067 ± 0.01 n = 11 units; Supplementary Fig. 2.3e). Finally, the F1 modulation of the firing of thalamic neurons was also poorly tuned to orientation, significantly less than the $F1_{Thal}$ recorded in cortical neurons (OSI = 0.11 ± 0.021; unpaired t-test, p= 0.0002; n = 11; Supplementary Fig. 2.3h). In fact, while in 55% of the cortical neurons the OSI of $F1_{Thal}$ was larger than 0.2, this value was reached by only 9% of the thalamic units recorded during cortical silencing (Supplementary Fig. 2.3h).

ON-OFF separation predicts preferred orientation of $F1_{Thal}$

If the separation between the peaks of the ON and OFF $EPSC_{Thal}$ subfields is a major determinant of the observed orientation tuning of $F1_{Thal}$, then the relative position of the ON and OFF peaks should predict the preferred orientation of $F1_{Thal}$.

To test this, we obtained both receptive field maps (Fig. 2.4a-b) and drifting grating orientation tuning curves (Fig. 2.4c-d) of thalamic excitation in the same neuron. The predicted preferred orientation derived from receptive field maps (RF_{Pref}) was determined by the angle of the line connecting the peaks of the ON and OFF subfields (Fig. 2.4b). The relationship between RF_{Pref} and the actual preferred orientation of $F1_{Thal}$ ($Grating_{Pref}$) can be seen by overlaying vectors indicating RF_{Pref} (black dashed line) and $Grating_{Pref}$ (blue line) on the polar orientation tuning curve (Fig. 2.4d-e). RF_{Pref} and $Grating_{Pref}$ were remarkably similar, differing by less than 30 degrees in 7 out of 8 cells (mean difference in preferred orientation: 19 ± 7 degrees; Fig. 2.4f-g).

Thus the separation of ON and OFF subfields is likely to be a key determinant of the preferred orientation of $F1_{Thal}$

Tuning of non-thalamic excitation

Is Q_{Tot}, that is the charge recorded in the absence of cortical silencing, also untuned to orientation and direction like Q_{Thal}? Comparison of the tuning curves for Q_{Tot} and Q_{Thal} revealed that Q_{Tot} was in fact significantly more selective for orientation and direction than Q_{Thal} (OSI Q_{Tot}= 0.049 ± 0.005, p=1.7e-4; DSI Q_{Tot} = 0.12 ± 0.01, p = 0.007; n = 42 cells; Fig. 2.5b-e). This suggests that under control conditions, when cortical activity is intact, the excitatory charge that is not of thalamic origin is, in contrast to Q_{Thal}, orientation and direction selective. We isolated this component of excitation by subtracting $EPSC_{Thal}$ from $EPSC_{Tot}$ ($EPSC_{Sub} = EPSC_{Tot} – EPSC_{Thal}$; Fig. 2.5a). Given the complete silencing of cortical activity upon PV cell photostimulation, $EPSC_{sub}$ must, in large part, reflect cortical excitation. Q_{Sub} (the charge integral of $EPSC_{Sub}$) was even more orientation and direction selective than Q_{Tot} (OSI Q_{Sub} = 0.083 ± 0.009; p = 1.4e-8; DSI Q_{Sub} = 0.18 ± 0.017; p = 2e-9; n = 42 cells) and more selective than Q_{Thal} (OSI p = 6e-7; DSI p=3.9e-6; n = 42 cells; Fig. 2.5f-i). Thus, in contrast to Q_{Thal}, both Q_{Tot} and Q_{Sub} are tuned to orientation and direction.

Similar to $EPSC_{Thal}$, F1 modulation of $EPSC_{Sub}$ was evident particularly at certain orientations (Fig. 2.6a). We quantified the orientation and direction selectivity of the F1 modulation of $EPSC_{Sub}$ ($F1_{Sub}$) and compared it to the tuning of Q_{Sub} (Fig. 2.6b-g). $F1_{Sub}$ was significantly more selective for orientation and direction than Q_{Sub} (OSI of $F1_{Sub}$: 0.24 ± 0.02, p = 1.2e-10; DSI of $F1_{Sub}$ = 0.38 ± 0.04; p = 4.4e-6; n = 42 cells; Fig. 2.6d

and f). Importantly, however, $F1_{Sub}$ and Q_{Sub} were tuned to the same orientation (mean difference between $F1_{Sub}$ and Q_{Sub} preferred orientation: 20 ± 3 degrees, n = 42 cells; Fig. 2.6e). Furthermore $F1_{Sub}$ and Q_{Sub} were also tuned to similar directions (Fig. 2.6g). Thus $F1_{Sub}$ exhibits orientation and direction selectivity that is co-tuned with Q_{Sub}.

Co-tuning of thalamic and non-thalamic excitation

Both $F1_{Thal}$ and $F1_{Sub}$ are orientation selective. Are these two sources of excitation tuned to the same or different orientations? The preferred orientations of $F1_{Thal}$ and $F1_{Sub}$ differed by only 20 ± 3 degrees on average (n= 42 cells; Fig. 2.7d, top) and the OSI of $F1_{Thal}$ and $F1_{Sub}$ were not significantly different (Thal: 0.22 +/- 0.015, Sub: 0.24 ± 0.02, p = 0.63; n = 42 cells; Fig. 2.7d, bottom). In addition $F1_{Thal}$ and $F1_{Sub}$ were also tuned to similar directions (Fig. 2.7e, top) yet DSI of $F1_{Thal}$ was significantly smaller than DSI of $F1_{Sub}$ (Thal: 0.23 ± 0.017, Sub: 0.37 ± 0.04, P = 0.03; n = 42 cells; Fig. 2.7e, bottom). Finally, we determined the phase difference between $F1_{Thal}$ and $F1_{Sub}$ at the preferred direction of thalamic excitation. We found that $F1_{Thal}$ and $F1_{Sub}$ were almost in phase (Fig. 2.7f), with $EPSC_{Thal}$ preceding $EPSC_{Sub}$, on average by 30.3 ± 5.5 degrees or 42 ± 8 ms given the temporal frequency of our stimulus (n = 42 cells; Fig. 2.7g). Thus $F1_{Thal}$ and $F1_{Sub}$ are co-tuned to orientation and have similar temporal phase.

Discussion

Here we describe the tuning properties of the thalamic and total excitation received by single neurons in L4 of mouse visual cortex using intracellular voltage clamp

recordings and optogenetic cortical silencing. Our recordings reveal that thalamic excitation is organized into spatially offset yet highly overlapping ON and OFF receptive fields. The relative position of the ON and OFF subfields is predictive of the orientation preference of thalamic excitation in response to drifting gratings. This orientation selectivity is observed in the F1 modulation of thalamic excitation ($F1_{Thal}$), but not in the thalamic excitatory charge (Q_{Thal}) demonstrating that it does not arise from the convergence of thalamic neurons that are themselves orientation selective. Finally, because the thalamic and cortical contributions to total excitation are tuned to the same orientation and share similar temporal phase, our data demonstrate a key function of visual cortex in amplifying tuned thalamic excitation.

We find that the thalamus contributes on average approximately 30% of the excitatory charge to a cortical neuron. This is consistent with previous studies using intracellular recording and cortical silencing in the cat visual cortex (37% (Ferster et al., 1996) and 46% (Chung & Ferster, 1998)) yet less than what was reported in rat auditory cortex (61% (Liu et al., 2007)). Our estimation of the thalamic contribution is likely to be an upper bound due to the facilitation of thalamic responses to visual stimuli upon disruption of corticothalamic feedback with cortical silencing (Olsen et al., 2012) (Supplementary Fig. 2.3). Additionally, the potential underestimation of total excitation (recorded without cortical silencing) in case of improper voltage clamp may further increase our estimate of the thalamic component. Finally, the two potential sources of under-estimation of the thalamic component, leakier postsynaptic membrane during cortical silencing and inhibition of transmitter release from thalamic afferents play only a minor role. PV cell photostimulation decreased input resistance of the recorded cells by

only 30%; given the perisomatic distribution of PV cell synapses, the conductance underlying this decrease in resistance is likely to be properly voltage clamped. Furthermore, the potential activation of presynaptic $GABA_B$ receptors on thalamic terminals via GABA release from photostimulated PV cells did not affect transmitter release (Supplementary Fig. 2.4).

We provide the first description, to our knowledge, of the ON and OFF receptive fields of thalamic excitation onto visual cortical neurons. The ON and OFF subfields of a single cell are highly overlapping, have little elongation, but exhibit spatially offset peaks. The average subfield width is 10 degrees, which is similar to the average width of the center receptive field of a neuron in the dorsal lateral geniculate nucleus (dLGN) of the mouse thalamus (9.8 degrees (Piscopo et al., 2013) and 11 degrees (Grubb & Thompson, 2003)). The receptive fields of thalamic excitation reported here are smaller than previously reported receptive fields of total synaptic excitation (Liu et al., 2010). A possible reason for this difference is that in our study intracortical connections are functionally eliminated via cortical silencing. If intracortical connections originate in part from cortical neurons whose receptive field is outside of or larger than the thalamic RF of the recorded neuron then intracortical connections would contribute to broadening the RF size.

We believe that the spatial offset of the ON and OFF subfields forms the basis for orientation selectivity of thalamic excitation. When the drifting grating is perpendicular to the axis connecting the ON and OFF peaks, it will simultaneously activate both ON and OFF subfields once per grating cycle resulting in strong F1 modulation (Fig. 2.4h, left). At the orthogonal orientation, the ON and OFF peaks will be activated sequentially

at opposite phases of the grating cycle, resulting in weak F1 modulation (Fig. 2.4h, right). We find that $F1_{Thal}$ is indeed well tuned for orientation, consistent with observations in cat visual cortex (Ferster et al., 1996).

In contrast, the excitatory charge over the stimulus period, Q_{Thal}, is poorly tuned, consistent with the Hubel and Wiesel feedforward model in which the receptive field structure of thalamic inputs rather than the tuning of individual thalamic neurons forms the basis of orientation selectivity in cortical neurons (Hubel & Wiesel, 1962). Indeed if the firing rate of thalamic neurons was tuned for orientation, the resulting Q_{Thal} should also be tuned, which is not what we observe. Thalamic neurons that are tuned to direction and orientation have been recently described in the mouse thalamus (Marshel et al., 2012; Piscopo et al., 2013). However, and consistent with our own dLGN recordings (Supplementary Fig. 2.3), they constitute a small fraction (11%) of the neurons in mouse dLGN, which appears to be dominated by cells with poor direction and orientation selectivity (Piscopo et al., 2013). Hypothetically, the F1 modulation but not the firing rate of thalamic neurons could be tuned for orientation. This could lead to the observed $F1_{Thal}$ tuning and concomitant lack of Q_{thal} tuning. This is, however, unlikely because the F1 tuning of dLGN neurons was poor (Supplementary Fig. 2.3). Furthermore, the few dLGN neurons with tuned F1 modulation also appear to exhibit similar tuning of their firing rates (Marshel et al., 2012). Nevertheless it is possible that orientation and/or direction selective dLGN neurons may contribute to the tuning properties of cortical neurons outside of L4, the layer that we targeted in this study.

It has been established in several species that the structure of the spike receptive fields of cortical simple cells also predicts the preferred orientation of spiking responses

(Lampl et al., 2001; Liu et al., 2011). Furthermore, the receptive field structure of populations of thalamic inputs in cat visual cortex predicts the preferred orientation of the target domain (Jin et al., 2011). Nevertheless our results are the first to demonstrate that the close relationship between receptive field structure and preferred orientation previously observed in the spiking output is already present in thalamic excitation onto single cortical neurons.

It is arguable that cortical silencing may affect orientation and direction tuning of thalamic neurons via the disruption of corticothalamic feedback. However, our recordings of dLGN units demonstrate little change to their tuning properties during cortical silencing (Supplementary Fig. 2.3). This is consistent with previous experiments addressing the impact of cortex on thalamic tuning properties which find effects on overall gain and spatial frequency tuning (Cudeiro & Sillito, 2006), but do not report changes in orientation or direction tuning.

While some functional properties of visual cortex such as spike rate (Niell & Stryker, 2010), surround suppression (Adesnik, Bruns, Taniguchi, Huang, & Scanziani, 2012), and inhibition (Haider, Häusser, & Carandini, 2013) are influenced by anesthesia, other properties such as orientation tuning (Niell & Stryker, 2010) remain relatively unaffected. Thus we believe that the mechanisms underlying orientation tuning revealed here in anesthetized animals are likely to apply under awake conditions.

We isolated the excitatory component that is not of thalamic origin ($EPSC_{Sub}$) by subtracting the thalamic excitation ($EPSC_{Thal}$) from the total excitation ($EPSC_{Tot}$). Because of the complete silencing of the cortex upon photostimulation of PV cells, $EPSC_{Sub}$ is likely to mainly reflect excitation mediated by cortical neurons. Furthermore

because of our overestimate of thalamic excitation during cortical silencing (discussed above) $EPSC_{Sub}$ is likely to be an underestimate of cortical excitation. Could the observed tuning of $EPSC_{Sub}$ simply result from the subtraction of an overestimated thalamic excitation from $EPSC_{Tot}$? If so this would bias the tuning properties of $EPSC_{Sub}$ to be actually anti-correlated with $EPSC_{Thal}$. However because $EPSC_{Sub}$ and $EPSC_{Thal}$ are co-tuned, the tuning properties of $EPSC_{Sub}$ are unlikely to be due to subtraction artifacts. In fact, the subtraction of an overestimated $EPSC_{Thal}$ likely underestimates the degree of co-tuning of thalamic and cortical excitation.

While $EPSC_{Sub}$ must largely reflect the synaptic excitation contributed by cortical neurons, it may also contain excitatory currents generated by active dendritic conductances, activated, for example, by the combination of thalamic and cortical inputs or synchronous activity. While our use of voltage clamp reduces such effects, we cannot rule out the possibility of such amplification.

Our finding that Q_{Sub} is orientation selective is consistent with the observation, in L2/3 of mouse visual cortex, that neurons tuned to the same orientation are more likely to excite each other (Ko et al., 2011). Our data suggest that such a rule may also apply in L4 although the relatively large Q_{Sub} at non-preferred orientations in some cells implies that the cortical connectivity is not exclusively orientation-specific. The fact that $EPSC_{Sub}$ is F1 modulated and that this F1 modulation is highly orientation selective may further imply specific connectivity among cortical neurons that are not only tuned to the same orientation but also share similar temporal phase. Novel methods for mapping the synaptic connectivity between functionally characterized neurons will address this possibility in the future (Bock et al., 2011; Briggman, Helmstaedter, & Denk, 2011; Jia,

Rochefort, Chen, & Konnerth, 2010; Ko et al., 2011; Lien & Scanziani, 2011; Marshel, Mori, Nielsen, & Callaway, 2010).

In conclusion, the fact that $F1_{Sub}$ and $F1_{Thal}$ are tuned to the same orientation and share the same temporal phase indicates that in the cortex, the excitation provided by thalamic inputs is amplified. Future experiments that selectively silence recurrent excitatory cortical synapses will help elucidate the impact of cortical amplification on the output of cortical neurons.

Methods

All experimental procedures were conducted in accordance with the National Institutes of Health guidelines and with the approval of the Committee on Animal Care at the University of California, San Diego. Data collection and analysis were not performed blind to the conditions of the experiments.

Animals

We used male and female transgenic mice heterozygous for PV-Cre (Jackson Labs #008069). Mice were bred by crossing homozygous PV-Cre C57/B6 fathers with ICR white wild-type mothers. All offspring had pigmented eyes. Mice were housed in a vivarium with a reversed light cycle at a maximum of 5 animals per cage. We report whole-cell voltage clamp recordings from 40 mice. Loose-patch recordings in Fig. 2.1b are from 2 mice. Combined loose-patch and LFP recordings in Supplementary Fig. 2.1 are from 4 mice. LFP recordings during pharmacological block of $GABA_B$ receptors in Supplementary Fig. 2.4 are from 6 mice. Thalamic units in Supplermentary Fig. 2.4 are from 3 mice.

Virus injection

Adeno-associated virus for Cre-dependent ChR2 expression (AAV2/1.CAGGS.flex.ChR2.tdTomato.SV40, Addgene 18917) was obtained from the University of Pennsylvania Viral Vector Core. Virus was injected into the right visual cortex of neonatal PV-Cre mice between postnatal day 0 and 2 as previously described (Atallah et al., 2012; Olsen et al., 2012). Pups were anesthetized on a cold pad (0° C).

Virus was loaded into a beveled glass micropipette (tip diameter 20-40 μm) mounted on a Nanoject II (Drummond) attached to a micromanipulator. Three bolus injections of 23 nl were made at a depth of 300-500 μm at each of three sites along the medial-lateral axis of V1.

Animal preparation for *in vivo* physiology

In vivo physiology experiments were performed on mice 1-3 months after neonatal virus injection. Mice were anesthetized by intraperitoneal injection of 1.5 g/kg urethane and 2-4 mg/kg chlorprothixene. During surgery this was supplemented by 1% isoflurane in O_2. Depth of anesthesia was monitored with toe-pinch response. 3 mg/kg dexamethosone was administered subcutaneously to reduce brain swelling. A thin layer of silicon oil was applied to the eyes to prevent drying. The scalp and fascia were removed and a metal headplate was mounted over the right hemisphere using dental cement mixed with black paint. A 2-3 mm diameter craniotomy was performed over V1 (centered 2.5 mm lateral to the midline, 1 mm anterior to the lambda suture). In whole-cell recording experiments, a partial durotomy was performed on the lateral side of the craniotomy using a hooked 27-gauge needle for insertion of patch pipettes. Otherwise the dura was left intact. A thin layer of 1.5% low melting point agarose dissolved in ACSF (in mM: 140 NaCl, 5 KCl, 10 D-Glucose, 10 HEPES, 2 $CaCl_2$, 2 $MgSO_4$, pH 7.4) was applied to the brain surface to reduce movement. The craniotomy was then kept submerged under a well of ACSF. Isoflurane was adjusted to 0-0.5% upon completion of craniotomy and/or durotomy surgery. At the end of the recording session, which lasted 4-

8 hours, mice were deeply anesthetized with 5% isoflurane and euthanized by decapitation.

In vivo physiology

Loose-patch recordings were obtained using glass patch pipettes (3-5 MΩ tip resistance) filled with 50 μM Alexa 488 hydrazide in ACSF. Recordings were targeted to ChR2-tdTomato negative neurons in L4 (350-450 μm below the pia surface) using the shadow-patch technique (Kitamura, Judkewitz, Kano, Denk, & Häusser, 2008) under a two photon laser scanning microscope (Sutter) coupled to a Ti:Sapphire laser (Coherent, Ultra II) tuned to 900-1,000 nm. Seal resistance of the loose patch was 10-100 MΩ. Spikes were recorded in current-clamp mode with zero holding current.

Whole-cell recordings were obtained using the blind patch technique (Margrie, Brecht, & Sakmann, 2002). Whole-cell patch pipettes (3-5 MΩ tip resistance) were filled with K^+ based internal solution (in mM: 135 K-gluconate, 8 NaCl, 10 HEPES, 4 Mg-ATP, 0.3 Na-GTP, 0.3 EGTA, pH 7.4) and 50 μM Alexa 488 hydrazide. The depth of the recorded neuron was obtained upon termination of the recording by identifying the soma and/or pipette tip under two photon microscopy and measuring the distance to the pial surface. Neurons were voltage clamped at the reversal potential of inhibition (-68 ± 0.8 - 69 ± 0.8 mV, n = 49) to record excitatory postsynaptic currents (EPSCs). The reversal potential of inhibition was determined by adjusting the holding potential to minimize the amplitude of the IPSC evoked by photostimulation of PV cells. Average series resistance across the duration of the recording was 49 ± 3 MΩ (n = 49). In 41/49 whole-cell recordings, local field potential (LFP) was concurrently monitored with a patch pipette

(3-5 MΩ tip resistance, 50 μM Alexa 488 hydrazide in ACSF internal solution) in L2/3 (150-250 μm below the pia) in current clamp mode.

Visual stimulation

Stimuli were created using Matlab with the Psychophysics Toolbox (Brainard, 1997) were displayed on a gamma-corrected LCD monitor (Dell, 44 x 27 cm, 60 Hz refresh rate, mean luminance 85 cd/m^2). The monitor was positioned 20 cm from the contralateral eye and repositioned such that the receptive field of the recorded neuron (as assessed by an experimenter-controlled white bar) was approximately centered. The ipsilateral eye was obscured from the monitor with a shield made of black tape.

Drifting gratings

Full field, full contrast drifting bar gratings with spatial frequency of 0.04 cycles per degree and temporal frequency of 2 Hz were displayed. Gratings were randomly presented at 12 evenly spaced directions. Stimulus duration was 1.5 or 1.7 s with a 2 s interstimulus interval in which a gray screen of mean luminance was displayed.

Receptive field mapping

The stimuli used to map receptive fields consisted of individually presented black (minimum luminance) or white squares (full luminance) against a gray background of mean luminance. The squares were 5 degrees in width and appeared in one of 64 locations of an 8x8 square grid covering 40x40 degrees. Stimuli were displayed for 100 ms followed by 200 ms of gray background before the next stimulus. Stimuli were

presented in blocks of 5 or 19 with a 3.5 s or 1.5 s inter-block interval, respectively. A gray screen was presented during the inter-block interval. For each stimulus presentation, the location and luminance of the square was randomized.

Photostimulation of PV cells

ChR2-expressing PV cells were photostimulated using a 470 nm blue LED (Thorlabs) coupled to the widefield epifluorescence illumination pathway of the two photon microscope. The LED illumination was delivered to the brain via a 20x water-immersion objective (1.0 NA, Olympus). The field of view of the objective was centered on the recorded neuron and focused at its depth coordinate. The total power out of the front of the objective was 1.3 or 2.3 mW. For drifting gratings and the 5-block flashed squares, the LED was turned on 0.64 s before the onset of visual stimulus and lasted 2.6 s. For the 19-block receptive field stimuli, the LED was turned on 0.57 s before the onset of visual stimulus and lasted 6.4 s. Thus the entire duration of visual stimulation was encompassed by the LED illumination period. Trials or blocks alternated between visual stimulus and LED + visual stimulus conditions.

To estimate the change in input resistance in the recorded neurons during PV cell photo-stimulation, cells were clamped at 2-4 different potentials (range: -50 to -80 mV) during an LED step lasting 1.8 s. The input resistance prior to LED onset was calculated by determining the current at each potential, fitting a line to the current-voltage relationship and determining the inverse of the slope of that line. The current prior to LED onset was quantified as the bottom 5^{th} percentile of the current amplitude distribution to exclude spontaneous synaptic activity. Input resistance during the LED

step was determined by plotting the average current during the last 1.1 s of LED illumination against the holding potential, performing a linear fit and determining the inverse of the slope of that fit.

Data analysis

All analysis was performed using custom written code in IgorPro (Wavemetrics).

Drifting gratings

The holding current (baseline, Fig. 2.3a top right) in a 540 ms window prior to the onset of visual stimulus was subtracted for each trial. This holding current was computed from the bottom 5th percentile of the distribution of current values, which should include the periods with the least amount of spontaneous excitatory activity. This was confirmed by visual inspection. Trials with the same visual stimulus and LED conditions were then averaged together (3-8 repeats per cell). Trial-averaged synaptic currents recorded during control conditions without LED illumination were designated $EPSC_{Tot}$ and those recorded during LED illumination were designated $EPSC_{Thal}$. $EPSC_{Sub}$ was generated by point-by-point subtraction of $EPSC_{Thal}$ from $EPSC_{Tot}$ ($EPSC_{Sub} = EPSC_{Tot} - EPSC_{Thal}$).

The excitatory charge (Q) was quantified as the time integral of the EPSC during the visual stimulus period (Fig. 2.3a, top right). F1 modulation was quantified by fitting a sinusoidal function with a periodicity matching the temporal frequency of the drifting grating (2 Hz) to the cycle-averaged response (average of 2-3 grating cycles; grating period 0.5 s). The results of this fit were used to derive F1 amplitude and phase values (Fig. 2.3a, bottom right).

Orientation selectivity index (OSI) was calculated as 1 - circular variance (Ringach et al., 2002) using the following equation:

$$OSI = \frac{\sqrt{\left(\sum r_k \sin(2\theta_k)\right)^2 + \left(\sum r_k \cos(2\theta_k)\right)^2}}{\sum r_k}$$

Where r_k is the response to the *k*th direction given by θ_k. Direction selectivity index (DSI) was calculated as $(R_{max} - R_{null})/(R_{max})$ where R_{max} is the response to the stimulus that produced the maximum response and R_{null} is the response to the direction 180 degrees away from that stimulus. As additional measures of orientation tuning, we also calculated the depth of modulation by orientation as well as the tuning width (Supplementary Fig. 2.5). The results for these measures of tuning are similar to those obtained by the OSI.

The population tuning curve for a particular parameter (i.e., Q or F1) was constructed by circularly shifting the tuning curves of all cells so that the preferred direction of a reference parameter occurred at 0 degrees and then averaging the tuning curves of all cells. The preferred direction was defined as the stimulus direction that evoked the largest response. The reference parameter could be the same or different from the parameter being plotted in the tuning curve. In figures showing population tuning curves of multiple parameters plotted on the same axis, if the population tuning curves were aligned to their own preferred direction, they are referred to as “self reference”. Otherwise, the tuning curves were aligned to the preferred direction of a common reference parameter stated in the figure.

Preferred orientation was calculated as the vector average of responses (Swindale, 1998) using the following equation:

$$a = \sum r_k \cos(2\theta_k) \; ; \; b = \sum r_k \sin(2\theta_k)$$

$$\text{Preferred orientation} = 0.5 \arctan(b/a) \text{ if } a > 0$$
$$\text{Preferred orientation} = 180 + 0.5 \arctan(b/a) \text{ if } a < 0$$

Where r_k is the response to the *k*th direction given by θ_k. Preferred orientation spanned the range of 0 to 180 degrees. Differences in preferred orientation were calculated by taking the absolute value of the difference. If this value was greater than 90 degrees, then it was adjusted to the complementary angle by subtracting it from 180. Preferred direction was defined as the stimulus that produced the maximum response and spanned 0 to 330 degrees. Difference in preferred direction was calculated by taking the absolute value of the difference. If this value was greater than 180 degrees, then it was adjusted to the complementary angle by subtracting it from 360.

Response to flashed squares

Responses to the same stimulus luminance, location, and LED conditions were averaged together (3-10 repeats per cell). The baseline activity for each average, defined as the average current level in a 30 ms window following stimulus onset was subtracted from each trace. We chose a late baseline window to limit the influence of large spontaneous fluctuations that often occurred during control trials in the absence of cortical silencing. While the baseline window occurred after the onset of the stimulus, it did not contain visually-evoked activity, as the latency to response was typically around 40 ms.

Receptive field of thalamic excitation

Raw receptive field maps of thalamic excitation were obtained from the average response to black (OFF) or white (ON) squares at each grid location during cortical silencing. The response was taken as the integrated excitatory charge across a response window starting 40 ms after stimulus onset and lasting 100 ms. This window allowed us to capture the response to the onset of the stimulus and avoid potential contamination by offset responses, which were occasionally observed. The response at each grid location was converted to a gray value to generate 8x8 heat maps of the raw receptive field. For each ON or OFF receptive field map, a set of background pixels was selected by eye that was clearly outside of the responsive region. The average value and standard deviation of the background pixels were calculated. Then, a 3x3 bilinear interpolation of the raw receptive field map was generated and z-scored using the previously calculated average and standard deviation of the background pixels. All pixels less than +2.5 z-scores were set to 0. Contiguous non-zero regions with area > 2 grid locations were designated as subfields. All other regions were set to 0. The interpolated and thresholded maps of the subfields were used for subsequent analysis and display in contour plots. Subfield area was calculated by counting all of the pixels in the subfield. Overlap area was the area of the region of overlap between ON and OFF subfields. Overlap index was equal to the overlap area as a fraction of the smaller subfield. The peak location of a subfield was determined as the center of mass of the set of pixels within 2-zscores of the strongest pixel. The subfield width along a given axis was defined as the linearly-interpolated full-width at half maximum of the subfield along that axis (as shown in the profile plots in Fig. 2.2c-d). This was calculated for both the axis between the ON and OFF subfields and the orthogonal axis. RF_{Pref}, the preferred orientation predicted from the receptive field

structure, was calculated as the orientation corresponding to gratings whose stripes are elongated perpendicular to the axis connecting the peak locations of the ON and OFF subfields. As shown in Figure 4d, horizontal gratings correspond to 0 degrees with clockwise rotations being positive.

Four neurons exhibited an OFF thalamic subfield but lacked sufficiently large ON responses to define an ON subfield according to the aforementioned criteria. In one case, the OFF thalamic subfield was situated on the edge of the grid used for receptive field mapping and so the presence or absence of an ON subfield could not be determined.

Simulation of separation between identical receptive field subfields

To ensure that the separation between the peaks of ON and OFF subfields that we measured was not due to noise in the estimate of peak location, we simulated the probability that a pair of identical subfields would exhibit a similar degree of peak separation given the variability of responses measured in pixels outside of the receptive field. For each subfield (n = 26 from 13 cells with 1 ON and 1 OFF subfield), the raw 8 pixel x 8 pixel heat map served as the underlying model subfield for our simulations. A noise value was added to each pixel to generate one simulated subfield. The noise was drawn from a Gaussian distribution centered at 0 with a standard deviation equal to the standard deviation of the responses in the background pixels (as defined in the previous section). The location of the peak of the simulated subfield was determined as stated in the previous section. The distance between peak locations for 1,000 pairs of simulated subfields (each starting from the same "true" subfield) was determined. The probability that the measured ON-OFF separation for a cell was less than the separation between

simulated identical subfields was calculated as the fraction of simulated distances that was greater than or equal to the measured values. Because each cell had an ON and an OFF subfield, we generated 2 probability values for each cell that used either the ON or the OFF subfield as the model receptive field. We refer to the larger of the two probability values in the text.

Statistical analysis

All error bars are presented as mean ± s.e.m and statistical significance was determined using two-sided paired t-tests. No statistical methods were used to pre-determine sample sizes, but our sample sizes are similar to those reported in previous publications in the field (Chung & Ferster, 1998; Ferster et al., 1996; Liu et al., 2010). Data distribution was assumed to be normal but this was not formally tested.

Figure 2.1 Isolating thalamic excitation

a, Schematic of experimental approach for isolating thalamic excitation recorded in response to visual stimulation in layer 4 neurons voltage clamped at the reversal potential for inhibition. Thalamic excitation is isolated by silencing cortical activity via photostimulation of ChR2-expressing PV cells. **b,** Optogenetic silencing of visually evoked cortical activity. Top: The spiking responses of two example cortical neurons recorded in the loose patch configuration with (LED, blue) and without (control, red) PV cell photostimulation are shown as raster plots. Gray rectangle, visual stimulus (1.5 s). Blue bar, LED illumination (2.6 s). Control and LED trials were interleaved, but separated here for clarity. Bottom, population peristimulus time histogram (PSTH) averaged across all cells and all stimulus directions (n = 14 cells, 2 mice). Note complete suppression of spiking during LED illumination. The high spontaneous activity and its stimulus-evoked reduction in cell 2 were rare. **c**, Total and thalamic excitation in response to flashed squares.Top, visually evoked EPSCs recorded in two example cortical neurons with (blue) and without (red) cortical silencing in response to a flashed square (5 degrees) at optimal location and luminance. Average of 8 (cell 1) and 4 (cell 2) trials. Gray rectangle, visual stimulus. Blue bar, LED illumination. Bottom, distribution of the fraction of excitatory charge contributed by the thalamus (n = 18 cells, 16 mice). **d**, Same as **c** for drifting gratings. The response to the preferred direction is shown. Average of 8 (cell 1) and 5 (cell 2) trials. Bottom, distribution of the fraction of excitatory charge contributed by the thalamus (n = 42 cells, 33 mice).

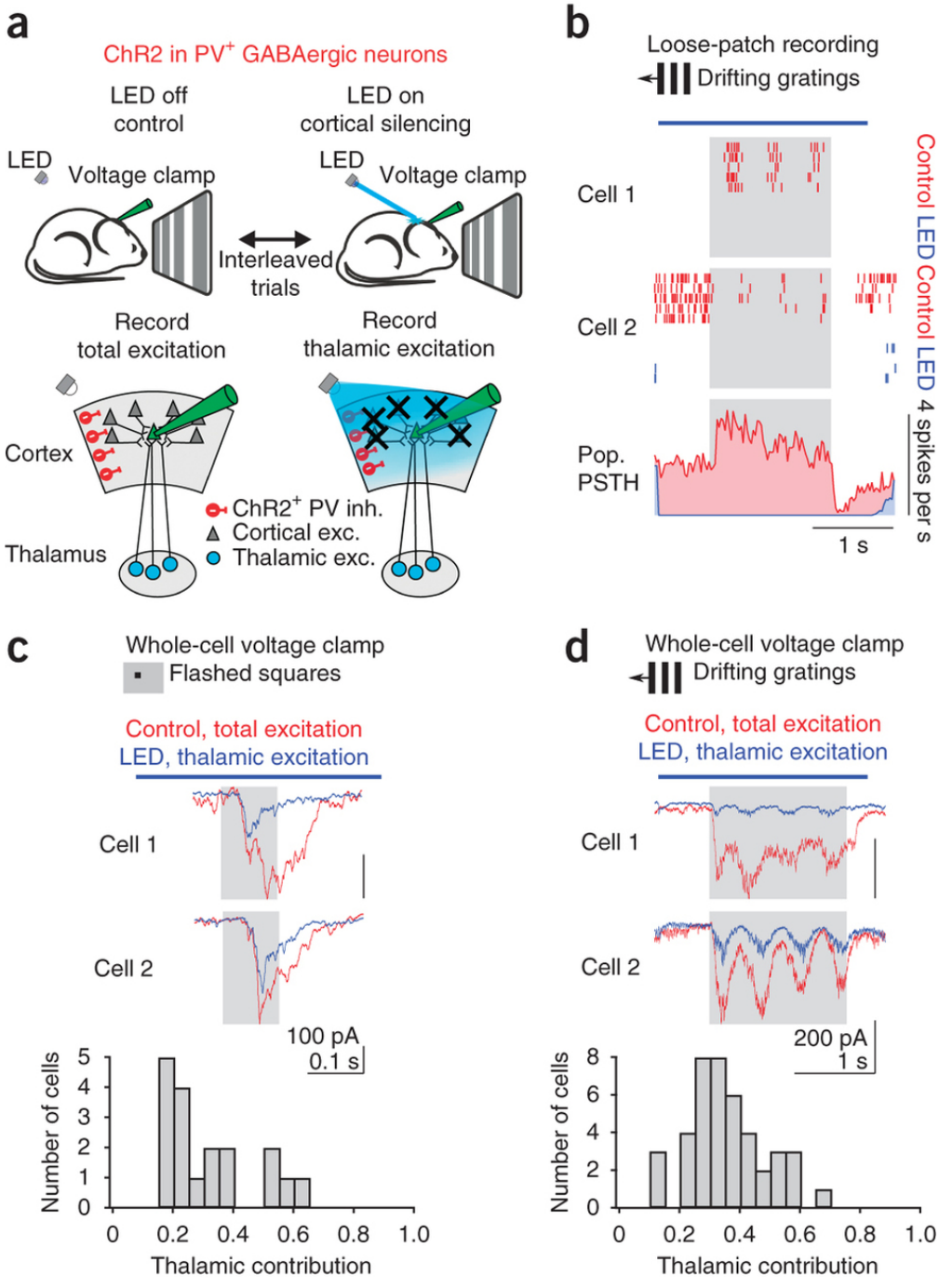
a
ChR2 in PV+ GABAergic neurons
LED off
control
LED on
cortical silencing
LED
Voltage clamp
LED
Voltage clamp
Interleaved
trials
Record
total excitation
Record
thalamic excitation
Cortex
Thalamus
ChR2+ PV inh.
Cortical exc.
Thalamic exc.
b
Loose-patch recording
Drifting gratings
Cell 1
Cell 2
Pop.
PSTH
Control LED Control LED
4 spikes per s
1 s
c
Whole-cell voltage clamp
Flashed squares
Control, total excitation
LED, thalamic excitation
Cell 1
Cell 2
100 pA
0.1 s
Number of cells
Thalamic contribution
d
Whole-cell voltage clamp
Drifting gratings
Control, total excitation
LED, thalamic excitation
Cell 1
Cell 2
200 pA
1 s
Number of cells
Thalamic contribution

Figure 2.2 Receptive field structure of thalamic excitation

a, Example cell. Isolated thalamic excitation ($EPSC_{Thal}$) in response to black ("OFF", magenta traces, left) or white ("ON", green traces, right) squares at each of 64 locations on an 8x8 grid. Stimuli appear at the beginning of each trace and last for 100 ms. The raw receptive field heat maps calculated from the thalamic excitatory charge (Q_{Thal}) evoked at each grid location and normalized to the peak ON response are depicted by the background gray-level of each trace. Average of 4 trials per location. **b,** Contour plot of the OFF and ON subfields for the cell in **a**. Each contour represents 2 z-scores. Filled magenta and green circles mark the peaks of the OFF and ON receptive fields, respectively. **c,** Profile plot of OFF and ON receptive fields in **c** along the axis connecting their peaks. **d**, Same as b and **c** for 3 additional neurons. **e,** Population average of OFF and ON receptive fields. Before averaging, the receptive fields for each cell were centered on the peak of the OFF subfield and rotated so that the peak of the ON subfield was directly to the right of the OFF. OFF and ON subfields were separately normalized. Top, heat maps of the population average OFF and ON receptive fields. Bottom, contour and profile plots of the population average receptive fields as in **b** and **c**. The outermost contour represents 10% of the peak and each additional contour is an increment of 20% of the peak. **f,** Quantification of subfield area (n = 26 subfields) and overlap between ON and OFF subfields (n = 13 cells). **g**, Distance between the peaks of ON and OFF subfields (n = 13 cells). **h,** Comparison of subfield width along the axis connecting the ON and OFF peaks (ON/OFF axis) or the orthogonal axis (n = 26 subfields). Black line, unity. Data in **e-h** are from 13 cells each exhibiting 1 OFF and 1 ON subfield from 12 mice. Error bars, mean ± s.e.m.

.

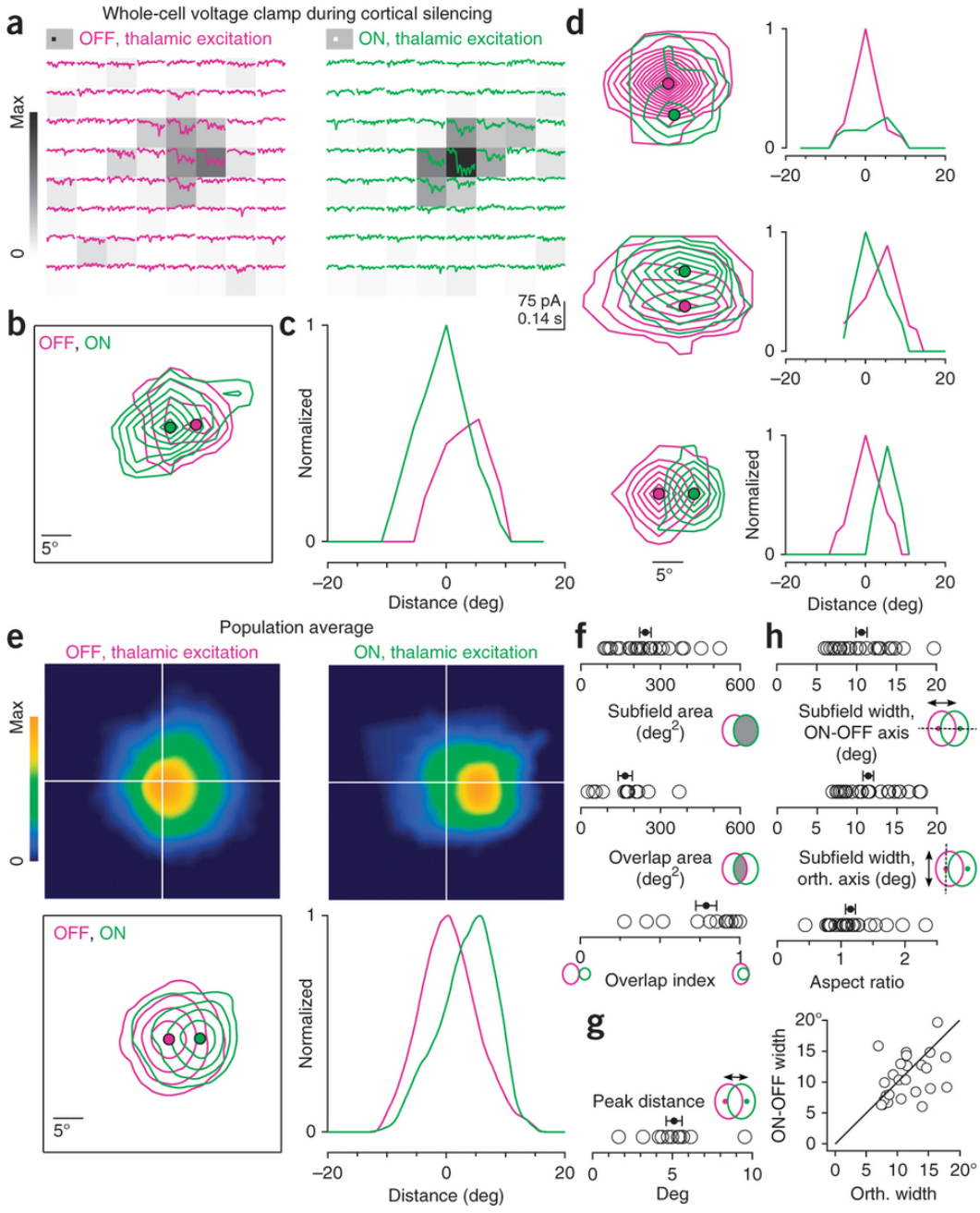
a
Whole-cell voltage clamp during cortical silencing
OFF, thalamic excitation
ON, thalamic excitation
Max
0
75 pA
0.14 s
b
OFF, ON
5°
c
Normalized
Distance (deg)
d
Normalized
Distance (deg)
e
Population average
OFF, thalamic excitation
ON, thalamic excitation
Max
0
OFF, ON
5°
Normalized
Distance (deg)
f
Subfield area (deg²)
Overlap area (deg²)
Overlap index
g
Peak distance
Deg
h
Subfield width, ON-OFF axis (deg)
Subfield width, orth. axis (deg)
Aspect ratio
ON-OFF width
Orth. width

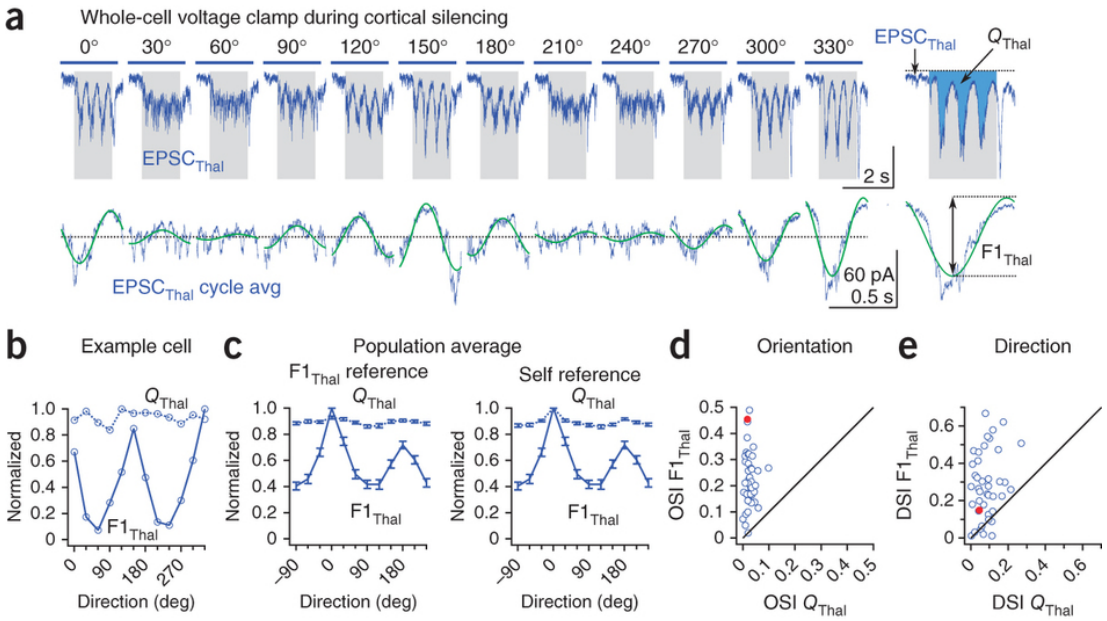

Figure 2.3 Orientation tuning of thalamic excitation

a, Example cell: Top, Isolated thalamic excitation ($EPSC_{Thal}$) in response to drifting gratings of various orientations (average of 8 trials per direction). Gray rectangle, visual stimulus (1.7 s). Blue bar, LED illumination (2.6 s). Bottom, F1 modulation of $EPSC_{Thal}$. Cycle average (blue) and best-fitting sinusoid (green) at the grating temporal frequency (2 Hz). The y-offset was removed to aid comparison of F1 amplitude across different orientations. Right, $EPSC_{Thal}$ and cycle average in response to 330 degree grating at expanded time scale showing how Q_{Thal} and $F1_{Thal}$ are determined. **b,** Orientation tuning curves of Q_{Thal} (dashed line) and $F1_{Thal}$ (solid line) for the neuron in (**a**). **c,** Population tuning curves of Q_{Thal} (dashed line) and $F1_{Thal}$ (solid line). Left, Population tuning curves in which Q_{Thal} and $F1_{Thal}$ tuning curves for each cell were equally shifted so that the preferred direction of $F1_{Thal}$ occurred at 0 degrees ($F1_{Thal}$ reference). Right, Population tuning curves in which Q_{Thal} and $F1_{Thal}$ tuning curves for each cell were independently shifted so that preferred direction of Q_{Thal} and $F1_{Thal}$ both occurred at 0 degrees (self reference). **d,** Orientation selectivity index (OSI) of Q_{Thal} plotted against OSI of $F1_{Thal}$ for each cell. **e,** Direction selectivity index (DSI) of Q_{Thal} plotted against DSI of $F1_{Thal}$ for each cell. Filled red markers in **d** and **e** denote the OSI and DSI values of the example cell. Data in **c-e** are from n = 42 cells from 33 mice. Error bars, mean ± s.e.m.

Figure 2.4 Separation of ON and OFF thalamic subfields predicts preferred orientation of thalamic excitation

a-d, Example recording of isolated thalamic excitation ($EPSC_{Thal}$) where both the ON and OFF receptive fields and the responses to drifting gratings at various orientations were obtained in the same cell. **a,** $EPSC_{Thal}$ in response to black and white squares. Average of 5 trials per location. **b,** Contour plot of the OFF and ON receptive field maps for the cell in **a**. Each contour represents 2 z-scores. Filled magenta and green circles mark the peaks of the OFF and ON receptive fields, respectively. Dashed black line connects the OFF and ON peaks to define the ON-OFF axis. The preferred orientation predicted from the ON-OFF axis, RF_{Pref}, is indicated by the small grating. **c,** $EPSC_{Thal}$ in response to drifting gratings of various orientations (average of 3 trials per direction). Gray rectangle, visual stimulus (1.7 s). Blue bar, LED illumination (2.6 s). **d,** Orientation tuning curves of $F1_{Thal}$ (blue) and Q_{Thal} (gray) in polar coordinates for the responses in **c**. The blue line indicates the preferred orientation of $F1_{Thal}$ ($Grating_{Pref}$) and the black dashed line corresponds to RF_{Pref}. **e,** Same as **b** and **d** for three additional cells. **f,** RF_{Pref} plotted against $Grating_{Pref}$ (n = 8 cells, 7 mice). Black line, unity. The dashed lines denote the region in which cells the difference between RF_{Pref} and $Grating_{Pref}$ is less than 30 degrees. The distributions of $Grating_{Pref}$ (n = 42, 33 mice) and RF_{Pref} (n = 13 cells, 12 mice) across the population of cells in which either value was measured are shown along the top and right, respectively. **g,** Absolute difference in RF_{Pref} and $Grating_{Pref}$ (DPref Ori) (n = 8 cells, 7 mice). Error bars, mean ± s.e.m. **h,** Diagram of how orientation tuning of $F1_{Thal}$ arises from spatially offset OFF and ON thalamic excitatory input. The area of the blue shaded region corresponds to Q_{Thal}. The difference between the peak and the trough of $EPSC_{Thal}$ corresponds to $F1_{Thal.}$

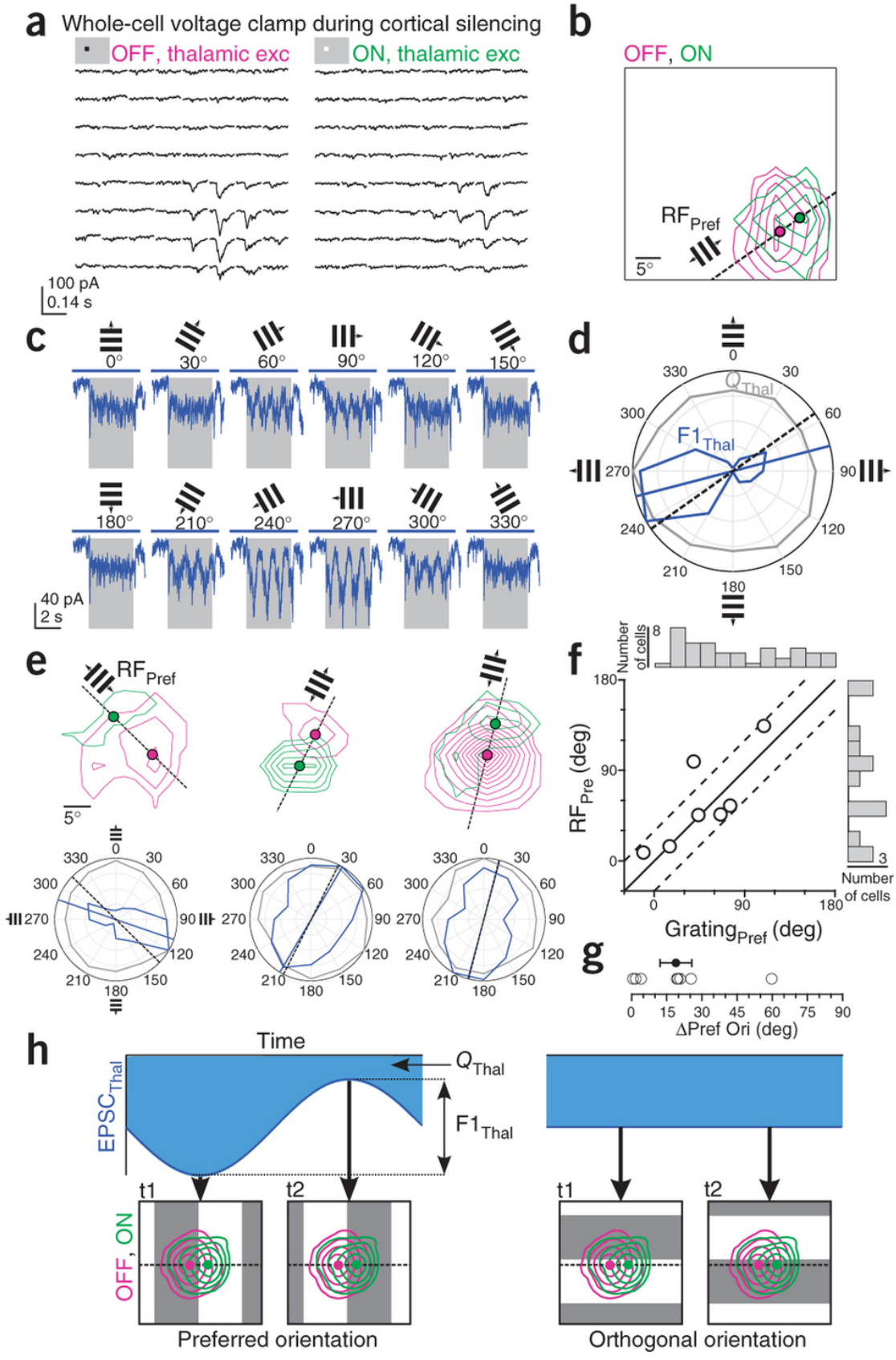
a
Whole-cell voltage clamp during cortical silencing
OFF, thalamic exc
ON, thalamic exc
100 pA
0.14 s
b
OFF, ON
RF Pref
5°
c
0°
30°
60°
90°
120°
150°
180°
210°
240°
270°
300°
330°
40 pA
2 s
d
Q Thal
F1 Thal
e
RF Pref
5°
f
Number of cells
RF Pre (deg)
Grating Pref (deg)
g
ΔPref Ori (deg)
h
Time
EPSC Thal
Q Thal
F1 Thal
t1
t2
OFF, ON
Preferred orientation
Orthogonal orientation

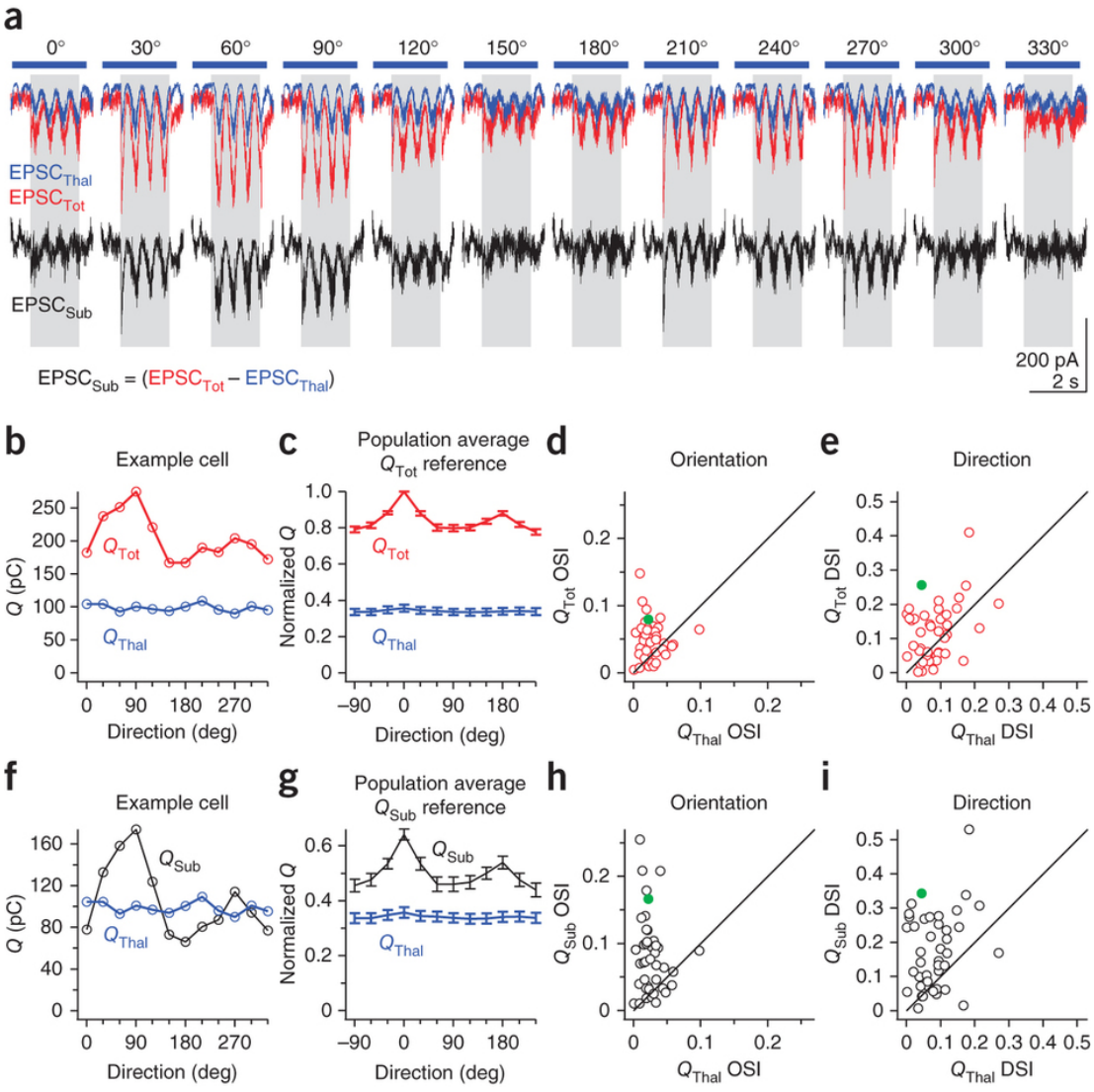

Figure 2.5 Tuning of non-thalamic excitatory charge

a, Example cell: Top, $EPSC_{Thal}$ (blue) and $EPSC_{Tot}$ (red) in response to drifting gratings of various orientations. Bottom, $EPSC_{Sub}$ derived from point-by-point subtraction of $EPSC_{Thal}$ from $EPSC_{Tot}$. Gray rectangle, visual stimulus (1.7 s). Blue bar, LED illumination (2.6 s). **b,** Orientation tuning curves of Q_{Tot} (red) and Q_{Thal} (blue) for the example cell in (**a**). **c,** Population tuning curves of Q_{Tot} (red) and Q_{Thal} (blue). Tuning curves are aligned to the preferred direction of Q_{Tot} (Q_{tot} reference) and normalized by the value of Q_{Tot} at its preferred direction. **d,** OSI of Q_{Tot} plotted against OSI of Q_{Thal} for all neurons. **e,** DSI of Q_{Tot} plotted against DSI of Q_{Thal} for all neurons. **f-i**, Same as (**b-e**) for Q_{Sub} (black) and Q_{Thal} (blue). Filled green markers in **d**, **e**, **h**, and **i** denote the OSI and DSI values of the example cell. Data in **c-e** and **g-i** are from n = 42 cells from 33 mice. Error bars, mean ± s.e.m.

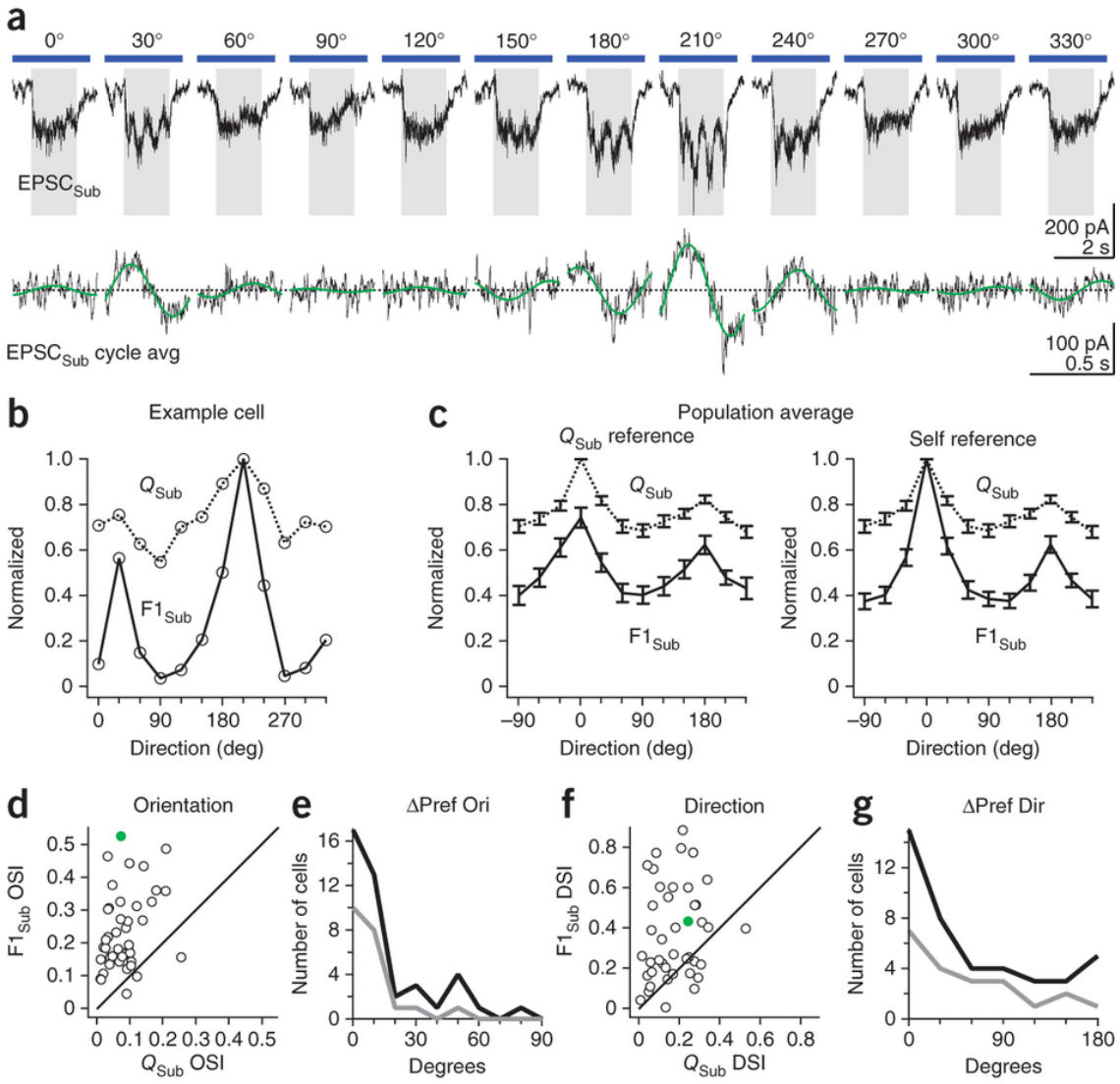

Figure 2.6 Tuning of non-thalamic excitatory F1 modulation

a, Example cell: Top, $EPSC_{Sub}$ in response to drifting gratings of various orientations. Gray rectangle, visual stimulus (1.5 s). Blue bar, LED illumination (2.6 s). Bottom, F1 modulation of $EPSC_{Sub}$. Cycle average (black) and best-fitting sinusoid (green) at the grating temporal frequency (2 Hz). **b,** Orientation tuning curves of Q_{Sub} (dashed curve) and $F1_{Sub}$ (solid curve) for the example cell in **a**. **c,** Population tuning curve of Q_{Sub} (dashed curve) and $F1_{Sub}$ (solid curve). Left, Population tuning curves in which Q_{Sub} and $F1_{Sub}$ tuning curves for each cell were equally shifted so that the preferred direction of Q_{sub} occurred at 0 degrees (Q_{sub} reference). Right, Population tuning curves in which Q_{Sub} and $F1_{Sub}$ tuning curves for each cell were independently shifted so that preferred direction of Q_{Sub} and $F1_{Sub}$ both occurred at 0 degrees (self reference). **d,** OSI of $F1_{Sub}$ is plotted against OSI of Q_{Sub} for all neurons. **e,** Distribution of absolute differences in preferred orientation (DPref Ori) between Q_{Sub} and $F1_{Sub}$. Dark curve, all cells (n = 42). Gray curve, cells in the top 50th percentile of $F1_{Sub}$ OSI (n = 21). **f-g,** Same as (**d-e**) for DSI and absolute differences in preferred direction (DPref Dir). Filled green markers in **d** and **f** denote the OSI and DSI values of the example cell. Data in **c-g** are from n = 42 cells from 33 mice. Error bars, mean ± s.e.m.

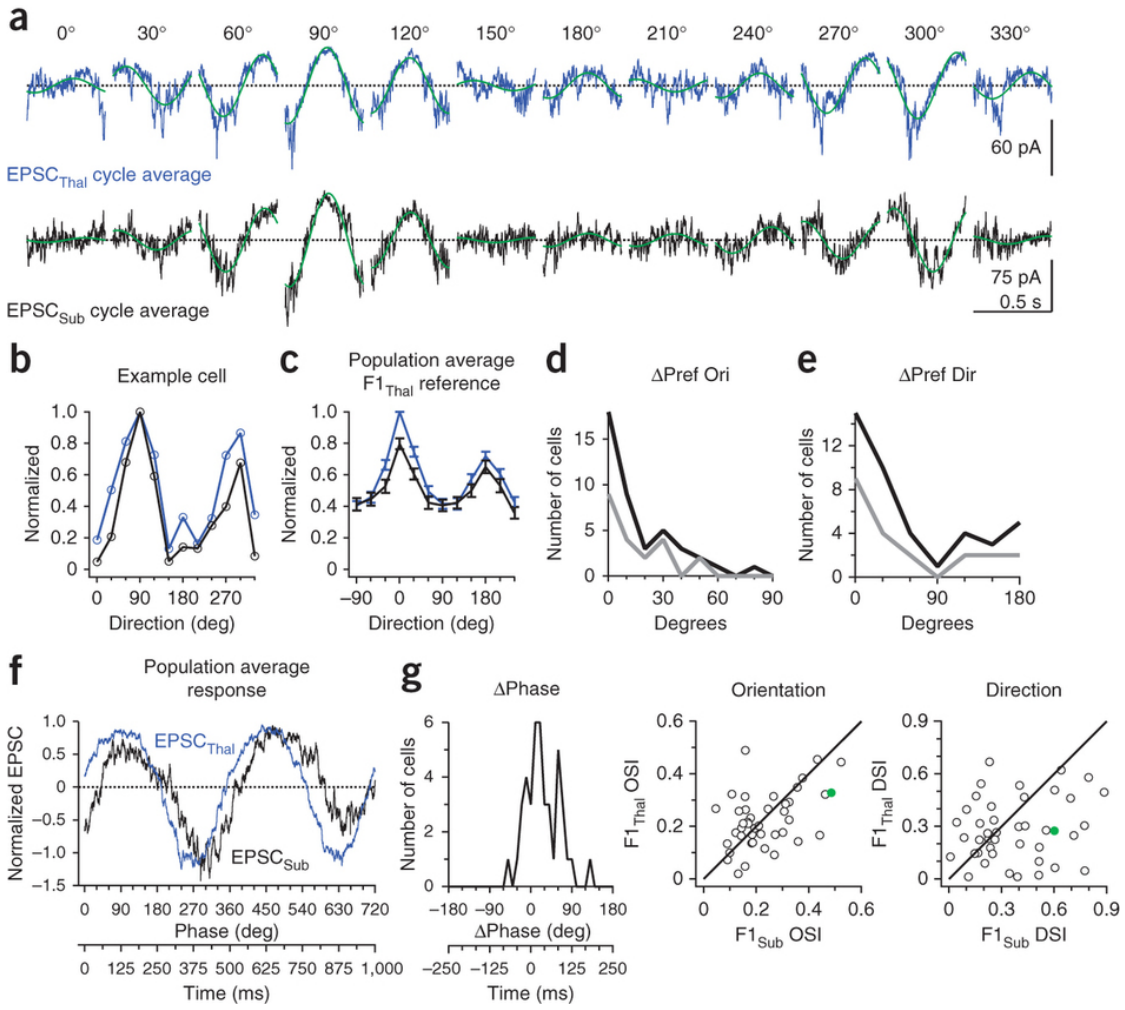

Figure 2.7 Co-tuning and phase relationship between thalamic and non-thalamic excitation

a, Cycle average of $EPSC_{Thal}$ (blue) and $EPSC_{Sub}$ (black) for an example cell. Green curves are the best-fitting sinusoids at the grating temporal frequency (2 Hz). **b**, Orientation tuning curves of $F1_{Thal}$ (blue) and $F1_{Sub}$ (black) for cell in **a**. **c,** Population tuning curves of $F1_{Thal}$ (blue) and $F1_{Sub}$ (black). $F1_{Thal}$ and $F1_{Sub}$ tuning curves were aligned to the preferred direction of $F1_{Thal}$ ($F1_{thal}$ reference) **d**, Top, distribution of absolute difference in preferred orientation (DPref Ori) between $F1_{Thal}$ and $F1_{Sub}$. Dark curve, all cells (n = 42). Gray curve, cells in the top 50th percentile of $F1_{Thal}$ OSI (n = 21). Bottom, OSI of $F1_{Thal}$ is plotted against OSI of $F1_{Sub}$ for all neurons. **e,** Same as **d** for absolute differences in preferred direction (DPref Dir) and DSI. **f,** Population average of $EPSC_{Thal}$ (blue) and $EPSC_{Sub}$ (black) over two grating cycles at the preferred direction of $F1_{Thal}$ and aligned to the F1 phase of $EPSC_{Thal}$. **g**, Distribution of F1 phase difference (DPhase) between $EPSC_{Thal}$ and $EPSC_{Sub}$ for responses from **f**. F1 phase of $EPSC_{Thal}$ is set to 0 degrees. Data in **c-g** are from n = 42 cells from 33 mice. Error bars, mean ± s.e.m.

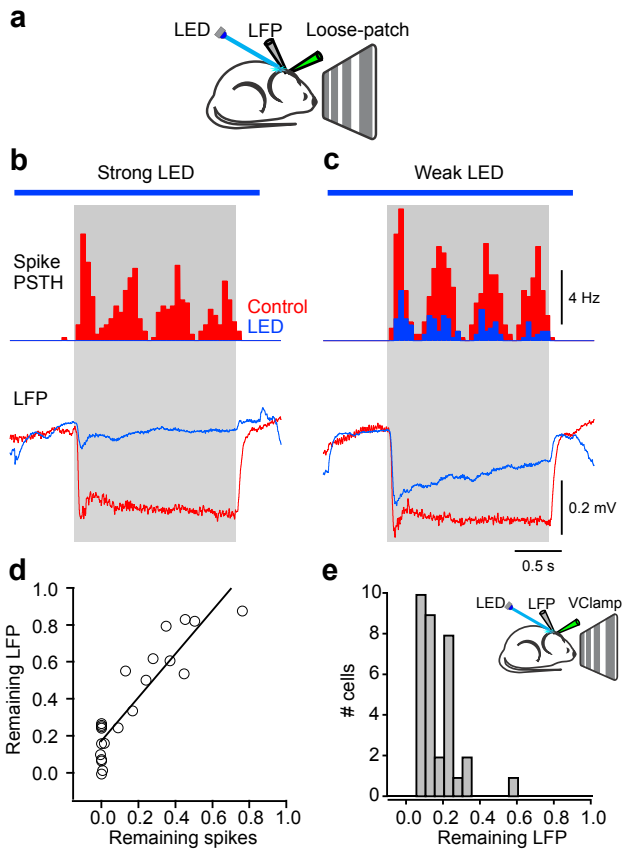

Supplementary Figure 2.1 Suppression of the local field potential is correlated with the degree of cortical silencing

a, Schematic of experimental setup. LFP electrode was inserted in L2/3 while loose-patch recordings were made in L4. **b,** Example responses during strong LED illumination (1.3 mW). Top, PSTH of loose-patch recording. Bottom, simultaneously recorded LFP on a second electrode. Red, control trials. Blue, LED trials. PSTH and LFP were averaged across all trials and stimulus directions. **c,** Responses from the same loose-patch and LFP recording in (b) during weak LED illumination (0.2 mW). **d,** The fraction of remaining LFP plotted against the fraction of remaining spikes during LED illumination. (n = 22 cell/LED intensity pairs from 11 cells in 4 animals, LED illumination ranged from < 0.1 mW to 1.3 mW). Black line is a linear fit (remaining LFP = 1.18 x remaining spikes + 0.17, r2 = 0.82). Note that complete cortical silencing reduces the LFP amplitude by ~80%. The remaining LFP likely reflects excitation from the thalamus. **e,** Distribution of remaining LFP during LED illumination for 34/42 neurons from our main drifting grating dataset in which LFP was monitored concurrently with whole-cell recording (schematized in the upper right). The average remaining LFP was 0.16 ± 0.017.

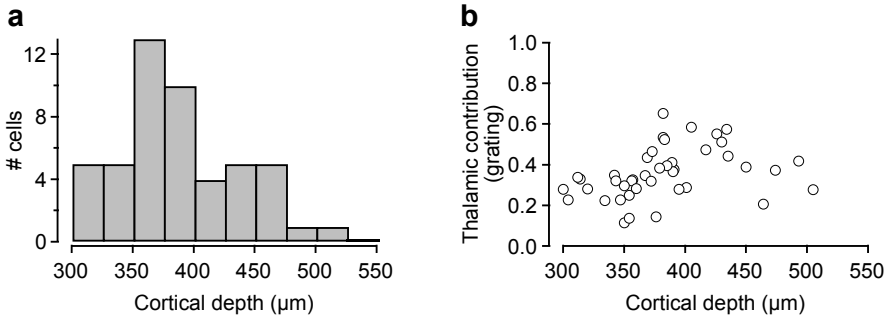

Supplementary Figure 2.2 Cortical depth of recorded neurons

a, Distribution of cortical depths for all whole-cell recordings analyzed in the study (n = 49 cells, 40 mice). Note that the study was restricted to cells within a depth range of 300-550 μm corresponding to cortical L4. **b,** Thalamic contribution to synaptic excitation during drifting grating plotted against cortical depth for neurons from Figure 1d (n = 42 cells, 33 mice).

Supplementary Figure 2.3 Tuning of isolated dLGN units

a, Schematic of experimental setup for recording single units from dLGN with and without cortical silencing. Recordings and photostimulation were performed as previously described (Ref 17). A small craniotomy was performed 2.5 mm posterior of bregma and 2 mm lateral of the midline and a 16-channel linear silicon probe (NeuroNexis a1x16-3mm-50- 177) was inserted to a depth of 2,500-3,300 μm. The probe was coated with DiO to label the recording site, which was confirmed to be in dLGN by post-mortem histology. To activate ChR2- expressing PV cells, the skull over the visual cortex was thinned and a blue (455 nm) fiber-coupled LED (1 mm diameter, Doric Lenses) positioned 5-10 mm illuminated the visual cortex with a power of 25 mW. Spike sorting of single units was performed as previously described (Ref 17). **b,** Spiking responses of a dLGN unit to drifting gratings of various orientations under control (red) and LED-illuminated cortical silencing (blue) conditions. Peri- stimulus time histogram (PSTH) of spiking is displayed below the raster plots. Gray line, visual stimulus (1.7 s). Blue bar, LED illumination (2.6 s). Note the strong F1 modulated spiking at all orientations. Inset, expansion of the grating cycle indicated by the black rectangle. **c,** Orientation tuning curve of the unit in **b** under control (red) and LED (blue) conditions. The response to each orientation was quantified as the average spike rate during the stimulus period. Control and cortical silencing conditions were separately normalized. **d,** Population tuning curves of dLGN single units under control (red) and LED (blue) conditions. Left, Population tuning curves in which control and LED tuning curves for each cell were equally shifted so that the preferred direction under control conditions occurred at 0 degrees. Right, Population tuning curves in which control and LED tuning curves for each cell were equally shifted so that the preferred direction under cortical silencing conditions occurred at 0 degrees. **e,** Orientation selectivity index of the average spike rate (OSI) under control conditions plotted against OSI under LED conditions (control OSI = 0.082 ± 0.02; LED OSI = 0.067 ± 0.01, not significantly different, $p = 0.31$). **f,** Same as **e** for direction selectivity index (control DSI = 0.33 ± 0.04; LED DSI = 0.27 ± 0.05, not significantly different, $p = 0.12$). **g,** Same as **e** for the average response magnitude across all directions (control response = 2.9 ± 0.4 Hz; LED response = 3.6 ± 0.6 Hz; not significantly different, $p = 0.2$). **h-i,** Same as **e-f** for F1 amplitude (control F1 OSI = 0.11 ± 0.024; LED F1 OSI = 0.11 ± 0.021; control F1 DSI = 0.42 ± 0.06; LED F1 DSI = 0.32 ± 0.06). F1 amplitude was determined by fitting the cycle average of the PSTH to a sinusoid at the temporal frequency of the grating (2 Hz). **j,** F1 OSI plotted against OSI of average spike rate during cortical silencing (LED on). Data in **d-j** are from 11 units from 3 mice. Error bars, mean ± s.e.m.

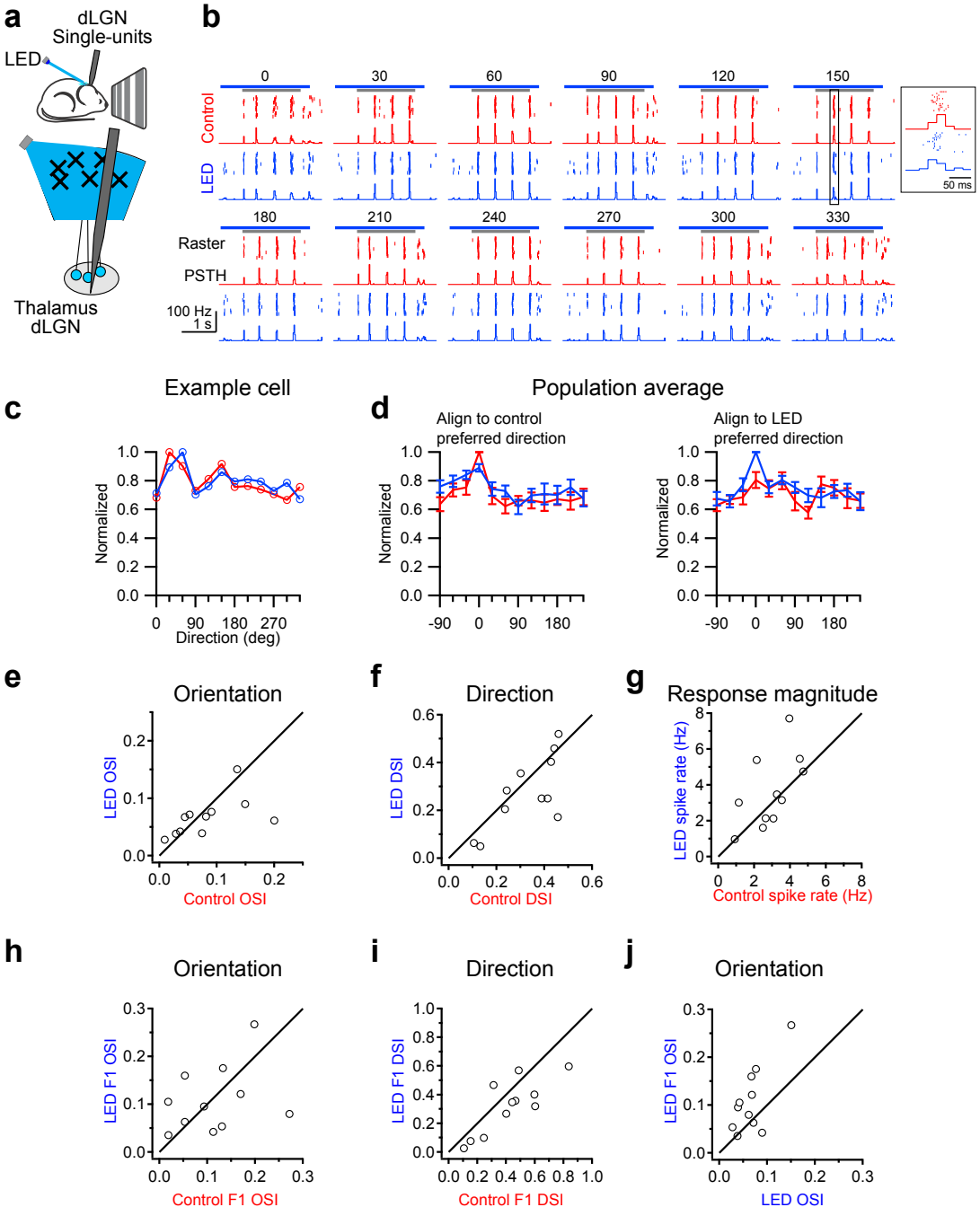
a
dLGN
Single-units
LED
Thalamus
dLGN
b
0
30
60
90
120
150
Control
LED
50 ms
180
210
240
270
300
330
Raster
PSTH
100 Hz
1 s
c
Example cell
Normalized
Direction (deg)
d
Population average
Align to control
preferred direction
Align to LED
preferred direction
Normalized
e
Orientation
LED OSI
Control OSI
f
Direction
LED DSI
Control DSI
g
Response magnitude
LED spike rate (Hz)
Control spike rate (Hz)
h
Orientation
LED F1 OSI
Control F1 OSI
i
Direction
LED F1 DSI
Control F1 DSI
j
Orientation
LED F1 OSI
LED OSI

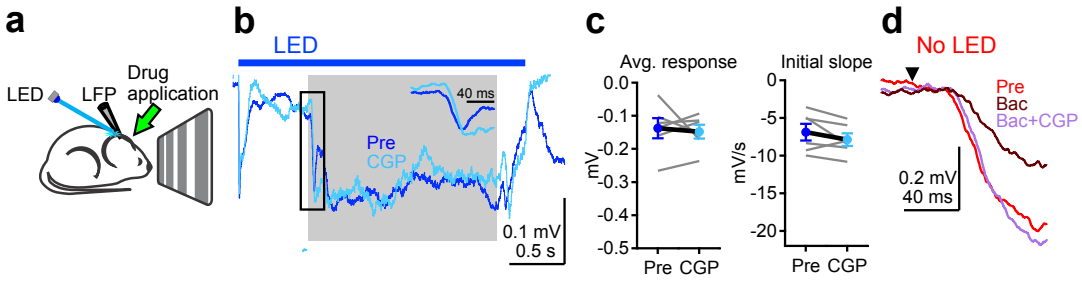

Supplementary Figure 2.4 Blocking $GABA_B$ receptors does not affect grating-evoked local field potential during cortical silencing

a, Schematic of experimental setup. To examine whether photostimulation of PV neurons could decrease transmitter release via activation of presynaptic $GABA_B$ receptors on thalamic terminals, we monitored changes in the grating-evoked LFP in L4 during LED illumination 15-45 minutes after application of the $GABA_B$ receptor antagonist CGP54626 (10 µM) to the cortical surface. In these experiments, a full durotomy was performed. **b,** Example grating-evoked LFP responses during LED illumination before (Pre, dark blue) and after CGP54626 application (CGP, light blue). Responses are the avearage across all stimulus directions (36 trials). Inset, expanded view of the boxed region during stimulus onset. Note that CGP54626 had little effect on neither the average response amplitude nor the initial slope at the onset of the response. **c,** Left, Average grating- evoked LFP over the duration of the stimulus (1.7 s) during LED illumination before and after CGP application. Right, initial slope of the first 20 ms of the response as obtained by a linear fit. CGP54626 did not significantly change the size of the average response (Pre: 0.14 ± 0.03 mV; CGP: 0.15 ± 0.02 mV; P = 0.73, n = 6 mice) nor the initial slope (Pre: Pre: -6.9 ± 1.1 mV; Post: -7.9 ± 0.8; P = 0.17, n = 6 mice). **d,** Onset of grating-evoked LFP before drug application (Pre, red), during application of $GABA_B$ agonist baclofen (Bac, dark red; 10 µM), and during application of a mixture of baclofen (10 µM) and CGP54626 (Bac+CGP, light purple). Responses are the average across all stimulus directions (36 trials). Note that baclofen reduces the initial slope by 50% however this effect is reversed by the addition of CGP54626 (Pre: -11.2 mV/s; Bac: -5.4 mV/ s; Bac+CGP: -11.7 mV/s). Thus, CGP54626 application in **d** was sufficient to reverse baclofen-mediated activation of $GABA_B$ receptors. The minimal effect of CGP54626 observed in **b-c** during LED illumination suggests that under our conditions, the photostimulation of PV cells did not significantly alter transmitter release from thalamic terminals via the activation of presynaptic GABA receptors. Error bars, mean ± s.e.m.

Supplementary Figure 2.5 Additional measures of orientation tuning

a, Schematic showing how depth of modulation by orientation (Mod) was calculated. For each tuning curve, the responses to opposite directions were averaged together and the tuning curve was circularly shifted so that the orientation producing maximum response was centered at 0 degrees. The tuning curves were then normalized to the maximum response (Max). The minimum values of the tuning curve on either side of the peak (Min_1 and Min_2) were averaged together (Min_{Avg}) and the depth of modulation was calculated as the difference between Max and Min_{Avg}. In most cases, $Min_1 = Min_2 = Min_{Avg}$. Mod ranges from 0 to 1. A value of 0 means that the response at the preferred orientation is the same as that of weakest orientation, 0.5 means that the response at the preferred orientation is half that of the weakest orientation, and 1 means that the response at the weakest orientation is 0. **b-f,** Mod for each OSI scatter plot from the main figures. **b,** Mod $F1_{Thal} = 0.58 \pm 0.03$, Mod $Q_{Thal} = 0.12 \pm 0.01$, significantly different p = 1e-10. **c,** Mod $Q_{Tot} = 0.19 \pm 0.01$, Mod $Q_{Thal} = 0.12 \pm 0.01$, significantly different p = 6e-5. **d,** Mod $Q_{Sub} = 0.3 \pm 0.02$, Mod $Q_{Thal} = 0.12 \pm 0.01$, significantly different p = 3e-8. **e,** Mod $F1_{Sub} = 0.65 \pm 0.02$, Mod $Q_{Sub} = 0.3 \pm 0.02$, significantly different p = 7e-16. **f,** Mod $F1_{Thal} = 0.58 \pm 0.03$, Mod $F1_{Sub} = 0.65 \pm 0.02$, significantly different p = 0.02. **g,** Schematic showing how orientation tuning width was calculated. The orientations at which the tuning curve reached a value of Mod/2 on either side of the peak of the tuning curve were determined by linear interpolation without smoothing. The difference in these two orientations was defined as the tuning width. Because the tuning width has little relevance in the case of tuning curves with very little selectivity, we calculated the tuning width only for $F1_{Thal}$ and $F1_{Sub}$, the parameters that exhibited the strongest tuning. **h,** Tuning width of $F1_{Thal}$ plotted against $F1_{Sub}$. Width of $F1_{Thal} = 76 \pm 3$ degrees, Width of $F1_{Sub} = 68 \pm 4$ degrees, not significantly different p = 0.084; Data in **b-f** and **h** are from n = 42 cells from 33 mice.

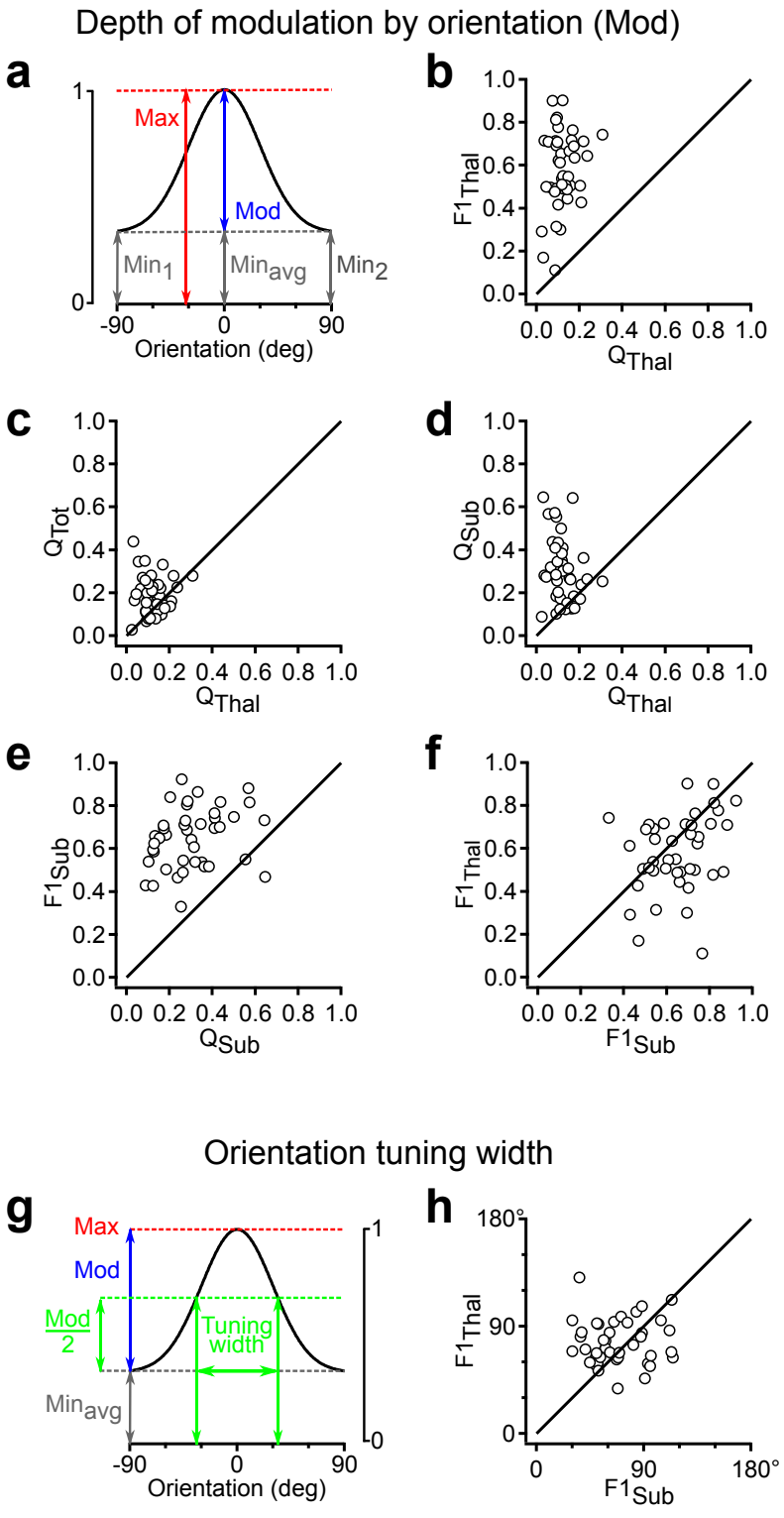
Depth of modulation by orientation (Mod)
a
Max
Mod
Min1
Minavg
Min2
Orientation (deg)
b
F1Thal
QThal
c
QTot
QThal
d
QSub
QThal
e
F1Sub
QSub
f
F1Thal
F1Sub
Orientation tuning width
g
Max
Mod
Mod 2
Tuning width
Minavg
Orientation (deg)
h
F1Thal
F1Sub

Acknowledgements

We thank J. Evora for help with genotyping and mouse husbandry, J. Isaacson, E. Chichilnisky, and the members of the Scanziani and Isaacson labs for helpful discussions of this project, and S. Olsen and K. Reinhold for help with dLGN recordings. This project was supported by the Gatsby charitable foundation, the Brain & Behavior Research Foundation and the Howard Hughes Medical Institute.

Chapter 2, in full, is a reprint of material as it appears in: Lien AD, Scanziani M (2013) Tuned thalamic excitation is amplified by visual cortical circuits. Nature Neuroscience 16:1315–1323. The dissertation author was the primary investigator and author of this paper.

References

1. Adesnik, H., Bruns, W., Taniguchi, H., Huang, Z. J., and Scanziani, M. (2012). A neural circuit for spatial summation in visual cortex. *Nature* 490, 226–31.

2. Anderson, J. S., Carandini, M., and Ferster, D. (2000). Orientation tuning of input conductance, excitation, and inhibition in cat primary visual cortex. *J. Neurophysiol.* 84, 909–26.

3. Atallah, B. V, Bruns, W., Carandini, M., and Scanziani, M. (2012). Parvalbumin-expressing interneurons linearly transform cortical responses to visual stimuli. *Neuron* 73, 159–70.

4. Bock, D. D., Lee, W.-C. A., Kerlin, A. M., Andermann, M. L., Hood, G., Wetzel, A. W., Yurgenson, S., Soucy, E. R., Kim, H. S., and Reid, R. C. (2011). Network anatomy and in vivo physiology of visual cortical neurons. *Nature* 471, 177–82.

5. Bosking, W. H., Zhang, Y., Schofield, B., and Fitzpatrick, D. (1997). Orientation selectivity and the arrangement of horizontal connections in tree shrew striate cortex. *J. Neurosci.* 17, 2112–27.

6. Boyden, E. S., Zhang, F., Bamberg, E., Nagel, G., and Deisseroth, K. (2005). Millisecond-timescale, genetically targeted optical control of neural activity. *Nat. Neurosci.* 8, 1263–8.

7. Brainard, D. H. (1997). The Psychophysics Toolbox. *Spat. Vis.* 10, 433–6.

8. Brecht, M., and Sakmann, B. (2002). Dynamic representation of whisker deflection by synaptic potentials in spiny stellate and pyramidal cells in the barrels and septa of layer 4 rat somatosensory cortex. *J. Physiol.* 543, 49–70.

9. Briggman, K. L., Helmstaedter, M., and Denk, W. (2011). Wiring specificity in the direction-selectivity circuit of the retina. *Nature* 471, 183–8.

10. Chapman, B., Zahs, K. R., and Stryker, M. P. (1991). Relation of cortical cell orientation selectivity to alignment of receptive fields of the geniculocortical afferents that arborize within a single orientation column in ferret visual cortex. *J. Neurosci.* 11, 1347–58.

11. Chung, S., and Ferster, D. (1998). Strength and orientation tuning of the thalamic input to simple cells revealed by electrically evoked cortical suppression. *Neuron* 20, 1177–89.

12. Cudeiro, J., and Sillito, A. M. (2006). Looking back: corticothalamic feedback and early visual processing. *Trends Neurosci.* 29, 298–306.

13. Ferster, D., Chung, S., and Wheat, H. (1996). Orientation selectivity of thalamic input to simple cells of cat visual cortex. *Nature* 380, 249–52.

14. Gilbert, C. D., and Wiesel, T. N. (1989). Columnar specificity of intrinsic horizontal and corticocortical connections in cat visual cortex. *J. Neurosci.* 9, 2432–42.

15. Grubb, M. S., and Thompson, I. D. (2003). Quantitative characterization of visual response properties in the mouse dorsal lateral geniculate nucleus. *J. Neurophysiol.* 90, 3594–607.

16. Haider, B., Häusser, M., and Carandini, M. (2013). Inhibition dominates sensory responses in the awake cortex. *Nature* 493, 97–100.

17. Hubel, D. H., and Wiesel, T. N. (1962). Receptive fields, binocular interaction and functional architecture in the cat's visual cortex. *J. Physiol.* 160, 106–54.

18. Jia, H., Rochefort, N. L., Chen, X., and Konnerth, A. (2010). Dendritic organization of sensory input to cortical neurons in vivo. *Nature* 464, 1307–12.

19. Jin, J., Wang, Y., Swadlow, H. A., and Alonso, J. M. (2011). Population receptive fields of ON and OFF thalamic inputs to an orientation column in visual cortex. *Nat. Neurosci.* 14, 232–8.

20. Kitamura, K., Judkewitz, B., Kano, M., Denk, W., and Häusser, M. (2008). Targeted patch-clamp recordings and single-cell electroporation of unlabeled neurons in vivo. *Nat. Methods* 5, 61–7.

21. Ko, H., Hofer, S. B., Pichler, B., Buchanan, K. a, Sjöström, P. J., and Mrsic-Flogel, T. D. (2011). Functional specificity of local synaptic connections in neocortical networks. *Nature* 473, 87–91.

22. Lampl, I., Anderson, J. S., Gillespie, D. C., and Ferster, D. (2001). Prediction of orientation selectivity from receptive field architecture in simple cells of cat visual cortex. *Neuron* 30, 263–74.

23. Lien, A. D., and Scanziani, M. (2011). In vivo Labeling of Constellations of Functionally Identified Neurons for Targeted in vitro Recordings. *Front. Neural Circuits* 5, 16.

24. Liu, B. H., Li, P., Sun, Y. J., Li, Y., Zhang, L. I., and Tao, H. W. (2010). Intervening inhibition underlies simple-cell receptive field structure in visual cortex. *Nat. Neurosci.* 13, 89–96.

25. Liu, B. H., Li, Y., Ma, W., Pan, C., Zhang, L. I., and Tao, H. W. (2011). Broad inhibition sharpens orientation selectivity by expanding input dynamic range in mouse simple cells. *Neuron* 71, 542–54.

26. Liu, B. H., Wu, G. K., Arbuckle, R., Tao, H. W., and Zhang, L. I. (2007). Defining cortical frequency tuning with recurrent excitatory circuitry. *Nat. Neurosci.* 10, 1594–600.

27. Malach, R., Amir, Y., Harel, M., and Grinvald, A. (1993). Relationship between intrinsic connections and functional architecture revealed by optical imaging and in vivo targeted biocytin injections in primate striate cortex. *Proc. Natl. Acad. Sci. U. S. A.* 90, 10469–73.

28. Margrie, T. W., Brecht, M., and Sakmann, B. (2002). In vivo, low-resistance, whole-cell recordings from neurons in the anaesthetized and awake mammalian brain. *Pflugers Arch.* 444, 491–8.

29. Marshel, J. H., Kaye, A. P., Nauhaus, I., and Callaway, E. M. (2012). Anterior-posterior direction opponency in the superficial mouse lateral geniculate nucleus. *Neuron* 76, 713–20.

30. Marshel, J. H., Mori, T., Nielsen, K. J., and Callaway, E. M. (2010). Targeting single neuronal networks for gene expression and cell labeling in vivo. *Neuron* 67, 562–74.

31. Nagel, G., Szellas, T., Huhn, W., Kateriya, S., Adeishvili, N., Berthold, P., Ollig, D., Hegemann, P., and Bamberg, E. (2003). Channelrhodopsin-2, a directly light-gated cation-selective membrane channel. *Proc. Natl. Acad. Sci. U. S. A.* 100, 13940–5.

32. Nelson, S., Toth, L., Sheth, B., and Sur, M. (1994). Orientation selectivity of cortical neurons during intracellular blockade of inhibition. *Science (80-.).* 265, 774–7.

33. Niell, C. M., and Stryker, M. P. (2010). Modulation of visual responses by behavioral state in mouse visual cortex. *Neuron* 65, 472–9.

34. Olsen, S. R., Bortone, D. S., Adesnik, H., and Scanziani, M. (2012). Gain control by layer six in cortical circuits of vision. *Nature* 483, 47–52.

35. Piscopo, D. M., El-Danaf, R. N., Huberman, A. D., and Niell, C. M. (2013). Diverse visual features encoded in mouse lateral geniculate nucleus. *J. Neurosci.* 33, 4642–56.

36. Reid, R. C., and Alonso, J. M. (1995). Specificity of monosynaptic connections from thalamus to visual cortex. *Nature* 378, 281–4.

37. Ringach, D. L., Shapley, R. M., and Hawken, M. J. (2002). Orientation selectivity in macaque V1: diversity and laminar dependence. *J. Neurosci.* 22, 5639–51.

38. Swindale, N. V (1998). Orientation tuning curves: empirical description and estimation of parameters. *Biol. Cybern.* 78, 45–56.

39. Usrey, W. M., Alonso, J. M., and Reid, R. C. (2000). Synaptic interactions between thalamic inputs to simple cells in cat visual cortex. *J. Neurosci.* 20, 5461–7.

Chapter 3. *In vivo* labeling of constellations of functionally identified neurons for targeted *in vitro* recordings

Preface

Historically, two parallel experimental approaches to neurophysiology have informed our understanding of how the brain works. At the systems level, *in vivo* extracellular recordings of neuronal spiking activity reveal how neurons encode information in the intact functioning brain but provide few details about the cellular and synaptic mechanisms by which activity arises. At the cellular level, *in vitro* intracellular recordings in brain slices provide detailed information about the cellular and synaptic properties of neuronal circuits but are blind to the specific *in vivo* functional response properties of recorded neurons. Novel methods that bridge the gap between systems-level and cellular-level neurophysiology are critical for understanding how cellular, synaptic, and circuit mechanisms underlie neuronal function *in vivo*.

To this end, I developed a technique to map the *in vivo* functional response properties of a neuronal population and fluorescently label specific neurons of interest for subsequent *in vitro* whole-cell recording in acute brain slices. The response properties of L2/3 neurons in the mouse visual cortex were mapped using *in vivo* two-photon calcium imaging. Functionally characterized neurons expressed a photo-activatable green fluorescent protein whose dim baseline fluorescence could be enhanced ~20-fold by two-photon photoactivation, allowing subsequent photolabeling of specific neurons of interest. Neurons that had been functionally characterized and photolabeled *in vivo* were easily identified and targeted for whole-cell recording in acute brain slices. This

technique helps bridge the gap between systems and cellular neuroscience by enabling investigation of cellular and synaptic properties of neuronal circuit elements with known *in vivo* functional properties. Such an approach opens up new possibilities for understanding how neuronal circuits underlie neuronal function in the intact brain.

Abstract

Relating the functional properties of neurons in an intact organism with their cellular and synaptic characteristics is necessary for a mechanistic understanding of brain function. However, while the functional properties of cortical neurons (e.g. tuning to sensory stimuli) are necessarily determined *in vivo*, detailed cellular and synaptic analysis relies on *in vitro* techniques. Here we describe an approach that combines *in vivo* calcium imaging (for functional characterization) with photo-activation of fluorescent proteins (for neuron labeling), thereby allowing targeted *in vitro* recording of multiple neurons with known functional properties. We expressed photo-activatable GFP rendered non-diffusible through fusion with a histone protein (H2B-PAGFP) in the mouse visual cortex and rapidly photo-labeled constellations of neurons *in vivo* at cellular and subcellular resolution using two-photon excitation. This photo-labeling method was compatible with two-photon calcium imaging of neuronal responses to visual stimuli, allowing us to label constellations of neurons with specific functional properties. Photo-labeled neurons were easily identified *in vitro* in acute brain slices and could be targeted for whole-cell recording. We also demonstrate that *in vitro* and *in vivo* image stacks of the same photo-labeled neurons could be registered to one another, allowing the exact *in vivo* response properties of individual neurons recorded *in vitro* to be known. The ability

to perform *in vitro* recordings from neurons with known functional properties opens up exciting new possibilities for dissecting the cellular, synaptic, and circuit mechanisms that underlie neuronal function *in vivo*.

Introduction

Understanding the connectivity, synaptic properties and intrinsic electrophysiological characteristic of neurons whose function has been established in response to sensory stimuli or during behavior is a major challenge in neuroscience. In fact while the function of individual neurons must be assessed in intact animals *in vivo*, connectivity, synaptic properties, and intrinsic electrophysiological characteristics of neurons are best determined on brain explants, *in vitro*. This holds true even for local connectivity patterns between neighboring neurons since, despite the existence of functional maps, neighboring neurons are not necessarily functionally identical (Ohki et al., 2005; Rothschild et al., 2010; Bandyopadhyay et al., 2010). Recent work relating sensory responses recorded *in vivo* with connectivity established *in vitro* has indeed revealed a tight correlation between function and connectivity among neurons in the mouse visual cortex (Ko et al., 2011; Bock et al., 2011).

Previous approaches for studying neurons with known *in vivo* functional properties have utilized *in vivo* intracellular or juxtacellular recording and staining of single neurons with dye-filled electrodes followed by *post hoc* morphological reconstruction (Gilbert and Wiesel, 1979; Pinault, 1996). The major drawback of this approach is that the recorded neurons are re-identified in fixed tissue, precluding targeted electrophysiology in acute brain slices. Additionally, neurons are recorded one at a time,

making this technique inherently low-yield. One recent study overcame some of these issues by combining *in vivo* calcium imaging with 3D registration techniques to assign functional properties to neurons in acute brain slices, however this technique relies on careful alignment of *in vivo* and *in vitro* image stacks (Ko et al., 2011).

We have developed an approach that allows us to fluorescently label constellations of neurons transfected with a non-diffusible photo-activatable fluorescent protein *in vivo*. In combination with *in vivo* calcium imaging of sensory responses, this approach allows an experimenter to rapidly fluorescently label constellations of neurons based on their functional properties. We demonstrate that these functionally-defined constellations can be targeted for subsequent detailed cellular and connectivity analysis *in vitro*. This approach, by greatly facilitating the identification and targeting of neurons *in vitro* whose function has been previously established *in vivo* will contribute toward integrating the experimental approaches of systems and cellular neuroscience.

Results

To photo-label neurons, we utilized photo-activatable GFP (PAGFP), a weakly fluorescent version of GFP that is converted to a strongly fluorescent form upon brief exposure to light of the appropriate wavelength (Patterson and Lippincott-Schwartz, 2002). To prevent diffusion of the photo-activated fraction throughout the cytoplasm of the neuron, which would result in substantial dimming of the fluorescence signal, we used a fusion protein containing PAGFP fused to the histone protein H2B (H2B-PAGFP), which is trafficked to the nucleus and integrated into the chromatin structure (Kruhlak et al., 2006; Testa et al., 2008).

We expressed H2B-PAGFP in the visual cortex of neonatal or juvenile mice through viral injection (see methods). To assess the expression pattern of H2B-PAGFP in layer 2/3 (L2/3) *in vivo*, we exposed the visual cortex and performed two photon imaging with 850 nm excitation light since non-photo-activated H2B-PAGFP is only weakly excitable at 950-1000 nm (Schneider et al., 2005) (Fig. 3.1b). Importantly, non-photo-activated PAGFP can be sufficiently imaged with 850 nm excitation at power levels that minimize its photo-activation (Schneider et al., 2005). We selected an arbitrary constellation of seven H2B-PAGFP expressing neurons for photo-activation (Fig. 3.1b, squares) with 750 nm light. Photo-activation increased the emission of PAGFP excited at 1000 nm by a factor of ~20 (23.0 ± 8.6 sd, n=7 cells). Photo-activated H2B-PAGFP was confined to the cell body of the neuron, consistent with the nuclear location of the fusion protein and was restricted to those neurons whose cell bodies were within the focal plane of the region excited at 750 nm (Testa et al., 2008) (Fig. 3.1b, XZ max). The slow diffusion of H2B-PAGFP also allowed us to test whether we could photo-activate the protein with sub-cellular resolution by performing linescans across somata with 750 nm light (Fig. 3.1c). The pattern of photo-activation was confined to path of the line scan, allowing different patterns to be imprinted onto each cell's nucleus. Thus, H2B-PAGFP is efficiently expressed in cortical neurons and can be used to brightly photo-label user-defined constellations of neurons with cellular and sub-cellular resolution *in vivo*.

Because calcium imaging with the indicator dye Oregon-Green BAPTA-1 AM (OGB) is one of the methods of choice to characterize the functional properties of cortical neurons *in vivo* (Stosiek et al., 2003; Ohki et al., 2005; Komiyama et al., 2010; Kerr et al., 2007) we tested whether we could combine the use of OGB with photo-activation of

H2B-PAGFP to label functionally-defined neuronal constellations. A potential caveat of this approach is the fact that the two fluorophores, OGB and PAGFP, have similar spectral properties. We bolus loaded OGB *in vivo* in L2/3 neurons of the primary visual cortex (V1) expressing H2B-PAGFP (Stosiek et al., 2003) (Fig. 3.1d, Pre images), presented visual stimuli consisting of drifting gratings of various orientation, and imaged OGB at 950-1000 nm excitation. The robust fluorescence change we observed in response to visual stimulation in OGB-loaded neurons (Ohki et al., 2005) (Fig. 3.1d, top) was not due to the lack of H2B-PAGFP expression in those neurons because subsequent scanning of the entire imaging plane at 750 nm lead to the photo-activation of H2B-PAGFP (fold-increase in somatic fluorescence: 2.9 ± 0.9 sd, n=26 cells, Fig. 3.1d, Post/Pre images). Thus, we can detect visually evoked calcium transients with OGB in individual neurons and subsequently label these same neurons *in vivo* by photo-activating H2B-PAGFP. These data show that despite spectral overlap, choice of proper wavelength and large differences in fluorescence magnitude and sub-cellular distribution allow one to combine OGB calcium imaging with H2B-PAGFP photo-labeling of neurons *in vivo.*

Can we perform targeted *in vitro* recordings from neurons that were selectively photo-labeled *in vivo* based on functional calcium imaging? We monitored visually evoked OGB responses in V1 L2/3 neurons expressing H2B-PAGFP and selected visually responsive neurons tuned to various orientations for photo-labeling (Fig. 3.1e, top row). After photo-activating all neurons of interest, the craniotomy was closed, the skin sutured and the animal allowed to recover and placed back in its home cage. Following a 72-hour survival period we cut coronal slices from the imaged and photo-labeled region of the visual cortex for *in vitro* electrophysiological recordings. During

this survival period OGB dissipated from the tissue while photo-labeled neurons could still be clearly detected, consistent with the strong expression and slow turnover of H2B-PAGFP (Testa et al., 2008) (Fig. 3.1e, bottom row), enabling targeted whole cell patch clamp recordings. These results indicate that photo-activation of H2B-PAGFP is a reliable tool for targeted labeling of selected cortical neurons *in vivo* for subsequent electrophysiological experiments *in vitro*.

To perform targeted *in vitro* recordings selectively from neurons with desired response properties to sensory stimuli it may be useful to register a labeled neuron in a slice to its original position *in vivo.* This would allow one to determine connectivity between neurons with known response properties (Ko et al., 2011) or compare intrinsic electrophysiological properties between neurons with different response properties to sensory stimuli. To illustrate the approach we compared input resistance (R_m) and resting membrane potential (V_{rest}) between visually responsive and non-responsive L2/3 neurons since both electrophysiological properties can influence the firing of neurons to synaptic excitation. Through OGB calcium imaging we characterized the response properties of L2/3 V1 neurons located within a single optical plane and photo-labeled all H2B-PAGFP expressing neurons in that plane (Fig. 3.2b). Neurons could be subdivided into those that responded to at least one stimulus direction (> 5 %DF to preferred stimulus) and those that did not (< 5%DF to preferred stimulus). We then cut coronal slices of the photo-labeled region of the cortex and performed targeted recordings from neurons with known response properties. To register the neurons in the slice with those recorded *in vivo* we created image stacks of the labeled region of the slice with the images parallel to the coronal plane (i.e. the surface) of the slice. We took advantage of the planes formed by

the photo-labeled neurons at each cortical depth that was imaged *in vivo* to align the *in vitro* with the *in vivo* image volume. In our coronal slices, these planes extend into the depth of the slice and may have some slant due to the slicing angle. We rotated the *in vitro* image stack such that photo-labeled neurons became co-planar, thus matching the *in vivo* imaging perspective (Fig. 3.2c*i*). Despite distortions possibly due to the to the slicing procedure itself, in the majority of cases even simple visual inspection allowed us to reliably match each individually labeled neuron in the slice to its original position, *in vivo* (compare Fig. 3.2b*i* to 3.2c*i*). This correspondence allows us to perform targeted electrophysiological *in vitro* recordings from neurons with desired response properties to sensory stimuli *in vivo.* We selectively recorded from photo-labeled L2/3 pyramidal cells identified as such via two-photon excitation at 1000 nm and IR oblique illumination (Fig. 3.2c*i*, right). Despite a relatively large neuron to neuron variability in %DF, R_m and V_{rest}, we did not find any correlation between the magnitude of visually evoked %DF and R_m or %DF and V_{rest} (Fig. 3.2d). The average V_{rest} of visually responsive pyramidal cells, measured immediately after breaking in was -62.3±10.1 mV and the average R_m was 141.3±21 MOhm (n=5 cells). There was no significant difference between visually responsive and non-responsive pyramidal cells (non responsive: V_{rest}: -67.5±7.6 mV and R_m: 175±81 MOhm, n=8 cells; p=0.29 for R_m, p=0.34 for Vrest). Thus, the responsiveness of L2/3 pyramidal cells to visual stimuli is not to be influenced by R_m and V_{rest}.

Discussion

Performing recordings *in vitro* from cortical neurons with known responses to sensory stimuli is a demanding task that requires unambiguous registration of large neuronal populations imaged *in vivo* with the neurons in the slice (Ko et al., 2011). This type of approach, however, is fundamental for a mechanistic understanding of brain function. We have developed a simple approach that greatly facilitates the recordings in brain slices from those exact same neurons whose response to sensory stimuli has been previously determined *in vivo*.

This approach is a substantial improvement over previous *in vivo* intracellular and juxtacellular recording and labeling methods (Gilbert and Wiesel, 1979; Pinault, 1996) because it allows an experimenter to functionally characterize of hundreds of neurons and then select subpopulations of interest for photo-labeling and targeted recording *in vitro*. Furthermore, use of the non-diffusible histone-fused H2B-PAGFP results in a much faster photo-activation protocol compared to the diffusible cytosolic form (one second versus tens of minutes) (Datta et al., 2008), while still resulting in strong fluorescence.

We have combined H2B-PAGFP for labeling with OGB for functional characterization. Despite the similar excitation and emission spectra of these two molecules, the difference in excitation of OGB and non photo-activated H2B-PAGFP, as well as the difference in strength, localization and retention in the neuron allows for a clear separation of the signals both *in vivo* and *in vitro.* Future developments will likely generate additional photo-activatable fluorescent proteins and calcium indicators with distinct excitation/emission spectra for an even better separation of fluorescence signals (Ivanchenko et al., 2007; Zhao et al., 2011). Furthermore, the generation of transgenic

mouse lines for both photo-activatable fluorescent proteins and genetically encoded calcium indicators will obviate problems associated with the variability of viral transfections and calcium dye loading. However, viral approaches and synthetic calcium indicators will still remain valuable options as they expand the range of organisms in which the tools can be used (Han et al., 2009; Ohki et al., 2005).

The method presented here will allow one to routinely perform multiple simultaneous recordings (to reveal, for example, the connectivity statistics) selectively between neurons with desired tuning properties, both within and across cortical layers and in a variety of cortical areas. Similarly, this technique will enable the assessment of synaptic strength and, using morphological analysis (Datta et al., 2008), the synaptic location between neurons of known function. Thus, the present approach will help reveal the matrix of connectivity, synaptic strength and synaptic location between cortical neurons contingent on their specific, individual function established *in vivo.*

Although the present study focuses on electrophysiological properties, our approach will also allow isolation of photo-labeled neurons (using FACS sorting or hand picking (Sugino et al., 2006)) to reveal the unique molecular or biochemical properties as well as gene expression profiles of functionally identified neurons.

In conclusion, the possibility of studying the same cortical circuit first *in vivo* and subsequently *in vitro* will certainly contribute in the effort to close the gap between systems and cellular neuroscience.

Methods

All procedures were conducted in accordance with the National Institutes of Health guidelines and with the approval of the Committee on Animal Care at UCSD.

AAV plasmid construction and virus production

Plasmid containing the H2B-PAGFP fusion gene was a gift from André Nussenzweig (Kruhlak et al., 2006). The H2B-PAGFP gene was subcloned into the pACAGW-ChR2-Venus-AAV plasmid (Addgene # 20071), replacing the ChR2-Venus insert. AAV2 serotype 9 was produced from the pACAGW-H2B-PAGFP-AAV plasmid by the Salk Viral Vector Core. Virus titer was $3x10^{12}$ GC/ml. The pACAGW-H2B-PAGFP-AAV plasmid was deposited to Addgene (plasmid #33000, http://www.addgene.org/33000/).

AAV delivery

We used C57BL/6J mice. AAV2.9CAG-H2B-PAGFP was delivered to the mouse visual cortex via intracranial injection of neonates (P0-1) or juveniles (P14-21). For neonatal injection, pups were anesthetized via a cooling pad. Virus was loaded into a beveled glass pipette with 20-40 μm tip diameter. The pipette was inserted into the right visual cortex through the skin and injections of 23 nl volume were made at 3 different depths from 100-600 μm at 1-3 sites using a Nanoject II (Drummond). For juvenile viral injection, mice were anesthetized with 2.5% isoflurane. An incision was made to expose the cranium and a small metal headplate was attached with cyanoacrylate glue to head-fix the animal. A small opening over the right visual cortex was made in the cranium with a

30-gauge needle and virus was delivered via a beveled glass pipette with 15-30 μm tip diameter. The pipette was inserted to a depth of 350 μm from the cortical surface and 50 nl of virus was injected over 5 minutes using a UMP3 microsyringe pump (WPI). Injections were made at 1-4 sites per animal with a separation of ~800 μm. After injection, the headplate was removed, the scalp was sutured, and the animal was given analgesic (0.1 mg/kg Buprenex, SC) and allowed to recover.

Craniotomy for imaging

Animals were used for imaging and photo-activation experiments two weeks to several months after virus injection. Mice were administered chlorprothixene (1 mg/kg, IP) and dexamethasone (2.6 mg/kg, SC) and then anesthetized with 1.5% isoflurane. A thin layer of silcone oil was applied to the eyes to prevent drying and maintain optical clarity. Once the mice reached a surgical level of anesthesia as evidenced by lack of response to toe or tail pinch, the cranium was exposed and a metal head plate was affixed over the right visual cortex with dental cement. After head-fixing the animal, a craniotomy of 1-2.5 mm diameter was performed with a micromotor drill (Foredom) and the dura was left intact. The exposed cortical surface was covered with a thin layer of 1.5% low-melting point agarose (Sigma) and a glass coverslip, which was sealed with Kwik-cast elastomer (WPI) or cyanoacrylate glue. In calcium imaging experiments, the coverslip was applied after dye-loading (see below). At the end of survival experiments, the coverslip was removed, the craniotomy was covered with Kwik-cast and dental cement, the scalp was sutured, analgesic was administered (0.1 mg/kg Buprenex, SC),

and the animal allowed to recover. Otherwise, animals were deeply anesthetized with isoflurane and sacrificed for acute slice preparation.

In vivo two photon imaging and photo-activation

Two-photon imaging and photo-activation was performed in upper L2/3 (100-300 μm depth) using a pulsed Ti:Sapphire laser (Chameleon Ultra II, Coherent; or Mai Tai, Spectra-Physics) coupled to a Sutter Moveable Objective Microscope. We used a 20x 0.95 NA water-immersion objective (XLUMPLFL20xW/0.95, Olympus). Green fluorescence emission light was filtered through a HQ535/50m-18deg aoi filter (Chroma) and collected via a photomultiplier tube (Hammamatsu). Non-photoactivated H2B-PAGFP was visualized using an excitation wavelength of 850 nm. Photo-activated H2B-PAGFP and OGB were imaged at 950-1000 nm excitation. All imaging and photo-activation was performed with Scanimage software (http://www.neuroptikon.org/projects/display/ephus/ScanImage). Laser power was 10-50 mW after the objective and image stacks were taken at 2 μm intervals before and after photo-activation. Calcium imaging of visual responses was performed at 2 or 4 frames/s.

Two-photon photo-activation of H2B-PAGFP was performed with at 750 nm excitation. Laser power was 20-70 mW after the objective. Photo-activation of single cells was performed by designating ~ 10 μm x 10 μm square ROIs around individual somata and scanning each ROI for ~ 0.5-1.5 s. Subcellular photo-activation was performed by scanning across a 250 μm line 512 times at 2 ms/line (~1 s). Full-field photo-activation was performed by scanning a 250 μm x 250 μm field of view with 512 lines 60 times at 2 ms/line (~1 minute).

Calcium indicator loading

Calcium indicator OGB1-AM (Invitrogen) was delivered to cortical neurons using the multi-cell bolus loading method (Stosiek et al., 2003). Briefly, 50 μg of dye was dissolved in 4 μl of 20% Pluronic/DMSO and then diluted to a final concentration of 1mM with a dye loading buffer (in mM: 140 NaCl, 2.5 KCl, 10 HEPES, pH 7.4). Dye solution also contained 50-100 μM Alexa 594 or 488 dye for visualization. This solution was loaded into a patch pipette that was guided into the cortex under the two-photon microscope to a depth of 200-300 μm and dye was pressure ejected for 1-2 minutes. Imaging was performed at least 45 minutes after loading.

Visual stimulation

Stimuli were generated in Matlab with Psychophysics Toolbox and displayed on an LCD monitor positioned 25 cm from the animal. Full contrast drifting square gratings with a spatial frequency of 0.04 cycle/degree and a temporal frequency of 1 Hz were presented sequentially at 12 different angles from 0 to 330 degrees. Gratings were presented for 4 seconds and were preceded and followed by a mean luminance gray screen for 4 s resulting in a 12 s epoch for each orientation. The full set of grating stimuli was presented 8 times. The mean luminance of the monitor during stimulus presentation was 97 cd/m^2.

Analysis of visual response

Image analysis was performed using custom-written scripts in ImageJ and IgorPro. Pixel-based orientation maps were generated by taking the average fluorescence signal of each pixel during the stimulus and subtracting the average fluorescence signal during the baseline period prior to the stimulus. This was done for each of the 6 orientations (responses to opposite directions were pooled), producing 6 images where the intensity value is the average response per pixel to each orientation. A local background subtraction was applied to reduce the contribution of neuropil signals and then each image was given a different color lookup table (Fig. 1E) and merged in RGB color-space to produce the final orientation map.

More detailed analysis of neuronal visual responses was performed by defining cell ROIs and averaging the OGB signal within an ROI. Each cell ROI had a complementary neuropil ROI that consisted of pixels within a 20 μm radius of the cell that were not part of other cells. This neuropil ROI was subtracted from the cell ROI to remove neuropil contamination. For each stimulus epoch, the fluorescence signal was expressed as $\%DF = (F - F_{baseline})/F_{baseline}$ where F is the fluorescence value of each time point and $F_{baseline}$ is the average fluorescence value during the 4 s pre-stimulus baseline period. Orientation tuning curves were constructed by plotting the mean %DF for each orientation.

Electrophysiology in acute slices

Acute cortical slices were prepared from previously imaged and photo-activated animals either immediately after *in vivo* experiments or after a survival period. 300 μm coronal slices were cut on a DSK microslicer in sucrose ACSF (in mM: NaCl 83, KCl

2.5, $MgSO_4$ 3.3, NaH_2PO_4 1, $NaHCO_3$ 26, glucose 22, sucrose 72, $CaCl_2$ 0.5) bubbled with carbogen. Slices were incubated in sucrose ACSF for 30 minutes at 34° C and then kept at room temperature. Individual slices were placed in a submersion-style recording chamber perfused with room-temperature ACSF (in mM: NaCl 119, glucose 22, $MgCl_2$ 1.3, KCl 2.5, NaH_2PO_4 1.3, $CaCl_2$ 2.5, $NaHCO_3$ 26) and imaged under two photon excitation at 1000 nm excitation with a 40x 0.8NA water immersion objective (LUMPLFLN40X/W, Olympus) to find the region containing photo-activated neurons. Individual photo-activated neurons were identified under the two photon and targeted for whole-cell patch clamp recording under oblique IR LED illumination detected via an IR CCD camera (IR-1000, Dage-MTI).

Whole-cell recordings were obtained using borosilicate patch pipettes (3-5 MOhm) containing potassium-based internal solution (in mM: potassium gluconate 135, NaCl 8, HEPES 10, NaGTP 0.3, MgATP 4, EGTA 0.3, Alexa 594 0.1). Signals were recorded on a Multiclamp 700B amplifier (Molecular Devices). Membrane potential was assessed immediately after break-in. Input resistance was measured by recording the amount of steady-state hyperpolarization in response to small negative current steps. Average values were expressed as the mean±s.d. The student t-test was used for statistical comparison.

In vitro and *in vivo* image registration

Image stacks were taken *in vivo* after photo-activation and *in vitro* prior to recording. After scaling the z-dimension of the *in vitro* stack to make it isotropic, the location of photo-activated neurons throughout the depth of the slice was noted. Because

the photo-activated neurons were restricted to a single plane or a series of well-spaced planes *in vivo*, they should form a plane that extends into the depth of the slice. We rotated the image stack such that the co-planar photo-activated neurons appeared in the same optical section. Once this was accomplished, the *in vivo* optical section of the photo-activated plane could be compared to this rotated *in vitro* optical section, and the corresponding neurons could be easily identified.

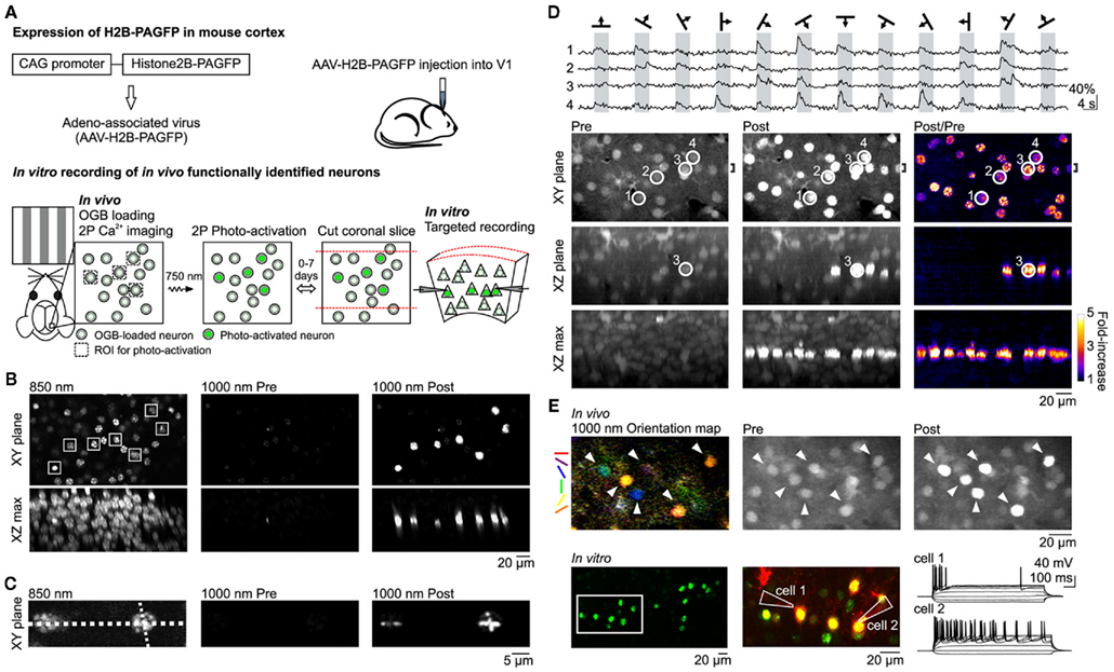

Figure 3.1 *In vivo* photo-labeling of functionally identified cortical neurons followed by *in vitro* targeted recording.

(A) Summary of method. **(B)** *In vivo* photo-activation of L2/3 cells expressing H2B-PAGFP via AAV infection. **(Top)** XYplane imaged at 850 nm (left) and 1000 nm excitation before (center) and after (right) photo-activation. Constellation of 7 neurons in the shape of the Big Dipper selected for photo-activation are indicated by white squares in the 850 nm image. **(Bottom)** Maximum intensity projections of the XZ plane through the entire field of view. **(C)** *In vivo* photo-activation with subcellular resolution. Line-scan photo-activation pattern is indicated by the dotted lines in the 850 nm image. **(D)** *In vivo* photo-activation is compatible with functional OGB Ca2+ imaging of visual responses. **(Top)** Traces show single trial OGB fluorescence responses to drifting grating stimuli in 4 neurons imaged with 1000 nm excitation. Cell locations are circled in the bottom images. **(Bottom)** Images taken with 1000 nm excitation show the cells before (left column) and after (center column) photo-activation of the entire imaging plane as well as the fold-increase in fluorescence (right column). Top row shows the XY plane. XZ plane (center row) and XZ max (bottom raw) images are maximum intensity projections through the region indicated by the bracket (shown on top row) and the entire field of view, respectively. **(E)** *In vitro* whole-cell recording of neurons functionally characterized and photo-activated *in vivo*. **(Top)** Orientation map shows the responsiveness and orientation tuning of each pixel in response to drifting gratings. Visually responsive neurons (arrowheads) were targeted for photo-activation. **(Bottom)** Green photo-activated neurons in an acute coronal brain slice from the region imaged *in vivo*. Two neurons in the region indicated by the white rectangle were targeted for whole-cell recording. Middle panel shows the photo-activated neurons in green and Alexa 594 dye, which was included in the internal solution of the patch pipettes, in red. The membrane potential response to hyperpolarizing and depolarizing current steps is shown to the right.

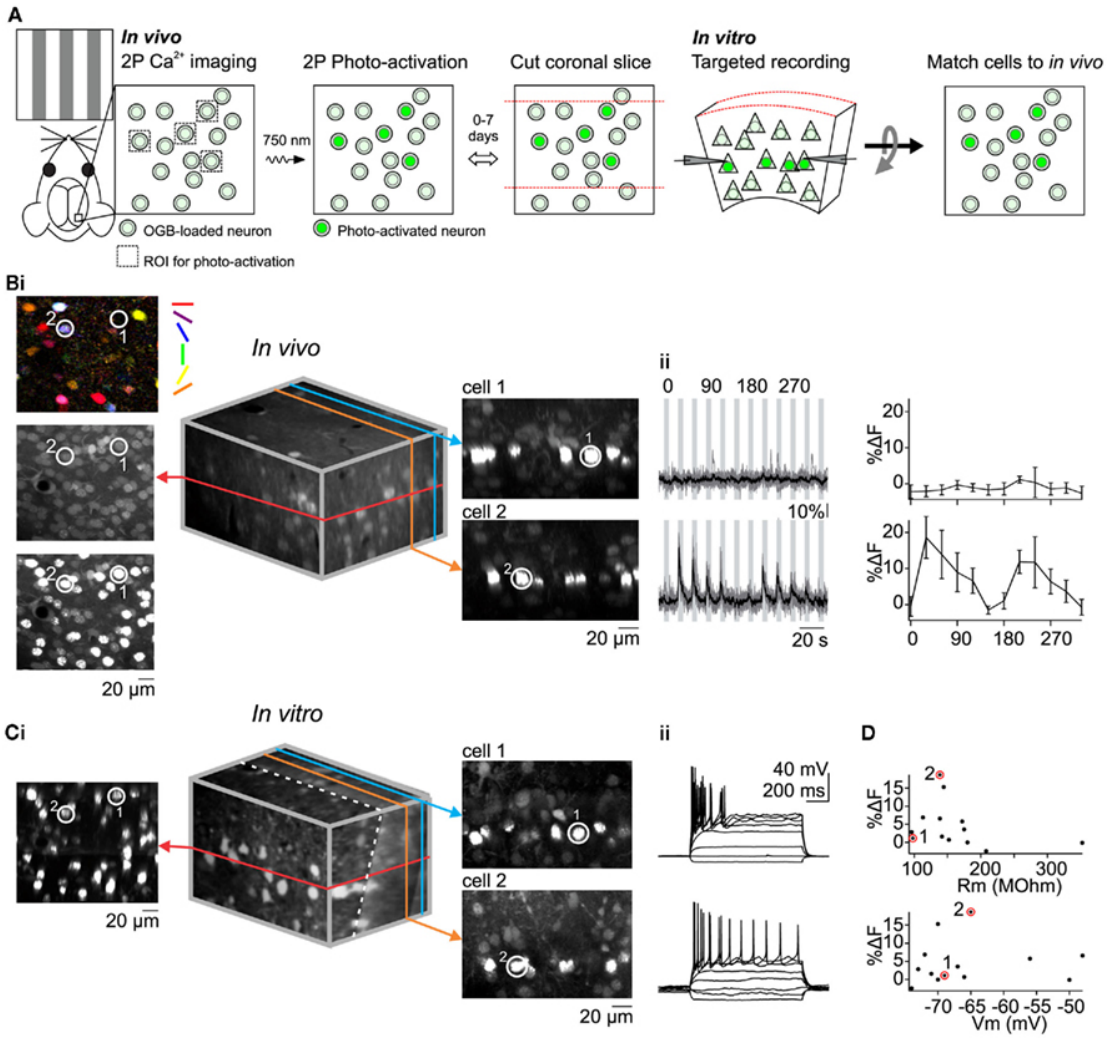

Figure 3.2 Matching *in vivo* and *in vitro* identities of photo-labeled neurons to correlate visual response properties with intrinsic electrophysiological properties.

(A) Summary of method. **(B)** *In vivo* Ca2+ imaging of visual responses followed by photo-activation of all imaged cells in a single plane. **(*i*, Left)** Pixel-based orientation tuning map and images before and after photo-activation. Encircled cells (1 and 2) were recorded later in vitro. **(*i*, Middle)** 3d reconstruction of *in vivo* image stack containing imaged and photo-activated plane (red). **(*i*, Right)** XZ optical sections containing cell 1 and cell 2. **(*ii*)** Visually-evoked Ca2+ signals (left) and orientation tuning curves (right) for cell 1 and 2. (**C**) *In vitro* image registration and whole-cell recording. **(*i*, Left)** Optical section containing photo-activated neurons including cells 1 and 2. **(*i*, Middle)** 3d reconstruction of *in vitro* image stack after rotation to register with the *in vivo* stack. The dotted white line denotes the slicing angle (i.e. main plane of the slice) and the red line denotes the optical section containing the cells that were photo-activated *in vivo*. Note that the *in vivo* (red) optical section is not exactly perpendicular to the plane of the slice **(*i*, Right)** XZ optical sections containing cells 1 and 2. Note the correspondence between *in vitro* and in vivo (B) images. **(*ii*)** Membrane potential response of cells 1 and 2 to hyperpolarizing and depolarizing current injection. **(D)** Magnitude of visual response to gratings is not correlated with input resistance or membrane potential. Size of the visual response to the preferred orientation recorded *in vivo* is plotted against the input resistance (top) and membrane potential (bottom) recorded *in vitro* (n=13 neurons). Data points corresponding to example cells 1 and 2 are circled.

Acknowledgments

We thank Jeff Isaacson and the members of the Scanziani and Isaacson lab for advice during the course of the study. We thank André Nussenzweig for the H2B–PAGFP fusion gene. This work was supported by the NIH grant NS069010, the Gatsby Charitable Foundation and the Howard Hughes Medical Institute. Chapter 3, in full, is a reprint of material as it appears in: Lien AD, Scanziani M (2011) In vivo labeling of constellations of functionally identified neurons for targeted in vitro recordings. Frontiers in Neural Circuits 5:16. The dissertation author was the primary investigator and author of this paper.

References

1. Bandyopadhyay, S., Shamma, S. a, and Kanold, P. O. (2010). Dichotomy of functional organization in the mouse auditory cortex. *Nat. Neurosci.* 13, 361-8.
2. Bock, D. D., Lee, W.-C. A., Kerlin, A. M., Andermann, M. L., Hood, G., Wetzel, A. W., Yurgenson, S., Soucy, E. R., Kim, H. S., and Reid, R. C. (2011). Network anatomy and in vivo physiology of visual cortical neurons. *Nature* 471, 177-82.
3. Datta, S. R., Vasconcelos, M. L., Ruta, V., Luo, S., Wong, A., Demir, E., Flores, J., Balonze, K., Dickson, B. J., and Axel, R. (2008). The Drosophila pheromone cVA activates a sexually dimorphic neural circuit. *Nature* 452, 473-7.
4. Gilbert, C. D., and Wiesel, T. N. (1979). Morphology and intracortical projections of functionally characterised neurones in the cat visual cortex. *Nature* 280, 120–125.
5. Han, X., Qian, X., Bernstein, J. G., Zhou, H.-H., Franzesi, G. T., Stern, P., Bronson, R. T., Graybiel, A. M., Desimone, R., and Boyden, E. S. (2009). Millisecond-timescale optical control of neural dynamics in the nonhuman primate brain. *Neuron* 62, 191-8.
6. Ivanchenko, S., Glaschick, S., Röcker, C., Oswald, F., Wiedenmann, J., and Nienhaus, G. U. (2007). Two-photon excitation and photoconversion of EosFP in dual-color 4Pi confocal microscopy. *Biophys. J.* 92, 4451-7.
7. Kerr, J. N. D., de Kock, C. P. J., Greenberg, D. S., Bruno, R. M., Sakmann, B., and Helmchen, F. (2007). Spatial organization of neuronal population responses in layer 2/3 of rat barrel cortex. *J. Neurosci.* 27, 13316-28.
8. Ko, H., Hofer, S. B., Pichler, B., Buchanan, K. a, Sjöström, P. J., and Mrsic-Flogel, T. D. (2011). Functional specificity of local synaptic connections in neocortical networks. *Nature* 473, 87-91.

9. Komiyama, T., Sato, T. R., O'Connor, D. H., Zhang, Y.-X., Huber, D., Hooks, B. M., Gabitto, M., and Svoboda, K. (2010). Learning-related fine-scale specificity imaged in motor cortex circuits of behaving mice. *Nature* 464, 1182-6.
10. Kruhlak, M. J., Celeste, A., Dellaire, G., Fernandez-Capetillo, O., Müller, W. G., McNally, J. G., Bazett-Jones, D. P., and Nussenzweig, A. (2006). Changes in chromatin structure and mobility in living cells at sites of DNA double-strand breaks. *J. Cell Biol.* 172, 823-34.
11. Ohki, K., Chung, S., Ch'ng, Y. H., Kara, P., and Reid, R. C. (2005). Functional imaging with cellular resolution reveals precise micro-architecture in visual cortex. *Nature* 433, 597-603.
12. Pinault, D. (1996). A novel single-cell staining procedure performed in vivo under electrophysiological control: morpho-functional features of juxtacellularly labeled thalamic cells and other central neurons with biocytin or Neurobiotin. *J. Neurosci. Methods* 65, 113-36.
13. Patterson, G. H., and Lippincott-Schwartz, J. (2002). A photoactivatable GFP for selective photolabeling of proteins and cells. *Science* 297, 1873-7.
14. Rothschild, G., Nelken, I., and Mizrahi, A. (2010). Functional organization and population dynamics in the mouse primary auditory cortex. *Nat. Neurosci.* 13, 353-60.
15. Schneider, M., Barozzi, S., Testa, I., Faretta, M., and Diaspro, A. (2005). Two-photon activation and excitation properties of PA-GFP in the 720-920-nm region. *Biophys. J.* 89, 1346-52.
16. Stosiek, C., Garaschuk, O., Holthoff, K., and Konnerth, A. (2003). In vivo two-photon calcium imaging of neuronal networks. *Proc. Natl. Acad. Sci. U.S.A.* 100, 7319-24.
17. Sugino, K., Hempel, C. M., Miller, M. N., Hattox, A. M., Shapiro, P., Wu, C., Huang, Z. J., and Nelson, S. B. (2006). Molecular taxonomy of major neuronal classes in the adult mouse forebrain. *Nat. Neurosci.* 9, 99-107.
18. Testa, I., Garrè, M., Parazzoli, D., Barozzi, S., Ponzanelli, I., Mazza, D., Faretta, M., and Diaspro, a (2008). Photoactivation of pa-GFP in 3D: optical tools for spatial confinement. *Eur. Biophys. J.* 37, 1219-27.
19. Zhao, Y., Araki, S., Wu, J., Teramoto, T., Chang, Y.-F., Nakano, M., Abdelfattah, A. S., Fujiwara, M., Ishihara, T., Nagai, T., et al. (2011). An expanded palette of genetically encoded Ca2+ indicators. *Science* 333, 1888-91.